



รายงานวิจัยฉบับสมบูรณ์

โครงการ การเตรียมและหาลักษณะเฉพาะทางโครงสร้างโครงข่าย
ออกไซด์ของโลหะทรานสิชันไฮบริดกับโมเลกุลอินทรีย์ที่เตรียมจาก
เทคนิคไฮโดรเทอร์มอลประยุกต์

โดย ผู้ช่วยศาสตราจารย์ ดร. อภินภัส รุจิวัตร์

กรกฎาคม พ.ศ.2551

รายงานวิจัยฉบับสมบูรณ์

โครงการ การเตรียมและหาลักษณะเฉพาะทางโครงสร้างโครงข่ายออกไซด์ ของโลหะทรานสิชันไฮบริดกับโมเลกุลอินทรีย์ที่เตรียมจากเทคนิคไฮโดรเทอร์ มอลประยุกต์

> ผู้ช่วยศาสตราจารย์ ดร. อภินภัส รุจิวัตร์ ภาควิชาเคมี คณะวิทยาศาสตร์ มหาวิทยาลัยเชียงใหม่

> สนับสนุนโดยสำนักงานคณะกรรมการการอุดมศึกษา และสำนักงานกองทุนสนับสนุนการวิจัย

(ความเห็นในรายงานนี้เป็นของผู้วิจัย สกอ. และ สกว. ไม่จำเป็นต้องเห็นด้วยเสมอไป)

กิตติกรรมประกาศ

ก่อนอื่นใดข้าพเจ้าใคร่ขอขอบคุณทาง สกว. และ สกอ. ที่ให้การสนับสนุน และ โดยเฉพาะอย่างยิ่งการ ให้โอกาสแก่นักวิจัยที่มีใจรักในการทำวิจัยพื้นฐาน ซึ่งปัจจุบันนี้อาจกล่าวได้ว่าได้รับการสนับสนุนน้อยมาก และมีผู้ที่เห็นความสำคัญและจำเป็นเพียงหยิบมือเท่านั้น นอกจากนี้โครงการวิจัยนี้คงไม่สามารถอุล่วงไปได้ ด้วยดีหากปราสจากนักศึกษาที่ตั้งใจเรียนรู้ และทุ่มเทให้แก่งานวิจัยอย่างจริงจัง ข้าพเจ้าจึงใคร่ขอขอบใจ นักศึกษาทุกคนไว้ ณ ที่นี้ด้วย หากปราสจาก "ครอบครัววิจัย IMR" เล็กๆครอบครัวนี้ ข้าพเจ้าคงทำอะไรได้น้อย กว่าที่วางแผนไว้มาก รวมทั้งขอบใจนักศึกษาทุกคนที่พิสูจน์ให้ข้าพเจ้าเห็นว่าการทุ่มเทให้กับการสร้างคนที่มี คุณภาพและจริยธรรมโดยผ่านการศึกษาจากงานวิจัยนั้นสามารถทำได้ และทำได้ดีเสียด้วย ซึ่งทำให้ข้าพเจ้าสุข ใจยิ่งกว่าความสำเร็จอื่นใด สุดท้ายข้าพเจ้าใคร่ขอขอบคุณ "ครอบครัวสุดที่รัก" ของข้าพเจ้าที่ให้ความเข้าใจ อดทนกับการไม่ใส่ใจในงานบ้านของข้าพเจ้า แต่ยังให้กำลังใจเสมอมาโดยไม่ปริปากบ่น ขอบคุณพ่ออี๊ดที่คอยดู ลูกเด้ให้ในช่วงเวลาที่ข้าพเจ้ากำลังเขียนรายงานฉบับนี้อยู่ ที่สำคัญที่สุดขอบคุณน้องเด้ที่เกิดมาแล้วทำให้แม่มี กำลังใจที่จะทำงานต่อไป ด้วยหวังใจว่าจะเป็นตัวอย่างที่ดีในการทำงาน การฝึกฝนตนเอง แก่คนร่นต่อไป

อภินภัส รุจิวัตร์ 14 กรกฎาคม 2551

บทคัดย่อ

รหัสโครงการ : RMU4880031

ชื่อโครงการ : การเตรียมและหาลักษณะเฉพาะทางโครงสร้างโครงข่ายออกไซด์ของ

โลหะทรานสิชันไฮบริดกับโมเลกุลอินทรีย์ที่เตรียมจากเทคนิคไฮโดร

เทอร์มอลประยุกต์

นักวิจัย : ผศ. ดร. อภินภัส รุจิวัตร์

ภาควิชาเคมี คณะวิทยาศาสตร์ มหาวิทยาลัยเชียงใหม่

E-mail address : apinpus@chiangmai.ac.th

ระยะเวลาโครงการ : 29 กรกฎาคม 2548 – 28 กรกฎาคม 2551

เนื่องจากข้อดีหลายๆประการของเทคนิคไฮโดรเทอร์มอล ความง่ายในการเตรียม เช่น ปฏิกิริยา ความไม่เป็นพิษต่อสิ่งแวดล้อม และศักยภาพในการนำไปปรับใช้ร่วมกับเทคนิคอื่นๆ ทำ ให้เทคนิคไฮโดรเทอร์มอลถูกนำไปประยุกต์ใช้ในการเตรียม และเลี้ยงผลึกเดี่ยวของสารประกอบ กลุ่มโครงข่ายออกไซด์ของโลหะทรานสิชันที่ไฮบริดกับโมเลกุลอินทรีย์ โลหะที่ทำการศึกษาคือ และวาเนเดียม เนื่องจากความหลากหลายของเคมีโคออร์ดิเนชั้น โคบอลต์ และสมบัติทาง แม่เหล็กของสารประกอบของชาตุทั้งสอง ส่วนโมเลกุลอินทรีย์ที่ใช้ในการวิจัย คือ สารประกอบได เอมีน ทั้งที่มีลักษณะเป็นโมเลกุลสายโซ่ยาว และโมเลกุลไดเอมีนที่มีโครงสร้างที่แข็งเกร็ง คือ 4,4'-ใบไพริดีน และ 1,4-ใดเอซาไบไซโคร[2.2.2]ออกเทน ทั้งนี้เพื่อศึกษาอิทธิพลของโครงสร้าง โมเลกุลอินทรีย์ที่มีต่อโครงสร้างผลึก ซึ่งพบว่าข้อมูลของโครงสร้างโมเลกุลสามารถถูกส่งต่อไปยัง โครงสร้างผลึก และดังนั้นควบคุมโครงสร้างผลึกได้ผ่านทางอันตรกิริยาประเภทต่างๆ ระหว่าง โมเลกุลอินทรีย์และองค์ประกอบอนินทรีย์ โดยเฉพาะอย่างยิ่งพันธะไฮโดรเจน ผลึกที่เตรียมได้ ส่วนใหญ่มีขนาดเล็กและมีลักษณะเป็นผลึกแฝด แต่ยังคงสามารถศึกษาโครงสร้างผลึกได้ด้วย เทคนิคการเลี้ยวเบนรังสีเอ็กซ์ของผลึกเดี่ยว ทั้งโดยใช้แหล่งกำเนิดรังสีเอ็กซ์แบบทั่วไป และแสง ซินโครตรอน ซึ่งในโครงการนี้มีโครงสร้างผลึกใหม่ที่ได้รับการเตรียมขึ้นหลายโครงสร้าง $[{V^{IV}}_4O_{10}{V^{V}}_2O_4](C_6H_{14}N_2).H_2O, \quad CoSO_4(C_2N_2H_{10}) \quad \text{list} \quad [V_{10}O_{27}(OH)].2(C_6N_2H_{14}).(C_6N_2H_{13}).$ $(C_6N_2H_{12}).2H_2O$ เป็นต้น โดยโครงสร้างหลังสุดนี้ถูกเตรียมขึ้นจากปฏิกิริยาที่มีการใช้การแผ่รังสี ไมโครเวฟ ร่วมกับเทคนิคไฮโดรเทอร์มอลในการเตรียมผลึกเดี่ยว เป็นที่น่าสังเกตว่านี่เป็นครั้ง แรกที่มีการประยุกต์ใช้ไมโครเวฟกับการเลี้ยงผลึกเดี่ยวอย่างแท้จริง นอกจากนี้สมบัติทางความ ร้อน และสมบัติแม่เหล็กของสารประกอบใหม่ที่เตรียมได้ยังได้รับการศึกษา และอภิปรายในเชิง องค์ความรู้ใหม่ด้านวิศวกรรมโครงสร้างผลึกด้วยการใช้สาร ของความสัมพันธ์กับโครงสร้าง แม่แบบ และอิทธิพลของสภาวะไฮโดรเทอร์มอลที่มีต่อการเติบโตของผลึกสามารถที่จะนำไปใช้ใน การออกแบบโครงสร้างสารประกอบอื่นๆในกลุ่มที่มีโครงสร้างใกล้เคียงกันได้ นอกเหนือจากองค์ ความรู้ใหม่ และผลงานวิจัยที่มีคุณภาพในระดับนานาชาติแล้ว โครงการวิจัยนี้ ยังช่วยในการเสริม ความแข็งแกร่งให้แก่การศึกษาและวิจัยด้านเคมีสภาวะของแข็ง และผลึกศาสตร์ในประเทศ รวม ไปถึงการเสริมสร้างการทำงานร่วมกันระหว่างกลุ่มวิจัยทั้งในและต่างประเทศ

คำหลัก : Modified hydrothermal synthesis, inorganic-organic hybrid,

oxide framework, vanadium, cobalt

ABSTRACT

Project Code : RMU4880031

Project Title : Preparation and Structural Characterization of Organically Hybrid

Transition Metal Oxide Frameworks Prepared By Modified

Hydrothermal Technique

Investigator : Asst. Prof. Apinpus Rujiwatra, Deptartment of Chemistry, Faculty

of Science, Chiang Mai University

E-mail address : apinpus@chiangmai.ac.th

Project Period : July 29, 2005 – July 28, 2008

Regarding numerous distinct virtues of the hydrothermal technique, e.g. handling facility, environmental benignity, and potential in combining with other techniques, the technique has been applied to the synthesis and single crystal growth of the transition metal oxide frameworks incorporated with organic molecules. The metals of interest were cobalt and vanadium due to their richness in coordination chemistry and versatility in catalytic and magnetic properties. The employed organic molecules were diaminoalkanes and more rigid 4,4'-bipyridine and 1,4-diazabicyclo[2.2.2]octane. This was to investigate the influences of the organic molecular structures on the framework architecture. It has been revealed that the molecular information can be conveyed to and hence regulate the hybrid framework registry via various inorganic-organic interactions particularly hydrogen bonds. Although nearly all of the obtained crystals were tiny and mostly twinned, the complete structural data could be characterized by single crystal X-ray diffraction using either laboratory X-ray source or synchrotron radiation. Numbers of new structures were synthesized and fully characterized, e.g. $[V_{4}^{IV}O_{10}V_{2}^{V}O_{4}](C_{6}H_{14}N_{2}).H_{2}O,$ $CoSO_4(C_2N_2H_{10})$ and $[V_{10}O_{27}(OH)].2(C_6N_2H_{14}).$ (C₆N₂H₁₂).(C₆N₂H₁₂).2H₂O, the latest of which were synthesized using a microwave assisted hydrothermal route. There was notably no prior report on the employment of the microwave heating in the growth of single crystals. The thermal and magnetic properties of the new structures were investigated and discussed in accordance with the structures. The established knowledge on the regulation of the frameworks using the organic template as well as the influences of the synthetic conditions on the crystal growth should be employed in further structural design and crystal growth of relevant structures. Besides the new knowledge and research works of international standard, this project should strengthen the fundamental study and research activities in solid state chemistry and crystallography in the country, as well as reinforce the cooperation with both national and international research groups sharing the common research interests.

Keywords: Modified hydrothermal synthesis, inorganic-organic hybrid, oxide

framework, vanadium, cobalt

หน้าสรุปโครงการ

EXECUTIVE SUMMARY

1. ชื่อโครงการ

(ภาษาไทย) การเตรียมและหาลักษณะเฉพาะทางโครงสร้าง โครงข่ายออกไซค์ของโลหะทรานสิชัน ไฮบริค กับโมเลกุลอินทรีย์ที่เตรียมจากเทคนิคไฮโครเทอร์มอลประยุกต์

(ภาษาอังกฤษ) Preparation and Structural Characterization of Organically Hybrid Transition

Metal Oxide Frameworks Prepared By Modified Hydrothermal Technique

2. รายละเอียดหัวหน้าโครงการ

ผศ. คร. อภินภัส รุจิวัตร์ ภาควิชาเคมี คณะวิทยาศาสตร์ มหาวิทยาลัยเชียงใหม่ จ.เชียงใหม่ 50200 โทรศัพท์ 0 5394 1906 โทรสาร 0 5389 2277

3. สาขาวิชาที่ทำการวิจัย

Solid state chemistry/ Materials chemistry

4. คำสำคัญของข้อเสนอโครงการ

Modified hydrothermal synthesis, Inorganic-organic hybrid,

Oxide framework, Vanadium, Cobalt

6. ระยะเวลาดำเนินงาน

29 กรกฎาคม 2548 - 28 กรกฎาคม 2551

7. ความสำคัญและที่มาของโครงการวิจัย

According to an exponential growth in global science and technology in the last few decades, the innovation and development of advanced materials serving as a major basis is a matter of unavoidable demand. Becoming knowledge based society and technology independent country, Thailand has naturally fallen into the same stream. Over the last thirty years, chemistry has made an increasing important contribution to science and technology of such materials, so much so that the terms solid state chemistry and/or materials chemistry have come into being. Fundamental research in solid state chemistry primarily needs to achieve three goals: (1) development of preparative techniques to prepare new compounds or to improve their properties, (2) discovery of new phases with desired properties from crystal chemical criteria, and (3) full characterization of new phases from chemical and structural points of view. Along this line, preparative chemistry plays very important role. Among various preparative techniques available nowadays, the so-called hydrothermal, which is also recognized by another name of solvothermal, technique has been garnering great interests from scientists and technologists of different disciplines, particularly in the last fifteen years. Due to various distinct virtues of the technique, it has been applied to the synthesis of many technologically important materials including the inorganic-organic hybrid (IOH) compounds, nearly all of which could be synthesized solely by this technique. The combination of inorganic and organic motifs, each of which retains its own structural information as well as properties, in the molecular level provides the IOH compounds the unique and novel properties reflecting partially through the vast structural complexity and diversity. The IOH compounds possessing particularly infinite framework structures have been moving toward the heart of the research activities in the field. The motivations are primarily due to their intrinsic potential, yet not currently well-defined, applications, e.g. as molecular sorbents, selective catalysts, magnetic materials, optical sensors and optoelectronic devices. Regarding the importance of the emerging science and technologies in solid state chemistry and/or materials chemistry as described, this project should result in a new knowledge in a field as well as a development of the in-house materials chemistry technologies. In addition, the research activities carried out under this project should contribute

to the fundamental foundation both academic-wise and technology-wise, both of which are still very much at the enfant stage in the country.

8. วัตถุประสงค์

- [1] To prepare new organodiamine transition metal oxide hybrid compounds by the modified solvothermal technique.
- [2] To establish new knowledge in the field and create research works of international standard.
- [3] To lay down the fundamental study and research activities in solid state chemistry and crystallography in the country.
- [4] To found the cooperation with both national and international research groups sharing the common research interests.

9. ระเบียบวิธีวิจัย

- 1. Grow single crystals of new organodiamine transition metal oxide hybrid compounds by the modified solvothermal technique. The metals of particular interest are cobalt and vanadium, whereas the experimented organodiamines are 1,2-diaminoethane, 1,3-diaminopropane, 1,4-diaminobutane, 1,5-diaminopentane, 1,6-diaminohexane, 4,4'-bipyridine and 1,4-diazabicyclo[2.2.2]octane.
- 2. Characterize the crystal structures by single crystal and powder X-ray diffraction, Fourier Transform Infrared spectroscopy, CHNS/O microanalysis and energy dispersive X-ray spectroscopy. The synchrotron radiation source has been applied in certain cases of single crystal X-ray diffraction experiment.
- Study the thermal properties of the crystals using thermogravimetric analyser, and the magnetic behavior by vibrating sample magnetometer.

It should be noted that due to the potential of the solvothermal technique and the common principle of the technique which is rather independent to the applied materials and/or

compounds, the technique has also been applied to the synthesis and development of the perovskite-based electroceramic powders, including lead titanate, lead zirconate, lithium niobate and barium zirconate, along the line with the proposed IOH compounds. This results in a number of international publications as listed later.

10. แผนการดำเนินงานวิจัยตลอดโครงการในแต่ละช่วง 12 เดือน

Research Activities	1-18	19-24	25-36
1. Grow single crystals of new Co - organodiamine hybrid			
compounds by the modified solvothermal technique.			
2. Characterize structure.			
3. Study thermal and magnetic properties.			
1. Grow single crystals of new V - organodiamine hybrid			
compounds by the modified solvothermal technique.			
2. Characterize structure.			
3. Study thermal and magnetic properties.			
1. Grow single crystals of new V - organodiamine hybrid			
compounds by the modified solvothermal technique using			
microwave heating.			
2. Characterize structure.			
3. Study thermal and magnetic properties.			

11. ผลงาน/หัวข้อเรื่องที่ตีพิมพ์ในวารสารวิชาการระดับนานาชาติ

- [1] Thapanon Settheeworrarit, Chaveng Pakawatchai, Santi Maensiri, Jumras Limtrakul, **Apinpus Rujiwatra***, Crystal structure, thermal and magnetic behavior of inorganicorganic hybrid [V^{IV}₄O₁₀V^V₂O₄](C₆H₁₄N₂).H₂O polymeric framework, *J. Inorg. Organomet. Polym. Mater.* 16(3) (2006) 231-239. (*impact factor, 1.44*)
- [2] Sanchai Lhuachan, Chaveng Pakawatchai, **Apinpus Rujiwatra***, Hydrothermal crystal growth, Structures and Thermal Properties of cobalt-4,4'-bipyridine based coordination polymeric materials, *J. Inorg. Organomet. Polym. Mater.* 17(3) (2007) 561-568. (*impact factor*, 1.44)

- [3] Thapanon Settheeworrarit, Chaveng Pakawatchai, Santi Maensiri, Apinpus Rujiwatra*, CRYSTAL STRUCTURES, THERMOGRAVIMETRIC AND MAGNETIC PROPERTIES OF FOUR ORGANODIAMINE TEMPLATED VANADIUM OXIDE FRAMEWORKS: INFLUENCES OF DIAMINOALKANE TEMPLATES, *J. Inorg. Organomet. Polym. Mater.* 18(2) (2008) 253-263. (impact factor, 1.44)
- [4] Sanchai Lauchan, Timothy J. Prior, Santi Meansiri, **Apinpus Rujiwatra***,

 COBALT(ETHYLENEDIAMINE)SULFATE: A PILLARED LAYERED

 COORDINATION POLYMER, *J. Inorg. Organomet. Polym. Mater.* 18(3) (2008) 352-357. (*impact factor*, 1.44)
- [5] Banlawee Yotnoi, Saranpong Yimgran, Timothy J. Prior, Apinpus Rujiwatra*,

 Microwave assisted crystal growth of a new organic decavanadate assembly:

 [V₁₀O₂₇(OH)].2(C₆N₂H₁₄). (C₆N₂H₁₃).(C₆N₂H₁₂).2H₂O, *Inorg. Chim. Acta*, Submitted (June 26, 2008). (*impact factor*, 1.713)
- [6] Weerachai Phutdhawong*, Duang Buddhasukh, **Apinpus Rujiwatra** and Chaveng Pakawatchai, *Synthetic Commun.* 36 (2006) 881-883. (*impact factor*, 0.977)
- [7] Apinpus Rujiwatra*, Nirawat Thammajak, Thapanee Sarakonsri, Rewadee
 Wongmaneerung, Supon Ananta, Influences of alkali reagents on phase formation and
 crystal morphologies of hydrothermally derived lead titanate, J. Cryst. Growth, 289(1),
 2006, 224-230. (impact factor, 1.95)
- [8] Apinpus Rujiwatra*, Saowalak Tapala, Sanchai Luachan, Orawan Khamman, Supon Ananta, One-Pot Hydrothermal Synthesis of Highly-Dispersed, Phase-Pure and Stoichiometric Lead Zirconate, *Mater. Lett.* 60(23) (2006) 2893-2895. (*impact factor*, 1.625)
- [9] A. Rujiwatra*, C. Wongtawan, W. Pinyo, S. Ananta, Sonocatalyzed Hydrothermal Preparation of Lead Titanate Nanopowders, *Mater. Lett.* 61 (2007) 4522-4524. (*impact factor*, 1.625)
- [10] O. Khamman, T. Sarakornsri, A. Rujiwatra, Y. Laosiritaworn, R. Yimniran, S. Ananta,

 Effects of Ball Milling Time and Calcination Condition on Phase Formation and Particle

- Size of Lead Zirconate Nanopowders Prepared by Vibro-milling, J. Mater. Sci. 42(20) (2007) 8438-8442. (impact factor, 1.081)
- [11] Saowalak Tapala, Nirawat Thammajak, Pitak Laorattanakul, Apinpus Rujiwatra*, Effects of microwave heating on sonocatalyzed hydrothermal preparation of lead titanate nanopowders, Mater. Lett. 62(21-22) (2008) 3685-3687. (impact factor, 1.625)
- [12] Apinpus Rujiwatra*, Nirawat Thammajak, Yotin Chimupala, Pitak Loaratanakul, Sonocatalyzed Ammonothermal Preparation of Fine Lithium Niobate Powders, Adv. Mater. Res. Accepted (May 2008).
- Suttipong Wannapaiboon, Apinpus Rujiwatra*, Ammonothermal preparation of barium zirconate fine powders, Adv. Mater. Res. Accept (May 2008).

สารบัญ

	เลขหน้า
กิตติกรรมประกาศ	i
บทกัดย่อ	ii
Abstract	iii
Executive Summary	iv
สารบัญ	ix
Chapter I : Introduction to principal techniques employed in	
the research project	
Hydro/solvothermal synthesis & crystal growth	1-3
Single crystal X-ray diffraction	1-7
Magnetic property	1-13
Bond valence sum calculation	1-17
References	1-18
Chapter II: Introduction to vanadium- and cobalt-based	
inorganic-organic hybrid compounds	
Chemistry of vanadium oxide frameworks	2-3
Survey on cobalt-organodiamine frameworks	2-23
References	2-33
Chapter III: Crystal structure, thermal and magnetic behavior	
of inorganic-organic hybrid	
$[{ m V^{IV}}_4{ m O}_{10}{ m V^{V}}_2{ m O}_4]({ m C}_6{ m H}_{14}{ m N}_2).{ m H}_2{ m O}$ polymeric	
framework	
Introduction	3-2
Experimental	3-2
Results and discussion	3-5
Conclusions	3-14
References	3-14
Chapter IV: Crystal structures, thermogravimetric and	
magnetic properties of four organodiamine	
template vanadium oxide frameworks :	
Influences of diaminoalkane templates	
Introduction	4-2

Experimental	4-4
Results and discussion	4-7
Conclusions	4-15
References	4-16
Chapter V: Hydrothermal crystal growth, structure and	
thermal of Co(II)-4,4'-bipyridine-based	
coordination polymer materials	
Introduction	5-2
Experimental	5-2
Results and discussion	5-5
Conclusions	5-14
References	5-14
Chapter VI : Cobalt (ethylenediamine)sulfate : A pillared	
layered coordination polymer	
Introduction	6-2
Experimental	6-2
Results and discussion	6-4
Conclusions	6-10
References	6-11
Chapter VII: Microwave assisted crystal growth of a new	
organic-decavanadate assembly:	
$[\mathrm{V}_{10}\mathrm{O}_{27}(\mathrm{OH})].2(\mathrm{C}_6\mathrm{N}_2\mathrm{H}_{14}).(\mathrm{C}_6\mathrm{N}_2\mathrm{H}_{13}).(\mathrm{C}_6\mathrm{N}_2\mathrm{H}_{12}).2\mathrm{H}_2$	
0	
Introduction	7-2
Experimental	7-3
Results and discussion	7-4
Conclusions	7-13
References	7-14
Chapter VIII : Summary of Project Outputs	
International publications	8-2
Human resources development	8-3
National and international research cooperation	8-4
Appendix: Reprints and submitted manuscript	A-1 – A-96

CHAPTER I

INTRODUCTION TO PRICIPAL TECHNIQUES EMPLOYED IN THE RESEARCH PROJECT

According to an exponential growth in global science and technology in the last few decades, the innovation and development of advanced materials serving as a major basis is a matter of unavoidable demand. Becoming knowledge based society and technology independent country, Thailand has naturally fallen in the same stream. Over the last thirty years, chemistry has made an increasing important contribution to science and technology of such materials, so much so that the terms solid state chemistry and/or materials chemistry have come into being. Fundamental research in solid state chemistry primarily needs to achieve three goals: (1) development of preparative techniques to prepare new compounds or to improve their properties, (2) discovery of new phases with desired properties from crystal chemical criteria, and (3) full characterization of new phases from chemical and structural point of view. Along this line, preparative chemistry plays very important role. Among various preparative techniques available nowadays, the so-called hydrothermal, which is also recognized by another name of solvothermal, technique has been garnering great interests from scientists and technologists of different disciplines, particularly in the last fifteen years. The term hydrothermal is the foremost and of geological origin, whereas the solvothermal analogue provides broader and more accurate meaning and is therefore preferable by chemists. Due to various distinct virtues of the technique, it has been applied to the synthesis of many technologically important materials including the inorganic-organic hybrid (IOH) compounds, nearly all of which could be synthesized solely by this technique. The combination of inorganic and organic motifs, each of which retains its own structural information as well as properties, in the molecular level provides the IOH compounds the unique and novel properties reflecting partially through the vast structural complexity and diversity. The IOH compounds possessing particularly infinite framework structures have been moving toward the heart of the research activities in the field. The motivations are primarily due to their intrinsic potential, yet not currently well-defined, applications, e.g. as molecular sorbents, selective catalysts, magnetic materials, optical sensors and optoelectronic devices.

HYDRO/SOLVOTHERMAL SYNTHESIS & CRYSTAL GROWTH

■ Definition of Solvo/Hydrothermal Reaction

Solvothermal technique is collectively referred to as a "chemie douce" or "soft chemistry"; a concept first introduced by Livage [1] and Rouxel [2]. This technique has been adopted for the preparation of a wide variety of compounds, including also the IOHs. Solvothermal synthesis can be defined as the synthesis by either homogeneous or heterogeneous chemical reactions of substances in a sealed liquid media at elevated temperature and pressure [3]. Since most of the solvothermal processes are carried out in water, the term "hydrothermal" is frequently misleadingly used to describe all kind of solvothermal reactions. The employed liquid media, and particularly water, plays a very important role in solvo/hydrothermal reaction, both as solvent and pressure transmitting medium. The pressure developed in the reaction vessel may correspond to the vapor pressure of the aqueous media above the aqueous phase or being controlled by an external pressure controller. Solvothermal reaction effectively provides a low temperature pathway for the preparation of framework and metastable materials by crystallizing them directly from the reaction solution while various thermodynamic variables such as temperatures, pressures and chemical compositions of the reaction mixture are controlled [4]. Understanding the mechanism of solvothermal reactions is particularly necessary in appropriate application and subjective development. However, under almost every solvothermal conditions, only few data are available at present, and only those for pure water and simple saltwater aqueous solutions are known [3,5].

In the hydrothermal reaction, the pressure-volume-temperature (PVT) data and the physico-chemical properties of water at high temperatures and pressures are of significant importance. The PVT curves shown in Figure 1.1 provides information on the behavior of pure water contained in a close reaction vessel filled to various percentages of volume capacity. The curves between the triple point (Tr; the point at which gas, liquid and solid phase coexist) and the critical point (C; 374 °C and 220 bars) represent the vapor pressure curves of water in which liquid and gas phases coexist. The liquid water is absent (dry-boiling) and the vapor phase is not saturated at the pressure below these curves, whereas the liquid water is under compression and the vapor phase is absent when the pressure is above these curves. When the

liquid water is further heated to higher temperature than C, the pressuretemperature (PT) relationship of water is determined by a degree of filling i.e. the volume of the reaction vessel that is originally filled with solution [4,6]. It may be worth nothing that the departure from the vapor pressure curve can occur even before the critical point when the filling capacity is higher than 60%. Figure 1.2 shows a closed two-phase region, in which the liquid and the gaseous phases are in equilibrium and coexist. With increasing temperatures, the density of the liquid phase decreases, while the density of the corresponding gas phase increases. This causes the liquid level to continuously rise up as shown in Figure 1.3. In any autoclave filled to more than 32% with water, the liquid will expand to completely fill the autoclave at some temperature below the critical temperature. The higher the percentage of filling, the lower the temperature the autoclave becomes filled with liquid. When the reaction vessel is completely filled with liquid water, the pressure within the vessel abruptly departs from the vapor pressure curves and rise up rapidly. The curves become more slanting as the degree of filling increases as pictured in Figure 1.1. If the autoclave is initially filled up to 32%, the liquid level remains however unchanged throughout the increase of temperature. When the vessel is filled with less than 32% capacity, which is rarely used, the liquid level on the other hand drops as the temperature increases because of the vaporization of water and the vessel undergoes dry-boiling at some temperatures below the critical temperature.

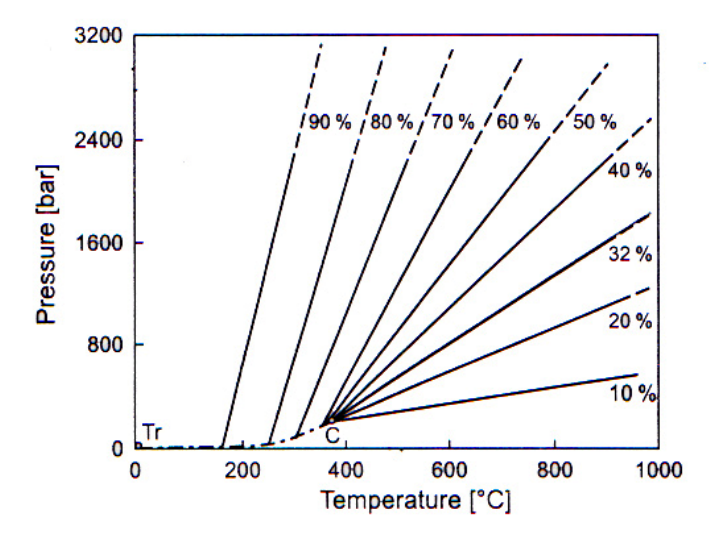


Figure 1.1 Relationship between pressure and temperature of pure water, with particular filling capacity [6].

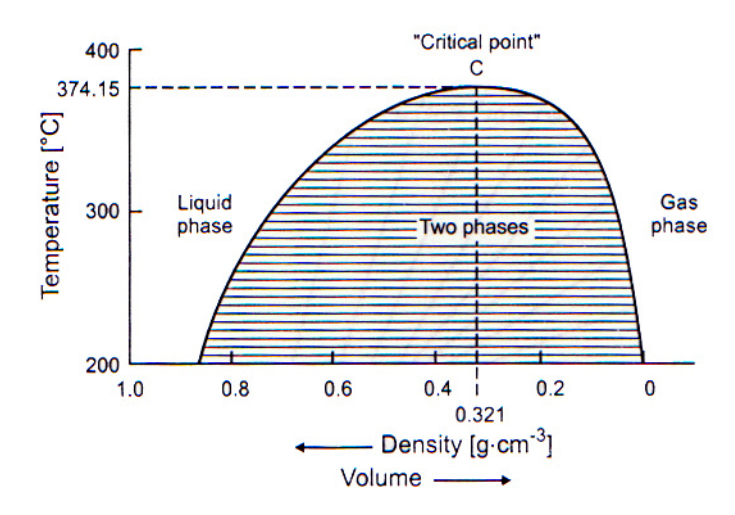


Figure 1.2 Density changes of vapor and liquid phases of pure water as a function of temperature [6].

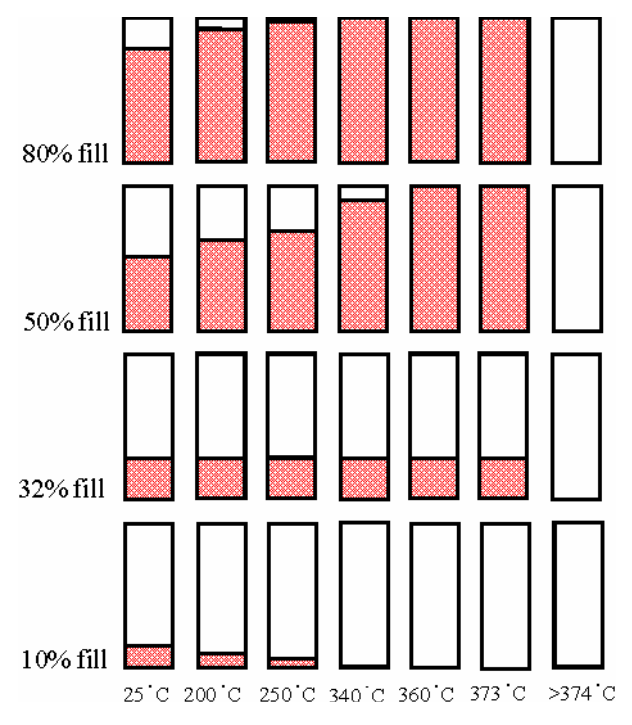


Figure 1.3 Changes of liquid level in closed reaction vessel, with particular degree of initial filling, as a function of temperature [7].

Usually hydrothermal reaction is performed with a degree of filling of 32%, and, with even more success, above 65% and autogenous pressure. It should keep in mind, however, that these data refer to pure water. Assuming that the solubility of the substances under hydrothermal condition is small and that only a very small portion is dissolved, these data may also be used for such solutions [8].

■ Advantages of Solvo/Hydrothermal Reaction in Crystal Growth

By imitating the formation process of crystalline minerals in nature, hydrothermal reactions have long been used in the crystallization of piezoelectric quartz crystals for electronic applications. The unique behaviors of the aqueous media under hydrothermal conditions give rise to many outstanding benefits over other conventional methods. Most importantly, since the viscosity of the aqueous media is lowered during hydrothermal treatment, diffusion processes are more rapid. The solvent extraction of solid precursors and crystal growth from solution is therefore facilitated. This is because the solute diffusion through the aqueous media to the growing crystal interface and the solvent diffusion away from the interface are enhanced. Moreover, these also enable the crystallization of single crystals from starting materials with sparing solubility [8]. The purity and perfection of the obtained single crystals are also significant, especially for those used in very precise and impurity-sensitive electronic equipments. If the diffusion process is too slow, as in conventional techniques, the concentration of the solute will decrease near the interface between the growing crystal and the solution. This fluctuation in concentration can lead to the formation of pertuberances at the crystal surface, resulting in dendritic growth which frequently entraps the impurity and solvent [8]. In addition, hydrothermal technique can also be defined as so-called "chimie douce" in which mild conditions are utilized [9, 10]. This character of hydrothermal reaction benefits in preventing the problems encountered when high temperatures are used such as poor stoichiometric control of volatile components and stress-induced defects caused by phase transformations that occur as the material is cooled down. Furthermore, the nature of direct crystallization from the reaction solution contributes to the ability to control rate and uniformity of the nucleation, growth and aging processes. This also affords the controllability over particle distributions, morphologies of the obtained crystals and aggregations [11]. Beside, being facile onepot technique, low cost instrumentations, low consumption of energy, costeffectiveness, environmental benignity, safety and possibility in modifying the technique are also the outstanding features of the hydrothermal technique. As for the synthesis of the IOH compounds, being "chimic douce" does favor he self-assembly process, and hence the success of the synthesis.

■ Instrumentation for Solvo/Hydrothermal Reaction

The reaction vessel used in hydrothermal synthesis and crystal growth must be a close system which is robust enough to withstand high pressure and corrosion. The constructive materials must have high mechanical strength and great resistance to corrosion by acid or base solutions. Hydrothermal syntheses throughout this study were performed in general purpose acid digestion bomb or so-called "hydrothermal bomb" as a common name. The bomb composes of a metal body as diagrammatically depicted in Figure 1.4 and a removable PTFE (Teflon) liner. The body of the reactor is made of thick-walled stainless steel. To compensate the creep effect of the enclosed PTFE liner according to its large thermal expansion and to maintain a constant loading on the PTFE seal, a spring-loaded closure is fitted with the reactor. The spring also helps maintaining the pressure in the liner throughout the operating cycle, and particularly during cooling process when PTFE vessel would otherwise relax and leak. The safety rupture disc is required to protect the bomb and the operator from the hazard of unexpected or dangerously high internal pressures. The rupture disc is installed above an inner corrosion disc, which serves as a corrosion barrier to protect the rupture disc from corrosive vapor [12].

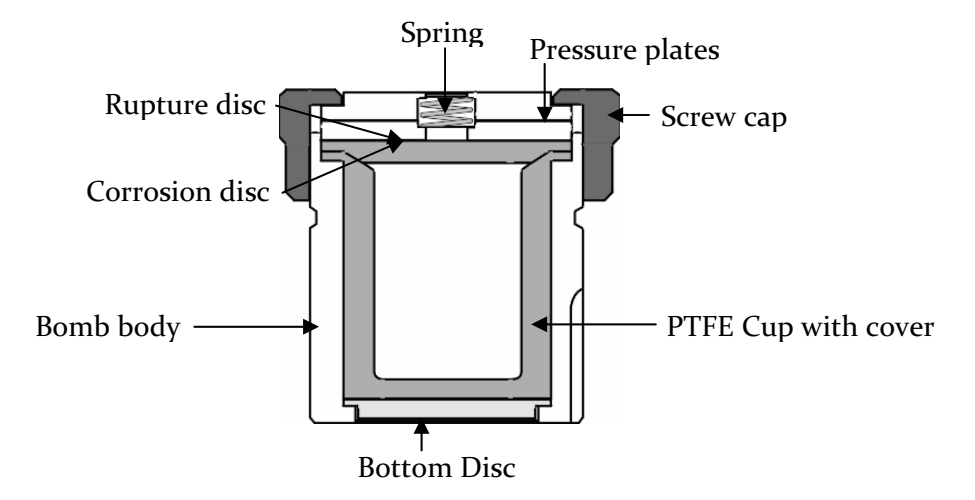


Figure 1.4 Diagram showing the components of general purpose acid-digestion bomb used in hydrothermal synthesis and crystal growth.

SINGLE CRYSTAL X-RAY DIFFRACTION

The capability of conventional stereomicroscope with sufficient magnifying power to clearly image small objects is limited by the wavelength of the visible light (400–700 nm). The objects which are much smaller than this range, including individual molecules or atoms do not give any significant scattering of visible light and therefore cannot be imaged by using typical optical microscopes. In an attempt to resolve the structures, it is necessary to replace long-wavelength visible light with shorter wavelength X-ray. The electrons in the atoms interact with X-ray and scatter them. The intensity variation, caused by interference effects of monochromatic radiations scattered from the electrons, and the patterns of scattered X-ray can be directly recorded, either on photographic films or on a variety of other X-ray sensitive detectors. Then the recombination can be performed mathematically to locate the positions where the electrons are dense and hence the positions of the atoms within the crystal structures [13].

■ Sample and Instrumentation

The sample must be a single crystal, of which all the unit cells are identical and aligned in the same orientation, so that they scatter cooperatively to give a clear diffraction pattern. A typical acceptable crystal size is a few tenths of a millimeter so that it is totally bathed in the incident X-ray beam throughout the diffraction experiment; however, very small crystals can be examined by using more intense X-ray generated from synchrotron radiation source. The quality of crystal samples are tested under a microscope with polarizing filter, to ensure that they are neither twin nor conglomerate, before glued with a minimum quantity of an amorphous glue or similar materials such as grease and perfluoropolyether oil to a fine glass fiber fixed onto a brass pin which is then attached to the goniometer head. The goniometer holds the crystal firmly in the X-ray beam and adjusts the position of the crystal in particular direction accurately.

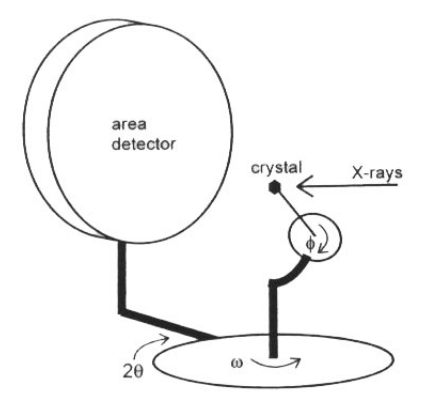


Figure 1.5 Schematic representation of a diffractometer equipped with an area detector [13].

The diffractometer generally used nowadays are all computer-controlled, with the X-ray generated from synchrotron radiation source or conventional X-ray tube of Mo source, and equipped with either an area detector, which provides various advantages over the classical photographic film and scintillation counter detector. The area detector can record over a considerably larger area and numbers of diffracted beam can be recorded simultaneously, resulting in less measurement time. Moreover, there is a high degree of redundancy of symmetry-equivalent data and several reflections are measured more than once. It also reduces the number of rotation axes involved in the classical four-circle diffractometer from four (i.e. 2θ , ω , φ and χ) to three axes (i.e. 2θ , ω and φ) as depicted in Figure 1.5 [13].

■ Data Collection and Reduction

The results of data collection are a list of reflections, usually thousands of them, each of which has its own hkl index and a measured intensity (I). In addition, each intensity has an associated standard uncertainty $(\sigma(I))$, which is a measure of precision or reliability of the measurement. However, the measured intensity is affected by several factors, for which corrections must be applied appropriately. This process is called "data correction". The so-called "Lorenz-polarization factors" associate with the data collection process, which is geometrical in nature and instrument-dependent, are the typical correction. A correction may also be needed for changes in the incident X-ray beam intensity or in the scattering power of the crystal during the experiments, which weakening the measured intensity of the diffracted beams. Absorption effects are also significant and a further correction must be applied. Many different types of absorption correction methods can be employed [13]. SADABS, for example, is designed for correcting the data obtained from Bruker charge-coupled device (CCD) and multi-wire proportional chamber (MWPC) area detectors. It provides useful diagnostics and can correct for errors such as variation in the volume of the crystal radiated, incident beam inhomogeneity, absorption by the crystal and crystal decay. Moreover, this program also improves the esds of the measured intensity [14].

The data reduction process includes the merging and averaging of repeated and symmetry-equivalent measurements in order to produce a unique, corrected and scaled set of data. This calculation affords a numerical measure of the agreement among equivalent reflections, which indicates the quality of the data and the appropriateness of the applied corrections [13].

■ Solving Crystal Structure

After the measurement and appropriate correction of diffraction data, the mathematical solution of the structure can be performed. This can be done by adding together the corrected amplitudes and phases of all the diffracted beams as expressed in equation 1.1,

$$\rho(xyz) = \frac{1}{V} \sum_{h,k,l} |F(hkl)| \cdot \exp[i\phi(hkl)] \cdot \exp[-2\pi i(hx + ky + lz)]$$
(1.1)

where $\rho(xyz)$ = electron density at the position *xyz*, V= unit cell volume (Å³), |F(hkl)|= structure factor for the reflection *hkl* , φ(hkl) = intrinsic phase of the diffracted beams relative to the original incident beam, $-2\pi i(hx + ky + lz)$ = phase shift relative to the unit cell origin.

The final exponential term can be calculated for the contribution of each reflection hkl to each position xyz. However, the intrinsic phase $\phi(hkl)$ of the different reflections are unknown from the diffraction experiment and can be regarded as "phase problem". Of the various methods available hitherto, two methods, i.e. Patterson and Direct methods are by far the most common. The former method is appropriate for the structures containing one or small number of atoms with significantly more electrons than the rest or so-called "heavy atoms", while the latter one is more suitable for the structures constructed from atoms of about equal electron densities [13,15,16].

The Patterson Synthesis

The Patterson method is based on an assumption that all diffracted beams are in phase ($\varphi(hkl) = 0$). Therefore, the electron density equation is shortened as shown in equation 1.2. The Patterson map shows an arrangement of atoms relative to each other as vectorial representations between pairs of atoms in the structure. The Patterson peaks, which are proportional in size to the atomic numbers of the two atoms concerned, show where the atoms lie relative to each other, but not where the atoms lie relative to the unit cell origin.

$$P(xyz) = \frac{1}{V} \sum_{h,k,l} |F(hkl)|^2 \cdot \exp[-2\pi i (hx + ky + lz)]$$
 (1.2)

Patterson map usually shows large regions of overlapped broad peaks, with significantly intense peaks due to the vectors involved with heavy atoms and inversion center due to the use of $|F_o(hkl)|^2$ term. If the structure contains only a few heavy atoms among a lot of lighter atoms, the Patterson map will show a small number of intense peaks standing out clearly above the background level [13,15,16].

Direct Method

The Direct method involves selecting the most important reflections (those which contribute most to the Fourier transform), working out the probable relationships among their phases, and trying different possible phases to see how well the probability relationship are satisfied. The process can be regarded simply as a sort of trial and error method, in which it is usually necessary to try many different sets of phases and use the relationships themselves to refine or improve them. When the solving is successful, most or all of non-hydrogen atoms in the structure will be located [13,15,16].

■ Structure Refinement

The rest of the atoms in the asymmetric unit of the proposed structure can be located by using a difference Fourier map ($|F_o|$ - $|F_c|$), as illustrated in Figure 1.6, followed by full-matrix least squares refinement. The processes of locating new atoms and refinements are repeated until the best fit of the proposed structure to the experimental data is achieved. If the atoms of the model structure are approximately in the right positions, there should be some degree of resemblance between the calculated diffraction pattern and the observed one, *i.e.* between the sets of $|F_c|$ and

 $|F_o|$ values. The most widely used assessment to compare these two data sets is a "residual factor" or "R-factor" which can be defined as shown in equation 1.3.

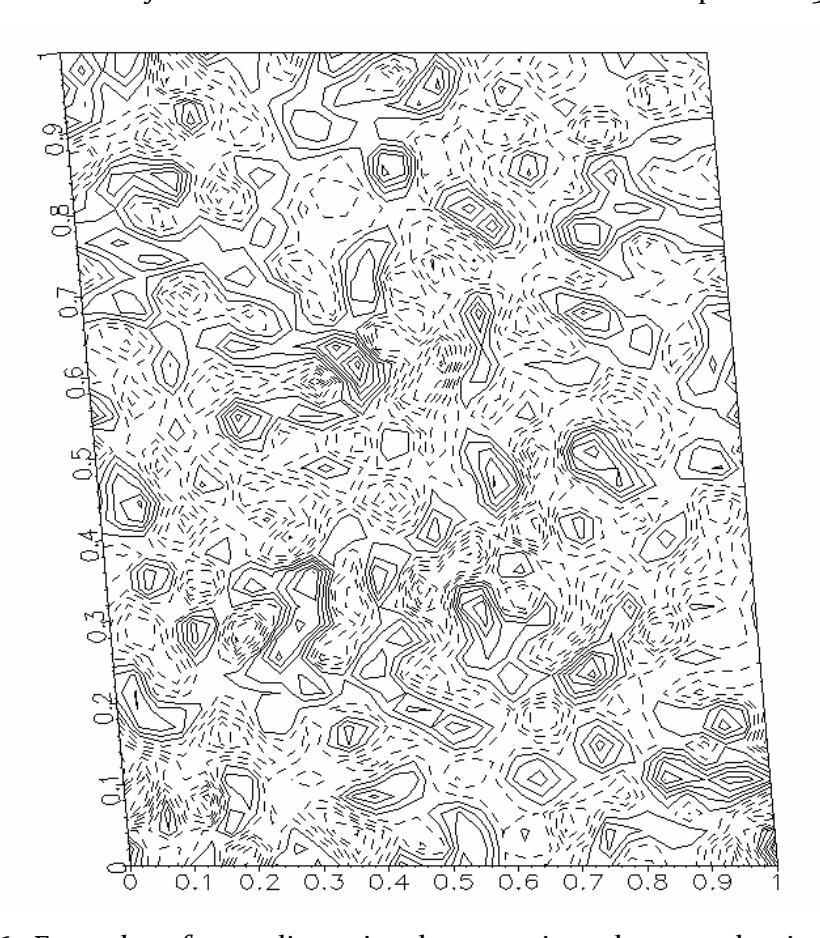


Figure 1.6 Example of two-dimensional successive electron density maps of $(V_{4}^{IV}O_{10}V_{2}^{V}O_{4})\langle C_{4}H_{14}N_{2}\rangle.$

$$R = \frac{\sum ||F_o| - |F_c||}{\sum |F_o|}$$
 (1.3)

If the weighting factors (w) are multiplied to different reflections, based on their standard uncertainty, another residual factor is obtained which is more meaningful than the basic *R* factor.

$$wR2 = \sqrt{\frac{\sum w(F_o^2 - F_c^2)^2}{\sum w(F_o^2)^2}}$$
 (1.4)

For a correct and complete crystal structure determined from well measured data, R factor is typically around 0.02-0.07. The value of wR2 is generally higher than those based on F values, by a factor of two or more [13,15,16].

If *n* is a number of the reflections and *p* is a total number of parameters refined, corresponding Goodness of Fit (*S*) can be defined as [13,15,16],

$$S = \frac{\sum \left[w\left(F_o^2 - F_c^2\right)^2\right]}{(n-p)^{1/2}}$$
 (1.5)

 $w = \frac{1}{[\sigma^2(F_o)^2]}$ (1.6)

when

MAGNETIC PROPERTIES

■ Principles of magnetism [17]

Magnetism is a property of bulk material to be attracted or repelled by an external magnetic field. When a material is placed in an external magnetic field (H_0) , a density of lines of force produced in the sample can be defined as magnetic induction (B). Besides the external field, the magnitude of B is also a function of magnetization (M), which is a magnetic moment of the material per unit volume.

$$B = H_0 + 4\pi M \tag{1.7}$$

The magnetic permeability of the substance (μ_0) is defined as B/H₀, leading to a new term of M/H_o or magnetic susceptibility per unit volume (χ_v) . This is the ratio of additional magnetic induction contributed by the sample to the induction generated by the field alone.

$$\frac{B}{H_0} = 1 + 4\pi\chi_{v} \tag{1.8}$$

The magnetic susceptibility is the major parameter providing a measure of response of a sample to an applied magnetic field, and therefore is usually considered

in the characterization of magnetic properties. The volume susceptibility can also be represented as specific susceptibility (χ_g), which is a susceptibility per unit mass.

$$\chi_{g} = \frac{\chi_{v}}{\rho \, (density)} \tag{1.9}$$

Molar susceptibility (χ_M), which is a susceptibility per mole, can be obtained by multiplying the χ_g with molecular weight (MW) or formula weight (FW) of the material.

$$\chi_M = \chi_g \times MW = \frac{\chi_V \times MW}{\rho} \tag{1.10}$$

Paramagnetic materials have positive χ_M whereas diamagnetic materials possess negative χ_M . The magnetic susceptibility can be varied depending on two major factors, namely temperature (T) and applied magnetic field (H_0) . Different behaviors of the materials as the function of temperature and/or applied magnetic field lead to classes of materials: paramagnetic, diamagnetic, ferromagnetic and antiferromagnetic. The characteristic field and temperature dependencies are summarized in Table 1.1 and shown in Figure 1.7 and 1.8.

Table 1.1 Magnetic classes categorized by magnetic behaviors of materials [17]

Classes	χ	χ(Τ)	χ(Η)	Origin of effect	
Diamagnetism	-	independent	independent	field induced circulation of	
				electron pairs	
Paramagnetism	+	dependent	independent	spin and angular momentum	
				of the electron	
Ferromagnetism	+	dependent	dependent	parallel alignment of unpaired	
				electron spins	
Antiferromagnetism	+	dependent	may dependent	Antiparallel alignment of	
				unpaired electron spins	

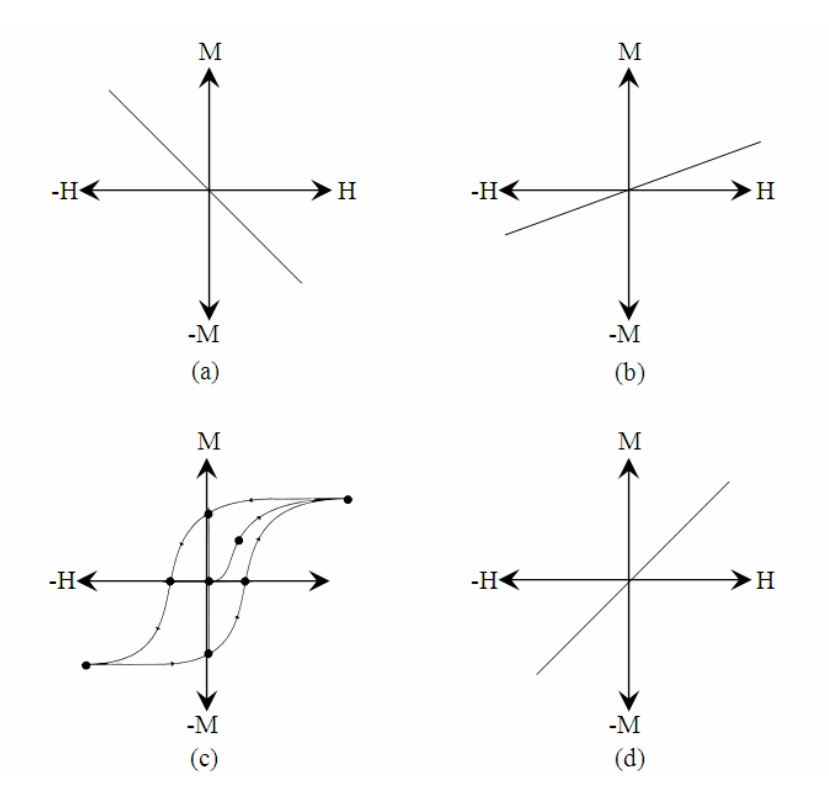


Figure 1.7 Field dependent magnetization curves, M(H), of each magnetic class; (a) diamagnetic, (b) paramagnetic, (c) ferromagnetic and (d) antiferromagnetic materials.

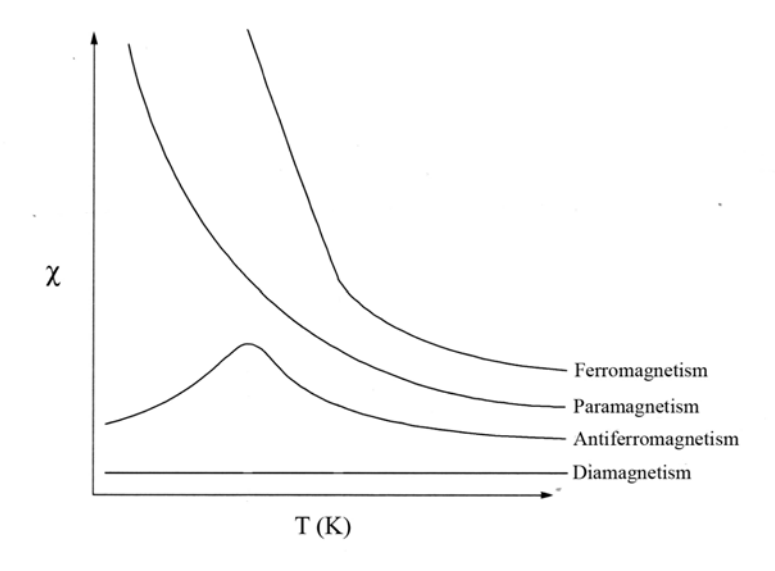


Figure 1.8 Temperature dependent susceptibility curves, $\chi(T)$, characteristic for each class of magnetic materials.

The magnetic properties of materials can be usefully expressed in terms of magnetic moment (μ) since this can be related directly to the number of unpaired

electrons. The relationship between χ and μ can be expressed as shown in equation 1.11.

$$\chi = \frac{N\beta^2 \mu^2}{3kT} \tag{1.11}$$

where N is Avogrado's number, β is Bohr magneton and k is Boltsmann's constant. Substituting for N, β and k gives the simplified equation.

$$\mu = 2.83\sqrt{\chi T} \tag{1.12}$$

The magnetic properties of unpaired electrons are regarded as arising from both, electron spin and electron orbital motion. Of most importance is the spin component. An electron may usually be visualized as a bundle of negative charge spinning on its axis. The magnitude of the resulting spin moment (μ_s) is 1.73 μ_B for a single electron.

$$\mu_s = g\sqrt{s(s+1)} \tag{1.13}$$

If only the electron spin contribution is assumed, the spin moment can be calculated from spin-only equation.

$$\mu_s = g\sqrt{S(S+1)} \tag{1.14}$$

where s is the spin quantum number ($\frac{1}{2}$) and g is the gyromagnetic ratio which is ~2.00 for the first row transition metals. S is the total spin quantum numbers of the unpaired electrons.

The contribution from orbital moment becomes more significant when the atomic number increases, and the magnetic moment can be calculated from equation 1.15.

$$\mu_{S+L} = g\sqrt{4S(S+1) + L(L+1)}$$
 (1.15)

where L is the orbital angular momentum quantum number for the ion [17].

BOND VALENCE SUM CALCULATION

For years, crystal chemists have been using the Bond Valence theory to assess the validity of various chemical structures. This theory was developed from the second rule of Pauling, that the charge (valence) Vj of ions has a tendency to be compensated with the valence strengths (s_{ij}) of the ions coordinated to the given ion $(Vj = \Sigma s_{ij})$ [18]. Since the bond strength is reciprocally related to bond distance, the bond strength can be directly calculated using bond distances and *vise versa* through exponential relationship:

$$s_{ij} = \exp\left[\frac{\left(R_0 - R_{ij}\right)}{b}\right] \tag{1.16}$$

where, R_{ij} = related bond distances,

 $R_{\rm o}$ = bond valence parameter (the bond length having a bond valence of 1),

b = the characteristic parameter of particular bond.

Since the strength of the bond also depends on the oxidation state of the center atom, one parameter model equation can therefore be deducted and effectively used in the determination of the oxidation state of particular atom from the lengths of the coordinated bonds [18,19].

$$V_{j} = \sum_{i=1}^{N} \exp \left[\frac{\left(R_{0} - R_{ij} \right)}{b} \right]$$
 (1.17)

REFERENCES

- [1] J. Livage, Chem. Scr. 28 (1988) 9.
- [2] J. Rouxel, Chem. Scr. 28 (1988) 33.
- [3] S. Feng and R. Xu, Acc. Chem. Res. 34 (2001) 239.
- [4] A. Rabenau, Angew. Chem. Int. Ed. Engl. 24 (1985) 1026.
- [5] G.R. Desiraju, Crystal Design: Structure and Function. John Wiley & Sons Ltd., (2003).
- [6]. U. Schubert, N. Hüsing, Synthesis of Inorganic Materials, Wiley-VCH, Weinheim (2000).
- [7] A. Rujiwatra, Synthesis and Characterization of Novel Framework Compound, D.Phil. Thesis, University of Oxford (2001).
- [8] R.A. Laudise, *C & EN*, September 28, (1987) 30.
- [9] S. Cheng, H.D. Hwang, G.E. Maciel, *J. Mol. Struct.* 470 (1998) 135.
- [10] J. Livage, Coord. Chem. Rev. 178-180 (1998) 999.
- [11] R.E. Riman, W.L. Suchanek, M. Lenka, Ann. Chim.-Sci. Mat. 27(6) (2002) 15.
- [12] PARR INSTRUMENT COMPANY, Parr Operating Instruction 249M: Parr Acid Digestion Bombs, Moline, IL (2000).
- [13] W. Clegg, Crystal Structure Determination, Oxford Chemistry Primers, Oxford Science Publications, New York (1998).
- [14] Bruker AXS, Inc., Bruker Advanced X-ray Solutions: SADABS User Manual (Area Detector Absorption and Other Corrections) Version 2.03 (2002).
- [15] C. Giacovazzo, H.L. Monaco, D. Viterbo, F. Scordari, G. Gilli, G. Zanotti, M. Catti, Fundamenal of Crystallography, Oxford University Press, Avon (1995).
- [16] B.D. Cullity, Elements of X-ray Diffraction, 3rd edn., Addison-Wesley Publishing Company, Inc., California (1956).
- [17] A.R. West, Solid State Chemistry and Its Applications, Replika Press Pvt. Ltd., India (2005).
- [18] V.S. Urusov, I.P. Orlov, Crystallogr. Rept. 44 (1999) 686.
- [19] V.R. Cooper, I. Grinberg, A.M. Rappe, Fundamental Physics for Ferroelectrics (2003) 220.

CHAPTER II

INTRODUCTION TO VANADIUM- AND COBALT-BASED INORGANIC-ORGANIC HYBRID COMPOUNDS

Stemmed from supramolecular origin, the inorganic-organic hybrid (IOH) materials have been defined as the materials which are based on molecular building blocks or derived from molecular precursors, and the materials that are based on collections of molecules [1]. The progress in the field has however brought about a broader concept, although no unanimous definition has been given. The IOH materials nowadays can generally and broadly are described as those comprising two components, namely inorganic and organic. Whereas the inorganic component provides strength, magnetic and electrical properties, the organic part prospers other functionalities, which otherwise cannot be found in the classical inorganic materials. The combination of the two components in molecular level therefore can give rise to novel structures with combined unique properties. These materials then facilitate scientists and technologists of the modern world to catch up with a demand for advanced technologies. Being distinct from the classical materials, the structures of the IOH materials can allegedly be roughly designed in prior to the syntheses. This is widely known as "crystal design", occurring at the forefront of the modern materials chemistry.

The IOH material was first found, although not yet recognized, in the middle of nineteen centuries, in the name of "Maya blue", which was well known as a robust pigment. The true nature and structure of the pigment was however revealed more than two centuries later and since then became an inspiration for the design of the novel IOH materials [2]. The contemplative design and development of the IOH materials began in the early of 1990s, apparently as an extension of an earlier work on three-dimensional cyanide frameworks. This was to generate larger cavities or voids in the framework structures by replacing the short cyanide ligands with larger ligands, e.g. nitriles, amines and carboxylates [2,3]. Such attempts have led to further extensive and more structural oriented research in the field. This can be reflected clearly from an exponential growth of a number of publications on the novel IOH structures and functionalities. It is found in the review by Robin and Fromm [4] that during the last 15 years the number of publications on coordination polymers, another yet more specific title for the IOH materials, has dramatically increased from 100 articles per year in 1990 to 1000 articles per year in 2004.

CHEMISTRY OF VANADIUM OXIDE FRAMEWORKS

■ Coordination Chemistry of Vanadium

In mineral chemistry, vanadium can exhibit four oxidation states, *i.e.* V^{II} , V^{III} , V^{IV} and V^{V} [10]. However, under mild reducing hydrothermal conditions which are usually employed in the preparations of the IOH structures of vanadium oxides, only V^{IV} and V^{V} are present [11]. The characteristic of both oxidation states is the presence of a short *vanadyl* bond, V=O, with bond distances in a range of 1.57-1.68 Å.

Tetravalent vanadium (V^{IV}) has a valence electronic configuration of $3s^23p^63d^t$ and exhibit two types of geometries, *i.e.* square pyramid and square bipyramid as illustrated in Figure 2.1. The square pyramidal geometry (Figure 2.1(b)) can be described as 4+1 coordination, *i.e.* four long bridging bonds in equatorial directions (1.80-2.12 Å) and a short vanadyl bond in the apical position. In general, the V^{IV} atom displaces off the basal-plane in the direction of the vanadyl O atom, causing the angles of $O_{(apical)}$ =V- $O_{(equatorial)}$ to deviate from orthogonality but in a range of 100-110°. The square bipyramid is similarly denoted as 4+1+1 coordination (Figure 2.1(d)), composing of four intermediate equatorial bonds (1.86-2.16 Å), one vanadyl bond in the axial position, and a very long bond located *trans* to the vanadyl bond. This *trans*-bond is lengthened as a consequence of *trans* influence of the multiply bonded oxo-group [12].

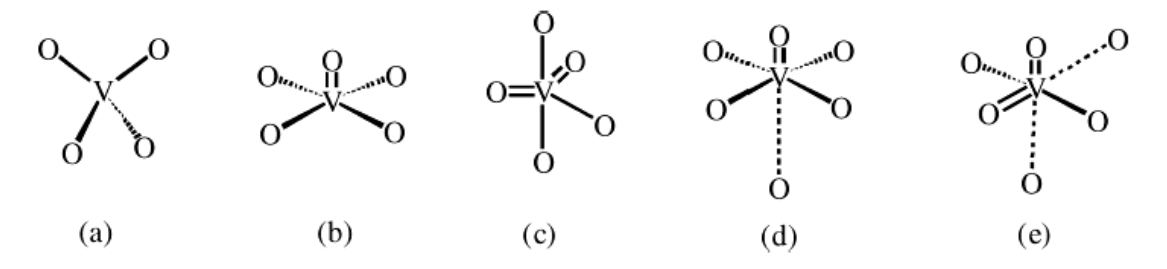


Figure 2.1 Coordination polyhedra adopted by V^{IV} and V^{V} ; (a) regular tetrahedral, (b) [4+1] square pyramid, (c) [3+2] distorted trigonal bipyramid, (d) [4+1+1] square bipyramid and (e) [2+2+2] distorted octahedral [11].

Pentavalent vanadium (V^V), with a valence electronic configuration of $3s^23p^6$, adopts four-, five-, and six- coordinations as also illustrated in Figure 2.1. The

four-coordinated V^V displays regular tetrahedral geometry (Figure 2.1(a)). The related bond distances can be varied in a range of 1.60-2.00 Å and distributed into a short (ca. 1.6-1.7 Å) terminal and long (ca. 1.8-2.0 Å) bridging bonds. The five-coordinate geometry reflects the effect of a number of vanadyl bonds on the $\boldsymbol{V}^{\boldsymbol{V}}$ coordination geometry. When there is only a single V=O bond, the ordinary [4+1] square pyramidal geometry (Figure 2.1(b)) is observed, whereas the presence of two V=O bonds in cis conformation results in a distorted [3+2] trigonal bipyramid (Figure 2.1(c)). The bond distances of bridging V-O bonds in the [4+1] square pyramid and the distorted [3+2] trigonal bipyramid can be varied from 1.74 Å to 2.04 Å. The six coordinate VV polyhedra can display either [4+1+1] square bipyramidal (Figure 2.1(d)) or [2+2+2] distorted octahedral geometries (Figure 2.1(e)), depending on the number of V=O bonds. The [2+2+2] coordination can be defined by two short V=O in cis orientation, two very long bonds (ca. 2.1-2.3 Å) trans to the V=O and two intermediate bonds (ca. 1.85-2.05 Å) *cis* to the V=O bonds [11,13]. Notably, when two V=O bonds are present, they are always arranged in *cis*-conformation in an order to maximize π -bonding to the metal t_{2g} orbitals, giving rise to a better electron distribution between vanadium and oxygen and hence less electronic repulsions [12].

■ Structural Chemistry of Vanadium Oxides

In addition to the richness of coordination chemistry of vanadium, the complexity in structures of the vanadium oxides also arises from the flexibility of the V-O-V bridge and type of polyhedral linkage mode. Various types of vanadium oxide polyhedra may fuse into discrete zero-dimensional polyoxovanadate oligomers or clusters [14], one-dimensional chains [15], two-dimensional layers [16] and three-dimensional networks [17], giving rise to a large structural diversity which can be troublesome to be christened. P.Y. Zavalji et al. have recently suggested the abbreviations which can be effectively used to designate the architectures of the vanadium oxide substructures and to describe the way in which the constructive polyhedra are linked to each other [17]. These abbreviations are summarized in Table 2.1. The most frequently found vanadium oxide building unit are tetrahedral (T), square pyramid (SP) and octahedral (O), which can be further linked in numerous fashions. Therefore, classes of vanadium oxides can be defined and named by their constructive polyhedra. As shown schematically in Figure 2.2, five classes and fourteen subclasses have been deducted. Surprisingly, the structure constructed from

only the T building unit has not yet been found up to the present, possibly because of the reductive conditions during hydrothermal treatments.

Table 2.1 Abbreviations used in defining the structures and connectivity patterns of vanadium oxide polyhedra [17].

Abbreviations	Definitions
T	Tetrahedral
TB	Trigonal bipyramid
SP	Square pyramid
O	Separated octahedral or octahedral sharing only two neighboring edges
U	SP with up-directed apex sharing only two neighboring edges
D	SP with down-directed apex sharing only two neighboring edges
u	SP with up-directed apex sharing at least two opposite edges
d	SP with down-directed apex sharing at least two opposite edges
o	Octahedral sharing at least two opposite edges
00	Closest packed double o chains
e	Empty site where SP or O is expected to locate
Q	Quadruple O chain
X	Crossed quadruple O chain
W	Wave-like O chain
Z	UuDd zig-zag chain
ZT	UuDd chain (or layer of these chains) with two corner-sharing to T
< >	Cluster or group of polyhedra
{}	One-dimensional chain
()	Two-dimensional layer
[]	Three-dimensional framework
/ / _n	Cyclic group
	Edge-sharing
	Corner-sharing
*	Apex sharing
	Sharing two corners with two following polyhedra or chains
:	Sharing two corners with one polyhedral or chain
n (integer)	Used before the formula to emphasize cell contents
ⁿ (superscript)	Shift along the chain (y-axis) relative to the previous chain in terms of
	polyhedra
_n (subscript)	Repeating number, usually used to describe double chains or layers

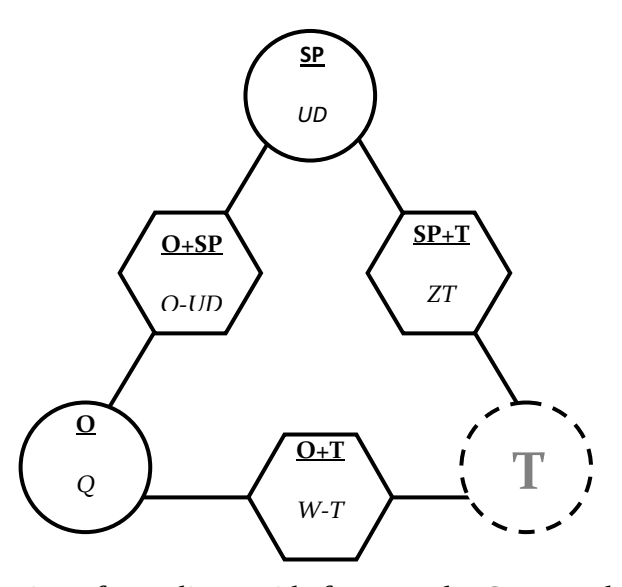


Figure 2.2 Classification of vanadium oxide frameworks. Structural classes and subclasses are shown in **bold** and *italic*, respectively [17].

Most of the structures in five classes of vanadium oxides are constructed from SP and O chains. Some chains exist as separated units, and some are linked into layers or frameworks.

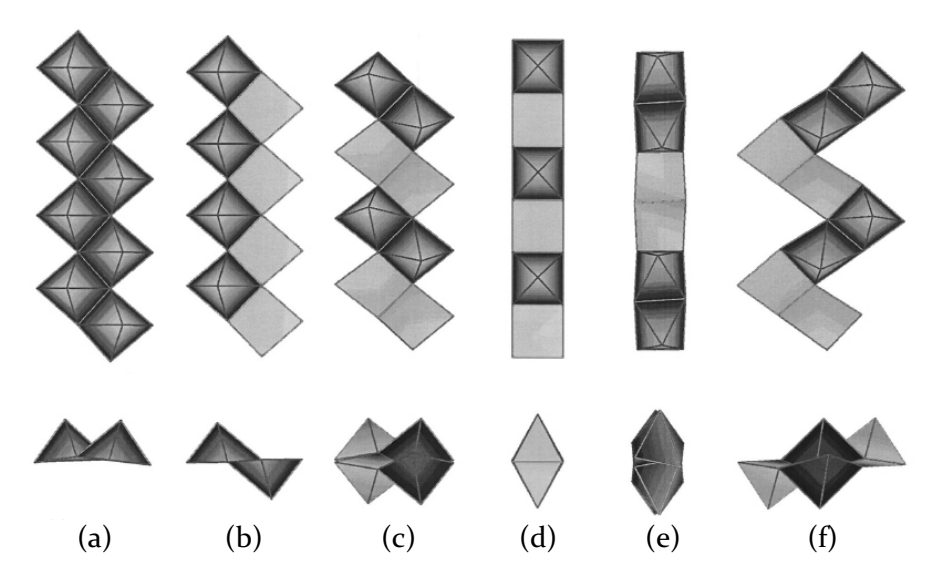


Figure 2.3 Various types of SP chains: (a) $\{UU\}$, (b) $\{UD\}$, (c) $\{UUDD\}$, (d) $\{ud\}$, (e) $\{uudd\}$, and (f) $\{z\}$ chains [17].

SP chains

There are six configurations of SP chains as depicted in Figure 2.3. The first type is the simplest {UU} chain. This chain is built up from the SPs which share their basal-edges in *cis*-conformation, in a way that the apexes of every SPs direct above the plane of the SPs' bases. Alternating U and D form the {UD} type, whereas

{UUDD} type displays a regular alternation of down- and up- directed SP pairs. The {ud} and {uudd} chains are produced when the SPs are fused in a *trans*-fashion. Finally, the {UuDd} or {z} chain is formed when both *cis*- and *trans*- edge sharing are present, which result as a zig-zag chain. Noteworthy, the apexes of the SPs in UU or DD dimers are substantially tilted, leading to a shortening and twisting of the {uudd} and {z} chain. This characteristic also participates in the formation of the SP rings and tunnels.

O Chains

Different types of O chains are produced from edge-sharing condensation of octahedra as shown in Figure 2.4. The chain of corner-shared octahedra is though not common. In the simplest {OO} chain, the Os share two adjacent edges whereas in the {o} chain, the opposite edges are shared. Two {OO} chains can be stacked along the z axis to form other two types of quadruple chains which are different only in the direction of translation between the two {OO} chains. The {X} chain is created when the {OO} chains are shifted half a diagonal along y axis, while x axis translation yield {Q} chain. In the other hand, when the Os share their opposite edges, {oo} chain is obtained. This chain can be used to derive wave-like {W} chain by removing every third Os.

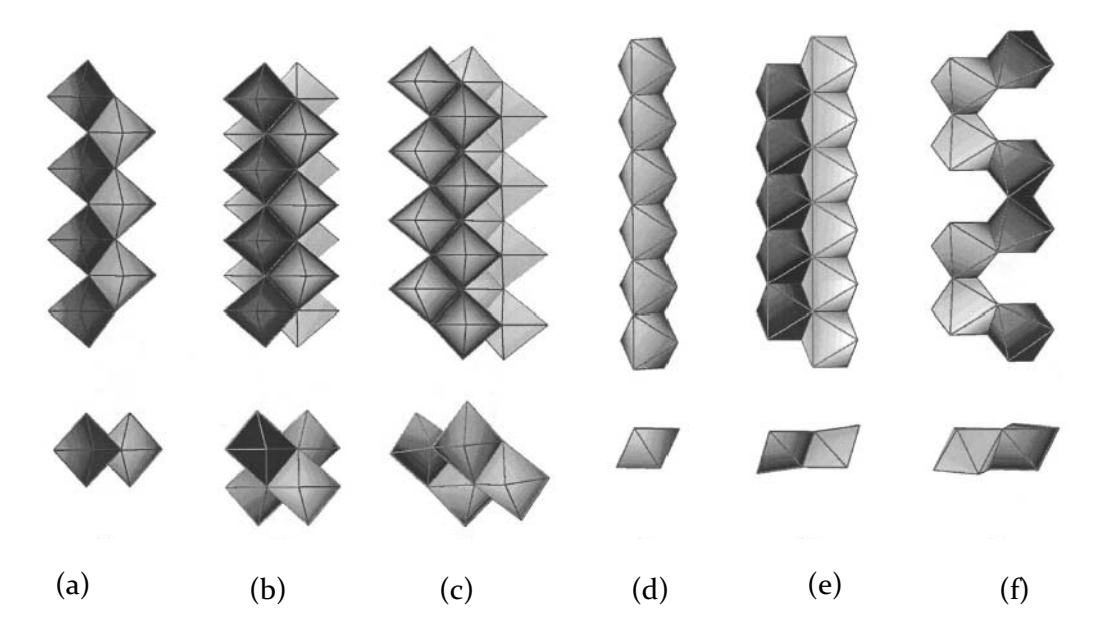


Figure 2.4 Various types of O chains: (a) {OO}, (b) {X}, (c) {Q}, (d) {o}, (e) {oo} and (f) {W} chains [17].

The symbols derived based on the abbreviations in Table 2.1, prototype compounds, space groups and structural construction details are summarized in Table 2.2-2.7. The relevant figures, showing examples of the architectures for each framework, are also given.

Class I. SP Structures; the frameworks are constructed from only SPs and can be divided into three subclasses, i.e. UD layers, UD hexagonal tunnels and ud layers.

Table 2.2 The classification of the SP class structures [17].

Structure symbols	prototype	Vanadium oxide architectures	Space group
Subclo	ıss 1: UD layer	s built from corner-sharing UD chains	
(2{UD}.)	α-V ₂ O ₅	The layer is constructed from	Pmmn
	α -Li _x V ₂ O ₅	corner-sharing {UD} chains	Pmmn,
	α' -NaV ₂ O ₄ F	which are transformed to each	Pmmn
	α '-NaV ₂ O ₅	other by reflection. The layers are	P2₁mn
	CaV_2O_5	translated along z axis with one	Pmmn
	$Cu_{o.64}V_2O_5$	layer per unit cell. The apex of	Pmmn
		each SP is opposite to the apex of	
		the SP in another layer.	
2(2{UD}.)	δ -LiV ₂ O ₅	The layer is similar to (2{UD}.),	Amma
		but every other (2{UD}.) layer is	
		shifted along y-axis for a half SP	
		with two layers per unit cell.	
2({UD}.{DU}.)	γ -LiV ₂ O ₅	Layered structure of corner-	Pnma
	γ - V_2O_5	sharing {UD} chains which are	Pnma
		transformed to each other by a	
		120° rotation around shared	
		corners. The rotation angles	
		alternate in sign within the layer.	
2({UUDD})	$(tma)V_4O_{10}$	Layered structure of corner-	B21ma
		sharing {UUDD} chains. The	
		chains are buckled due to the	
		presence of two equally directed	
		SPs in pairs which put their	
		apexes apart.	

Table 2.2 The classification of the SP class structures [17]. (continued)

Structure symbols	Prototype	Vanadium oxide architectures S	pace groups
Subclass 2: U	ID hexagonal ti	unnels built from corner-sharing {UD} cl	nains.
{/{UD}./ ₆ }	Cs _{0.3} V ₂ O ₅	Six {UD} chains share their corners into an independent hexagonal pipe. Cs atoms fill the space inside	P6 ₃ /m
[{/{UD}./ ₆ }.3{UD}.]	Cs _{0.35} V ₃ O ₇	and between the pipes. {/{UD}./ ₆ } hexagonal pipes which share their faces with each other. Cs atoms occupy only inside the	P6 ₃ /m
		channels.	1 .1
2({ud}¹)	Li _x V _{2-δ} O _{4-δ} Li _x V _{2-δ} O _{4-δ} .H ₂ O	Layer of SPs alternating up and down in strict chessboard order. Each SP shares four edges to neighboring SPs with opposite apex orientations. 1/6 of V sites are vacant and occupied by Li atoms.	P4/nmm I4/mmm
2(2{udue} ⁻¹)	CaV ₃ O ₇	Chessboard layer similar to 2({ud}¹) layer but 1/4 of V sites are empty.	Pnam
({ududedudue} ⁷)	CaV ₄ O ₉	Chessboard layer similar to 2({ud}¹) layer with 1/5 empty V sites. The sequence of the layer in both vertical and horizontal directions are identical, <i>i.e.</i> 'ududedudue'.	P4/n
2({uddueduude} ⁸)	(ppd)V ₄ O ₉	Layer similar to ({ududedudue} ⁷) but the sequence of the layer in perpendicular directions are completely different; "uddue" in horizontal and "udude" in vertical.	P112,/a

Class II. SP+T Structures; the frameworks are built up from the combination of SPs and Ts, and can be classified into three major subclasses, *i.e.* U-T, UD-T and Z-T layers.

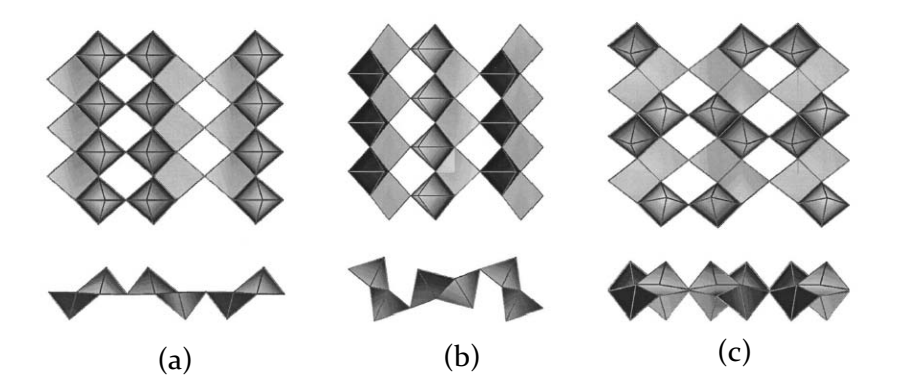


Figure 2.5 UD layers constructed from corner-sharing SP chains; (a) $(2\{UD\}.)$, (b) $2(\{UD\}.\{DU\}.)$ and (c) $2(\{UUDD\}..)$ [17].

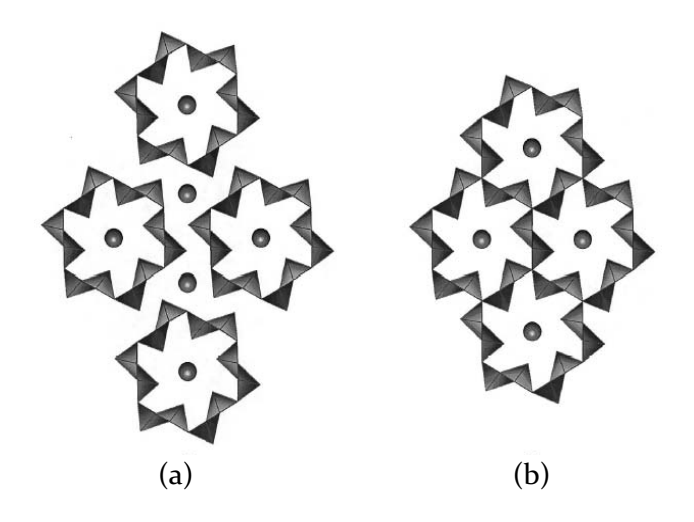


Figure 2.6 UD hexagonal tunneled structures constructed from enwrapped SP layers; (a) $\{/\{UD\}./_6\}$ and (b) $[\{/\{UD\}./_6\}._3\{UD\}.]$ [17].

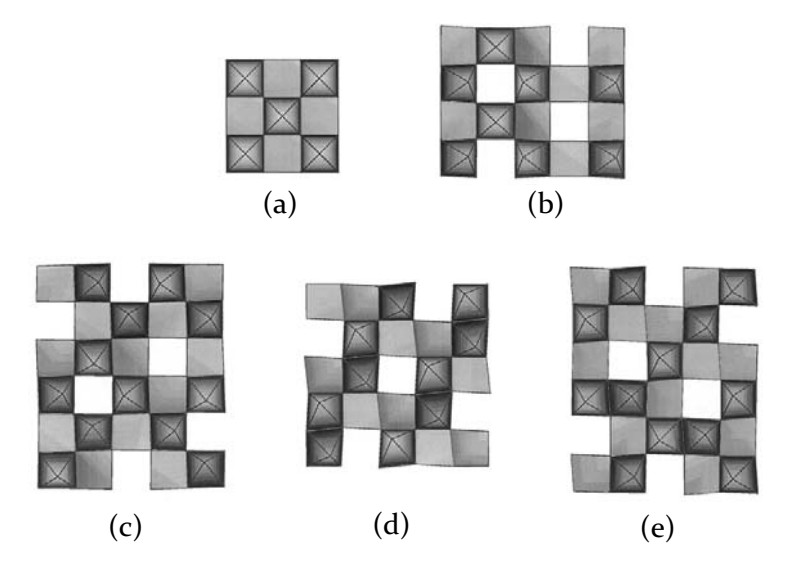


Figure 2.7 Chessboard-like layers built from basal-edges sharing SPs; (a) $2(\{ud\}^1|)$, (b) $2(\{udue\}^{-1}|)$, (c) $(\{ududedudue\}^7|)$, (d) $2(\{uddue\}^3|)$ and (e) $(\{uddueduude\}^8|)$ [17].

Table 2.3 The classification of SP+T class structures [17].

Structure symbols	Prototype	Vanadium oxide architectures Space g	roups
Subclass 1: U-T str	uctures, SPs are	separated units and joined into layer by sharing the	ir corners
		with Ts.	
(/U./ ₃ .2T.)	$K_3V_5O_{14}$	Triangle cycles of three SPs sharing their	P31M
		corners together. The cyclic units are further	
		linked into layer by sharing the remaining	
		corners of the base with isolated Ts.	
2(U./T./ ₄ .)	$Cs_2V_5O_{13}$	Cyclic tetramer of corner-sharing Ts. The	I4MM
		cycles share corners with isolated SPs to form	
		layer.	
(U.〈T.T›.)	$Rb_2V_3O_8$	Pyrovanadate groups $\langle V_2 O_{7^{\flat}}$ are linked into	P4bm
	$K_2V_3O_8$	layer via corner-sharing with isolated SPs.	P4bm
	$(NH_4)_2V_3O_8$		P4bm
	$(H_3O)_2V_3O_8$		P4bm
Subclass 2	: UD-T structure	s, ‹UD› dimers which are linked into layer by	
	sharing their co	orners with Ts and other dimers.	
(UD.2T)α	CsV ₂ O ₅	Oppositely directed SP dimers which are	P_{2_1}/c
		linked into layer by sharing corners with	
		separated Ts. Ts apexes alternate from row	
		to row.	
(UD.2T)α'	$Ca(V_2O_5)_2.5H$	(UD.2T) α layer with Ts apexes alternate	$P\overline{1}$
	$_{2}O$	along the row.	$P\overline{1}$
	$enH_2(V_2O_5)_2$		P21/n
	$(\text{prda})(\text{V}_2\text{O}_5)_2$		$P\overline{1}$
	$(\mathrm{ppd})(\mathrm{V_2O_5})_{\scriptscriptstyle{2}}$		
(UD.2T)β	$(\mathrm{ppd})(\mathrm{V_2O_5})_{\scriptscriptstyle{2}}$	The (UD) dimers are linked through	p21/n
		separated Ts. The dimers are rotated by 90°	
		to each other.	
({{ <uud>.}₂:</uud>	$(en_2Cu)_2(V_2O$	«UUD» and «DDU» trimers of edge-sharing	$P\bar{1}$
⟨T.T⟩}2T.)	₅) ₅	SPs share their corners to form { <uud>.}</uud>	
		chains. The chains are linked into layer	
		through Ts. Half of the Ts are coupled into	
		⟨V₂O ₇ ⟩ unit and share four corners to link	
		two chains into double chain. The double	
		chains are then linked into layer via	
		separated Ts.	

Table 2.3 The classification of SP+T class structures [17]. (continued)

Structure symbols	s Prototype	Vanadium oxide architectures Space	ce groups
({{ <uud>.}₂:</uud>	$(en_{2}Cu)_{2}(V_{2}O_{5})_{5}$	«UUD» and «DDU» trimers of edge-	$P\overline{1}$
⟨T.T⟩}2T.)		sharing SPs share their corners to	
		form { <uud>.} chains. The chains</uud>	
		are linked into layer through Ts.	
		Half of the Ts are coupled into	
		$\langle V_2 O_7 \rangle$ unit and share four corners	
		to link two chains into double	
		chain. The double chains are then	
		linked into layer via separated Ts.	
({U∢UD>₄D.T.	$(tma)_{5}(V_2O_5)_{9}$	«UD» dimers, «UUD» trimers and	$P\bar{1}$
UDD.T.UD.T.}.)		(UUDUDUDUDD) groups are	
		linked into chain via corner-	
		sharing and separated Ts. The	
		chains are then linked into layer	
		through corner-sharing.	
Subclass 3: Z-T	structures, {UuDd} zig-	zag chains linked into layer by sharing corner.	s with Ts.
({UuDd}:T.)α	$(tma)V_3O_7$	{UuDd} chains are joined into layer by	p2 ₁
		separated Ts sharing two corners with	
		one chain and one corner with another	
		chain. Every chain within the layer is	
		uniformly oriented and Ts apexes	
		alternate along the row.	
({UuDd}:Τ*)α'	$(DABCO)V_6O_{14}.H_2O$	Similar to ({UuDd}:T.) α layer but the	p_{2_1}
		layer is wavily twisted.	
({UuDd}:T.)β	$(en)_2 ZnV_6O_{14}$	Similar to ({UuDd}:T.) α layer but SPs in	p_{2_1}/a
	$(en)_2 CuV_6O_{14}$	adjacent chains are not uniformly	p_{2_1}/a
		oriented. Ts apexes alternate along the	
		row.	
({UuDd}:T*.)β'	$(ma)V_3O_7$	Similar to ({UuDd}:T.) β layer but the	p_{2_1}/a
		layer is wavily twisted.	
({UuDd}:T.)γ	$(en)_2 NiV_6 O_{14}$	SPs in the neighboring $\{UuDd\}$ chains are	$pb2_{i}a$
		oppositely directed. Ts apexes alternate	
		every two Ts rows.	
({UuDd}:T.)δ	Hypothetical	Similar to ({UuDd}:T.) γ layer, but one	$p_{2_{1}2_{1}2}$
		SP shift is observed in adjacent chains.	

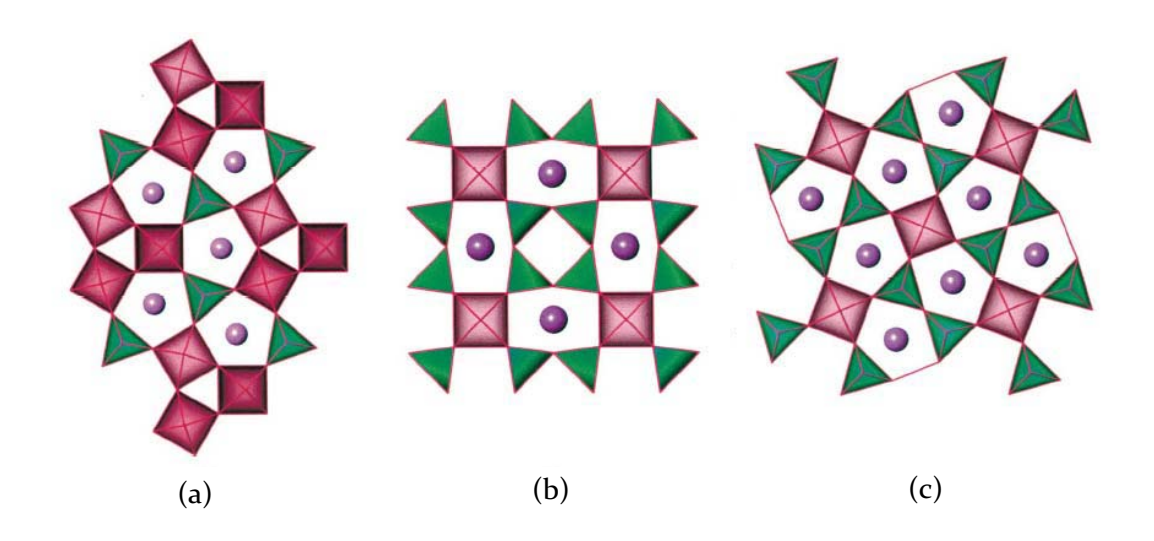


Figure 2.8 U-T layers constructed from separated SPs linked through separated Ts: (a) $(/U./_3.2T.)$, (b) $2(U./T./_4.)$ and (c) $(U.\langle T.T \rangle.)$ [17].

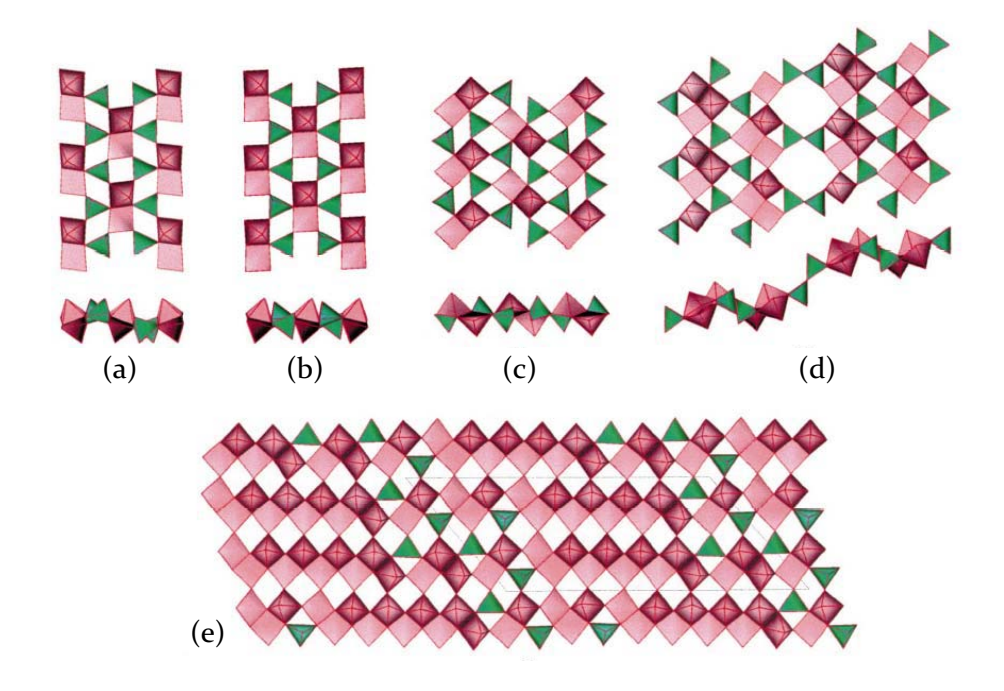


Figure 2.9 UD-T layers built up from $\langle UD \rangle$ dimers and Ts: (a) α-(UD.2T..), (b) α'-(UD.2T..), (c) β-(UD.2T..), (d) ({{ $\langle UUD \rangle .}_2:\langle T.T \rangle }..2T.)$ and (e) ({ $U\langle UD \rangle_4D.T.UDD.T.UD.T.$ }.) [17].

Class III. O Structures; the frameworks are built up from only Os in the form of quadruple chains. To clarify further descriptions of octahedra linkages, four corners of quadruple chain are marked as depicted in Figure 2.11. The frameworks in this class can be classified into three subclasses, *i.e.* Q, X and o structures.

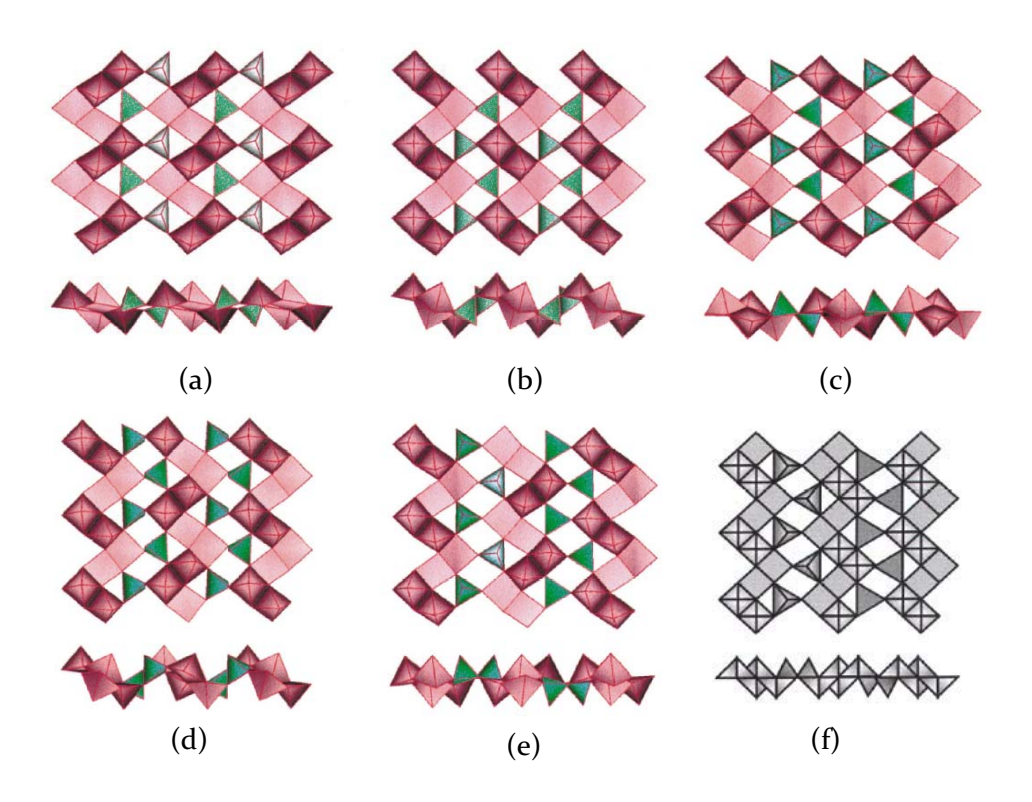


Figure 2.10 Z-T layers constructed from the linkage of {UuDd} chains through separated Ts: (a) ($\{UuDd\}:T.$) α , (b) ($\{UuDd\}:T^*$) α' , (c) ($\{UuDd\}:T.$) β , (d) $(\{UuDd\}:T^*)\beta',$ (e) $(\{UuDd\}:T.)\gamma$ and (f) hypothetical $(\{UuDd\}:T.)\delta$ [17].

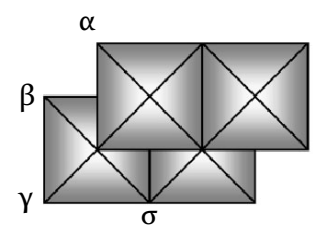


Figure 2.11 Numeration scheme of the shared corners in {Q} chain [17].

Table 2.4 The classification of O class structures [17].

Structure symbols	Prototype	Vanadium oxide architectures	Space groups
Subclass 1: Q structu	ures, the struct	ures are constructed from quadruple oc	tahedra {Q} chains.
{Q}	β-AgVO ₃	Single {Q} chain.	Ст
	$Ag_{\sim 3}V_4O_{\scriptscriptstyle 12}$		Cm
	β -SrV ₂ O ₆		Pcmn
	α -SrV ₂ O ₆		Pcmn
	PbV_2O_6		Pcmn

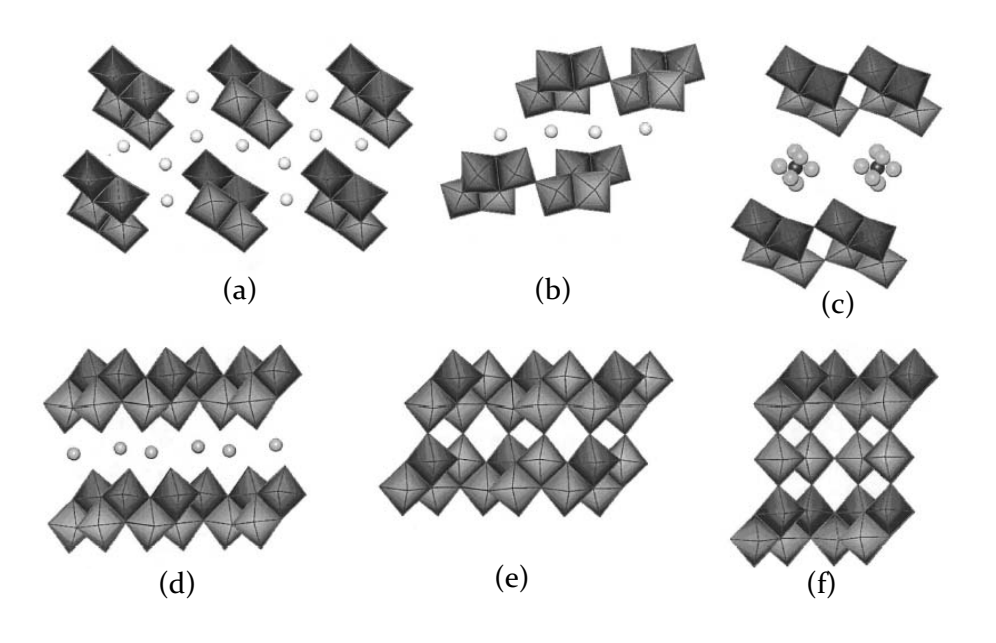
Table 2.4 The classification of O class structures [17]. (continued)

Structure symbols	Prototype	Vanadium oxide architectures	Space groups		
({Q}.)	$Ag_{1.92}V_4O_{11}$	{Q} chains are linked into layer	C2/m		
	$Cu_{\scriptscriptstyle 1.82}V_{\scriptscriptstyle 4}O_{\scriptscriptstyle 11}$	through β corner-sharing.	Cm		
({Q}:)	$(tma)V_8O_{20}$	{Q} chains are linked into layer	C2/m		
		through α and β corner-sharing.			
({Q})	δ -Na _{0.56} V ₂ O ₅	{Q} chains are linked into layer	C2/m		
	$\tau\text{-Na}_{o.64}V_{\scriptscriptstyle 2}O_{\scriptscriptstyle 5}$	through edge-sharing. The layers	C2/m		
	δ -Ag _{0.68} VO ₅	are separated by metal ions and	C2/m		
	ϵ -Cu _{o.828} V ₂ O ₅	water of crystallization.	C2/m		
	$\upsilon\text{-Ca}_{o.6}V_{2\text{-x}}O_5$		C2/m		
	$\delta\text{-}K_{o.486}V_{2}O_{5}$		C2/m		
	$Ti_{o.5}V_2O_5$		C2/m		
	$Ni_{0.25}V_2O_5.H_2O$		C2/m		
	$Ca_{0.25}V_2O_5.H_2O$		C2/m		
	$Ca_{0.72}V_2O_5.H_2O$		C2/m		
2({Q})	$\rho\text{-}K_{o.5}V_{\scriptscriptstyle 2}O_{\scriptscriptstyle 5}$		Ccmm		
[({Q}).]	VO_2	$({Q})$ layers are linked into 3D	C2/m		
		framework through corner-			
		sharing.			
[({Q}).({OO}.).]	V_6O_{13}	$({Q})$ layers are sandwiched	C2/m		
		with ({OO}.) layers through	P_{2_1}/a		
	$\text{Li}_{x}\text{V}_{6}\text{O}_{\scriptscriptstyle{13}}$	corner-sharing.	C2/m		
Subclass 2: X stru	ctures, the struct	ures are constructed from crossed quadru	ple {X} chains		
[({X}:):]	VO ₂	{X} chains are linked into 3D framework	P ₄₂ /ncm		
		via corner-sharing			
[({X}:):({OO}.):]	β - V_6O_{13}	{X} chains are linked into layer <i>via</i>	Cmma		
		corner-sharing. The layers are			
		sandwiched with ({OO}.) layer			
		through corner-sharing.			

Class IV. O+SP Structures; the frameworks are fabricated from the combination of Os and SPs, and can be categorized into two subclasses, *i.e.* Q-UD and O-UD structures.

Table 2.4 The classification of O class structures [17]. (continued)

Structure symbols	Prototype Va	nadium oxide architectures Spa	ce groups					
Subc	lass 3 : o and oo structu	res, the structures contain single {o} chains						
	and/or double {oo} chai	ns of opposite edge-sharing octahedra.						
[2{0}.]	}.] δ -VO ₂ Rutile structure formed by corner-sharing {o} chains.							
[2{oo}.] ^{1x2}	VO(OH)	Rutile structure constructed from {oo} double chains which are linked into 3D framework through corner-sharing with {o} chains, providing 1×2 tunnels.	Pbnm					
[4{00}.] ^{2x2}	$K_{2-x}V_8O_{16}$, $x = 0.2$ $Tl_{2-x}V_8O_{16}$, $x = 0.26$ $Bi_{2-x}V_8O_{16}$, $x = 0.38$	3D Hollandite structure constructed from corner-sharing {oo} double chains, providing large 2×2 tunnels.	I4/m					
	$Ba_{2-x}V_8O_{16}$, $x = 0.81$ $(Pb_{1.32}V_{0.35})V_8O_{16}$		I112/m					
({oo}.)	$H_6V_4O_{10}$	Layered structure formed from corner-sharing {oo} double chains	C2/m					
({oo}.{o}.)	$H_{10}V_6O_{16}$	Layered structure formed from alternating {o} and {oo} chains which are linked through corner-sharing.	C2/m					



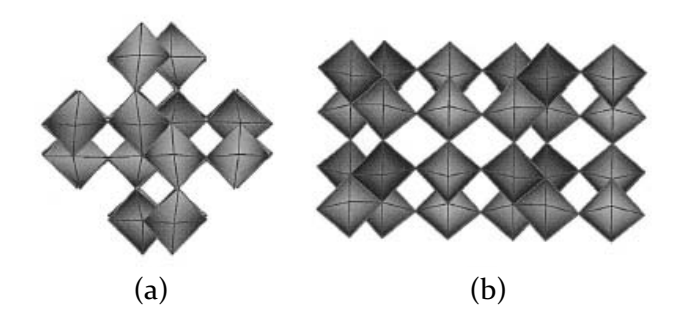


Figure 2.13 Three dimensional frameworks constructed from $\{X\}$ chains: (a) $[(\{X\}:):]$ and (b) [({X}:):({OO}.):] [17].

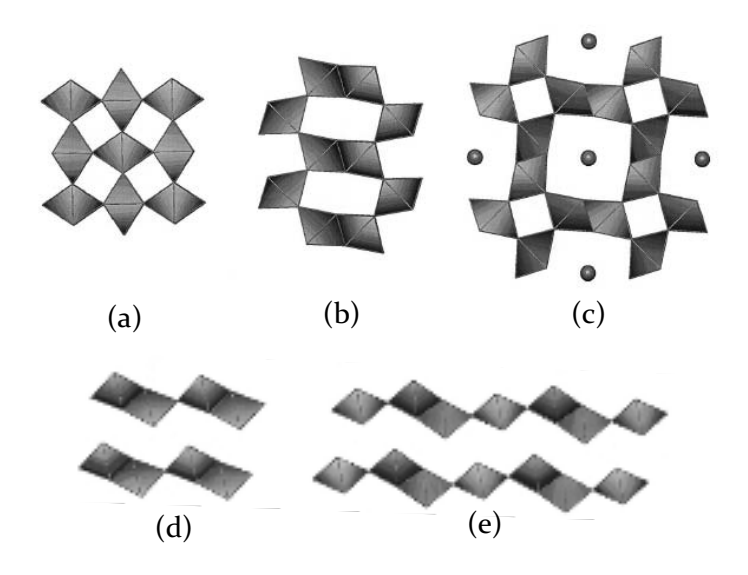


Figure 2.14 o and oo structures built up from the linkages of {o} and {oo} chains: (a) ${{\left[{2\{o\}.} \right]},\left(b \right)\left[{2\{oo\}.} \right]^{1\times 2},\left(c \right)\left[{4\{oo\}.} \right]^{2\times 2},\left(d \right)\left({\{oo\}.} \right) \text{ and }\left(e \right)\left({\{oo\}.\{o\}.} \right)\left[{17} \right].}$

Table 2.5 The classification of O+SP class structures [17].

Structural sy	tructural symbols Prot		Vanadium oxide architectures	Space groups				
Subclass 1: Q)-UD struc	tures, the structi	ares are constructed from quadruple octo	ahedra {Q} chains				
	and square pyramid {UD} chains.							
β({Q}.{UD}.)	Li _{1.2} V ₃ O ₈	Q} chain	s are linked into layer through β corner	$P2_1/m$				
		sharing w	rith {UD} chains. The layers are sandwis	shed by				
		Li⁺ ions.						
$\delta'(\{Q\}.\{UD\}.)$	V ₃ O ₇ .H ₂	O {Q} chain	is are linked into layer through δ corner	r- Pnma				
		sharing w	rith {UD} chains. The layered structure	is Pnma				
		stabilized	by H-bonds.					

Table 2.5 The classification of O+SP class structures [17]. (continued)

Structure symbo	ols Prototype	Vanadium oxide architectures Space	e groups
$\delta[(\{Q\} \{UD\}).$	$Ba_{o.4}V_3O_8$	{Q} chains are joined into layer via two	P_{2_1}/m
{UD}.]	$(VO)_{o.4}.H_2O$	corner-sharing. The layers are constructed	
		into 3D structure through corner-sharing	
		with {UD} chains.	
[{Q}.(.{UD}*)*]	V_4O_9	{UD} chains are joined into layer via corner-	Pnma
		sharing. The layers are linked into 3D	
		framework through corner-sharing with $\{Q\}$	
		chains.	
[({Q}.).{UD}.]	$\beta\text{-Ag}_{0.333}V_2O_5$	{Q} chains are jointed into layer via corner-	C2/m
	β -Cu _{0.55} V ₂ O ₅	sharing {UD} chains. The layers are linked	Cm
	$Na_{0.333}V_2O_5$	into 3D framework through corner-sharing	C2/m
	$Na_{0.287}V_2O_5$	with {UD} chains.	C2/m
	β -Li _{0.3} V ₂ O ₅		C2/m
	β '-Li _{0.48} V ₂ O ₅		C2/m
	$K_{0.33}V_2O_5$		C2/m
	$Cu_{0.261}V_2O_5$		C2/m
	$\beta - Pb_{0.333}V_2O_5$		C2/m
[({Q}:{Q}.).2{UD}.]	β -Li _x V ₁₂ O ₂₉ , x	[({Q}.).{UD}.] layers are joined into double	C2/m
	= 1.5, 2.1	layer through α and β corner sharing {Q}	C2/m
	$Cu_{x}V_{12}O_{29}, x =$	chains. The double layers are then linked into	
	1.2, 1.5, 1.7	3D framework <i>via</i> β corner-sharing {Q}	
	0	chains	
[({Q}:{Q}.{Q}.).		[({Q}.).{UD}.] double layers sandwished by a	P_{2_1}/m
3{UD}.]	= 1.2, 1.7	single (Q.UD) layer by sharing only β corners.	
Subclass 2:		the structures are constructed from {O} chains ar	ıd
((1120))		are pyramid {UD} chains.	·
({UDO}.)	,	Corner-sharing {O} chains which are linked	P_{2_1}/m
		into 3D network through edge-sharing with	P_{2_1}/m
	1 9	⟨UD⟩ dimers.	P_{2_1}/m
[[00]]	CsV ₃ O ₈	T	P_{2_1}/m
	,	Two types of Os, single {O} chains and edge-	C2/c
(O.}.{UD}*]		sharing pairs of O { <oo>:} are linked into 3D</oo>	
		network through corner-sharing with two	
		types of SPs chains, {UD} and {UU}.	

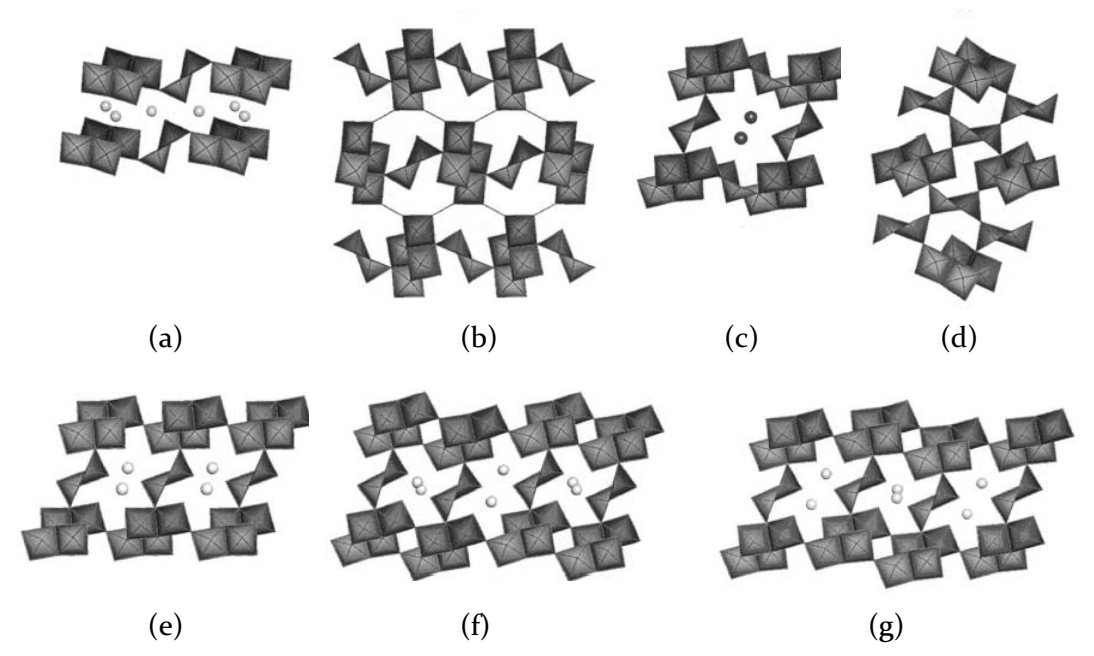


Figure 2.15 Q-UD structures fabricated from {Q} chains and {UD} chains: (a) $\beta(\{Q\}.\{UD\}.), (b) \ \delta'(\{Q\}.\{UD\}.), (c) \ \delta[(\{Q\}|\{UD\}|).\{UD\}.], (d) \ [\{Q\}.(.\{UD\}^*)^*], (e)$ $[(\{Q\}.).\{UD\}.], (f) \ [(\{Q\}:\{Q\}.).2\{UD\}.]) \ and \ (g) \ [(\{Q\}:\{Q\}.\{Q\}.).3\{UD\}.] \ [17].$

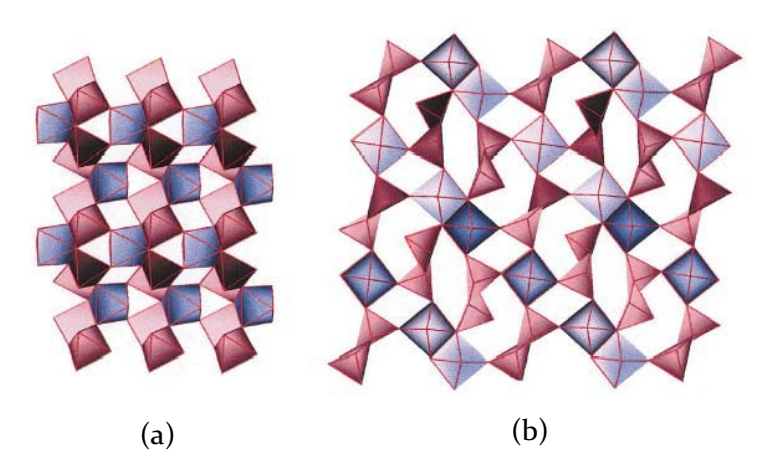


Figure 2.16 O-UD structures composing of Os and SPs chains or dimers: (a) ({UDO}.) and (b) [.{<OO>:}.2{UU}*{O.}.{UD}*] [17].

Class V. O+T Structures; the structures in this class are fabricated from the combination of Os and Ts. They can be subdivided into three subclasses, i.e. O-T, W-T and o-T structures.

Table 2.6 The classification of O+T class structures [17].

Structure symbols	Prototype	Vanadium oxide architectures	Space groups				
Subclass 1:	O-T structures	, the structures are built from separated Os and Ts.					
({O.}.T.)	Sr ₂ V ₃ O ₉	Chains of corner-sharing Os with Ts additional link each pair of Os	I2/a				
		along the chain. The chains are					
		then joined into 3D network					
		through separated Ts.					
(O.〈T.T.〉.)	BaV ₃ O ₈	Separated Os and V ₂ O ₇ groups	$P_{2_{j}}$				
(3.1.1)	24.30%	which are joined into double layer	121				
		by sharing corner with Os.					
(O.{2T.}.)	(phen)V ₃ O ₇	Chains of Ts which are linked into	P2/c				
(((),(=1,),)	(Pitell) 1307	double layer through corner-	1 = 7 0				
		sharing with Os					
Subclass 2: W-T stri	ictures, the stru	actures are constructed from wave-like o	ctahedral {W} chain				
({W}:T.)	NiV ₂ O ₆	{W} chains are linked into layer by	P1				
(()/	1111200	separated Ts with Ni atoms occupy	<i>T</i> 1				
		octahedral sites between the					
		layers.					
[({W}:T.).]	FeV ₂ O ₆ H _{0.5}	Similar to ($\{W\}$:T.) layer but $1/3$ of	$P_{2_1 2_1 2_1}$				
	2 0 0.9	V atoms are substituted with Fe					
		atoms to form 3D framework.					
[({W}:2T.).]	β-MgV ₃ O ₈	{W} chains are linked into layer by	C2/m				
	1 0 , 0	Ts <i>via</i> corner-sharing. The layers	·				
		are then jointed into 3D					
		framework through corner-					
		sharing. Half of the V atoms in					
		octahedral sites are substituted					
		with Mg atoms.					
(U {W}:T.)	σ-	{W} chains are linked into double	$P\overline{1}$				
•	$Zn_{0.25}V_2O_5$.	layer by Ts and SPs. The layers are	-				
	H ₂ O	separated by Zn ions and water of					
		crystallization.					

Table 2.6 The classification of O+T class structures [17]. (continued)

Structure symbols	Prototyp	e Vanadium oxide architectures Space groups						
Subclass 3: O-T struct	Subclass 3 : O-T structures, the structures are built up from layers of octahedral and separated Ts.							
((OoOee) ₂ T)	BaV ₇ O ₁₆ .n	Two sheets of edge-sharing O with two of P_{42}/m						
	H_2O	five octahedral sites are not occupied.						
		Four empty sites, two from each layer are						
		linked by separated Ts to form 3D						
		network.						

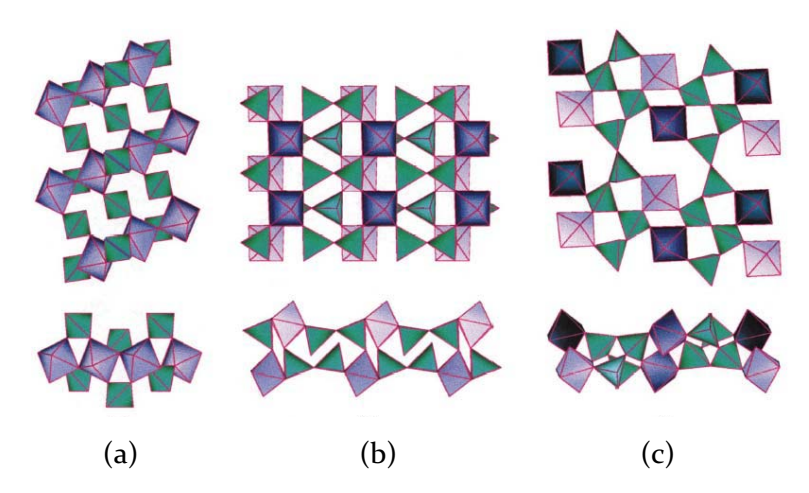


Figure 2.17 O-T structures constructed from the combination of Os and Ts: (a) $(\{O.\}.T.)$, (b) $(O.\langle T.T.\rangle.)$ and (c) $(O.\{2T.\}.)$ [17].

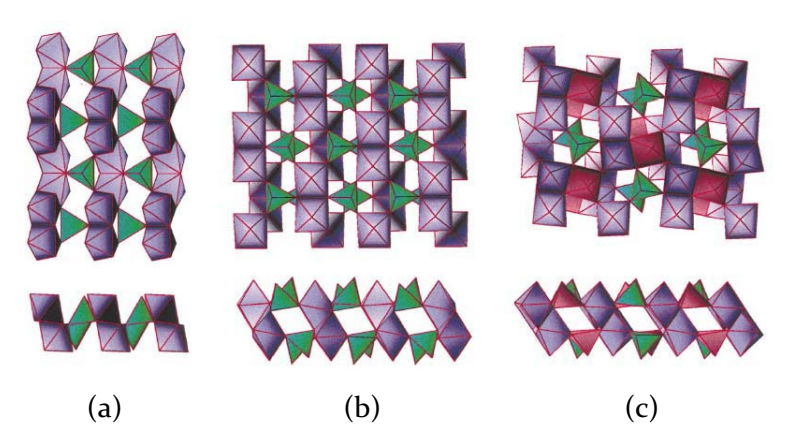


Figure 2.18 W-T layers built up from wave-like octahedral $\{W\}$ chains linked through Ts and SPs: (a) $(\{W\}:T.)$, (b) $[(\{W\}:2T.).]$ and (c) $(..U|\{W\}:T.)$ [17].

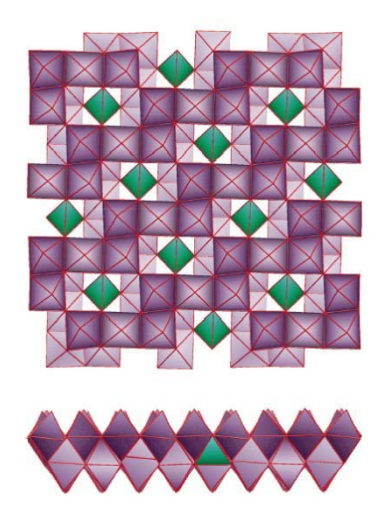


Figure 2.19 ((OoOee)₂..T..) octahedral double layer sheets with incorporated Ts [17].

As mention earlier, vanadium oxides exhibit a very wide range of chemical compositions and several types of architectures. Table 2.7 shows the relation between structure distribution and chemical compositions. The letters C, L and N shown in the table abbreviate one-dimensional chain, two-dimensional layer and threedimensional network, respectively.

Table 2.7 Structural types displayed by vanadium oxides with their chemical compositions [12].

			Stoichiometries and O:V ratios											
Class	Subclass	VO ₂	V ₆ O ₁₃	V_4O_9	V ₇ O ₁₆	V_3O_7	V ₁₂ O ₂₉	V_9O_{22}	V ₂ O ₅	V ₅ O ₁₃	V_3O_8	V ₄ O ₁₁	V ₅ O ₁₄	VO ₃
		2	2.17	2.25	2.29	2.33	2.42	2.44	2.5	2.6	2.67	2.75	2.8	3
SP+T	U-T			L						L	L		L	
	UD-T								L					
	Z-T					L								
SP	ud	L	L	L		L								С
	UD								L					С
	UD pipes					N			L					
O+T	O-T										L			L+C
	W-T	N							L					L
	oe-t				L									
O+SP	O-UD					N					L			
	Q-UD			N			N	N	N		L			
0	Q	N	N						L			L		C
	X	N	N											
	0	N							L		L			C

SURVEY ON COBALT-ORGANODIAMINE FRAMEWORKS

The IOH compounds of metal transitions, particularly the magnetic ions, *e.g.* cobalt (Co), nickel (Ni) and iron (Fe), with *trans*-diamines, *e.g.* ethylenediamine (en), 1,3-diaminopropane (1,3-dap), 1,4-diaminobutane (1,4-dab), 1,5-diaminopentane (1,5-dap), 1,6-diaminohexane (1,6-dah), 1,4-diazabicyclo[2.2.2]octane (DABCO) and 4,4'-bipyridine (4,4'-bipy), have been widely studied in the aspects of preparation and crystal structure characterization. According to the literature survey conducted on the following databases, *i.e.* American Chemical Society, Scifinder Scholar, Science direct, Blackwell Synergy and International Union of Crystallography, there are over 760 articles reported on the magnetic IOH compounds during 1958-2007. The numbers of the publications on these compounds have been generally increasing especially in the last decade, as shown in Figure 2.20. Among the studied diamines, it is distinct statistically that en has enjoyed its major enrollment, as shown in Figure 2.21. This may be due to the readily availability and inexpensive cost of en compared to the other diamines.

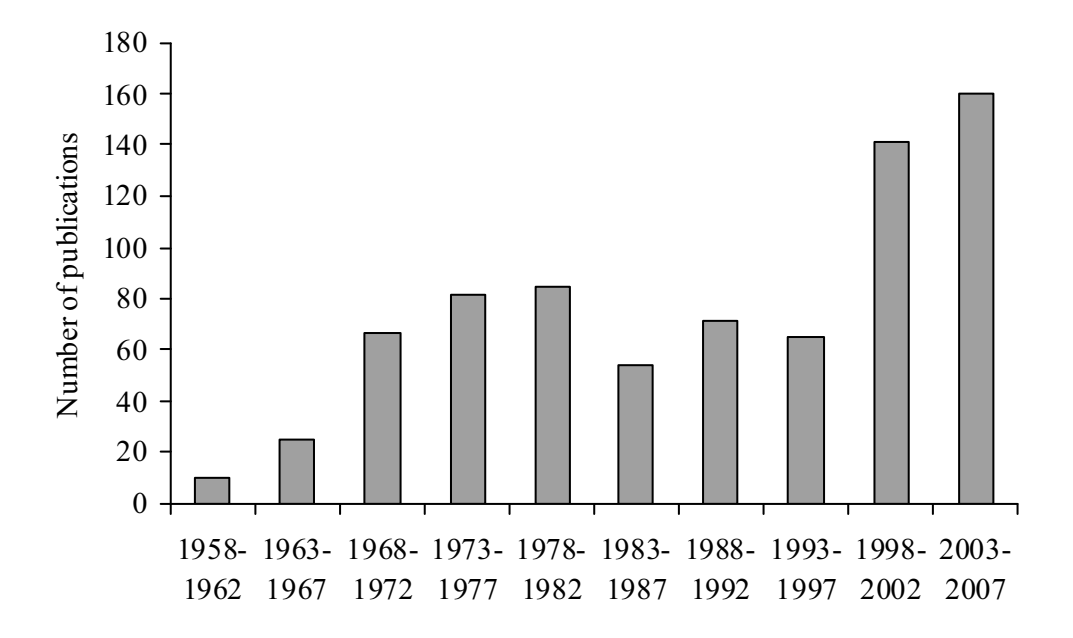


Figure 2.20 Numbers of publications on metal-diamine IOH compounds reported during 1958 to 2007 (metal = Co, Ni and Fe; diamine = en, 1,3-dap, 1,4-dab, 1,5-dap, 1,6-dah, DABCO and 4,4'-bipy).

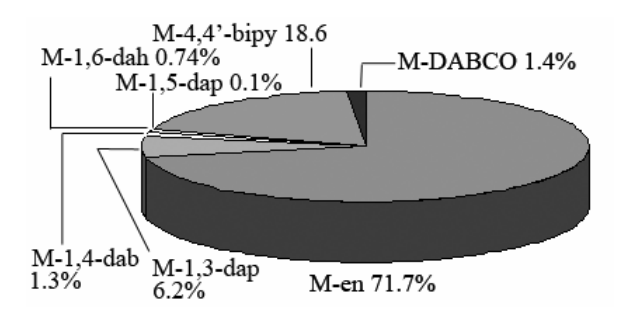


Figure 2.21 Percentages of publications on metal-diamine IOH compounds during 1958 to 2007 classified by type of the diamine molecules (M = Co, Ni and Fe).

The reported diamines plays various roles in the IOH structures, e.g. as a bridging ligand or linker, chelating ligand, monodentate ligand and uncoordinated guest (Figure 2.22). It can be noticed from that there are relation between the diamine functionalities with the IOH structures. Almost every diaminoalkanes show chelating effect in ligating to the metals, whereas the more rigid DABCO and 4,4'bipy favor a bridging role. This can be accounted for by structural flexibility of the formers and the steric hindrance and rigidity of the latters. This is however not the case for 1,6-dah, of which only the bridging role has been reported.

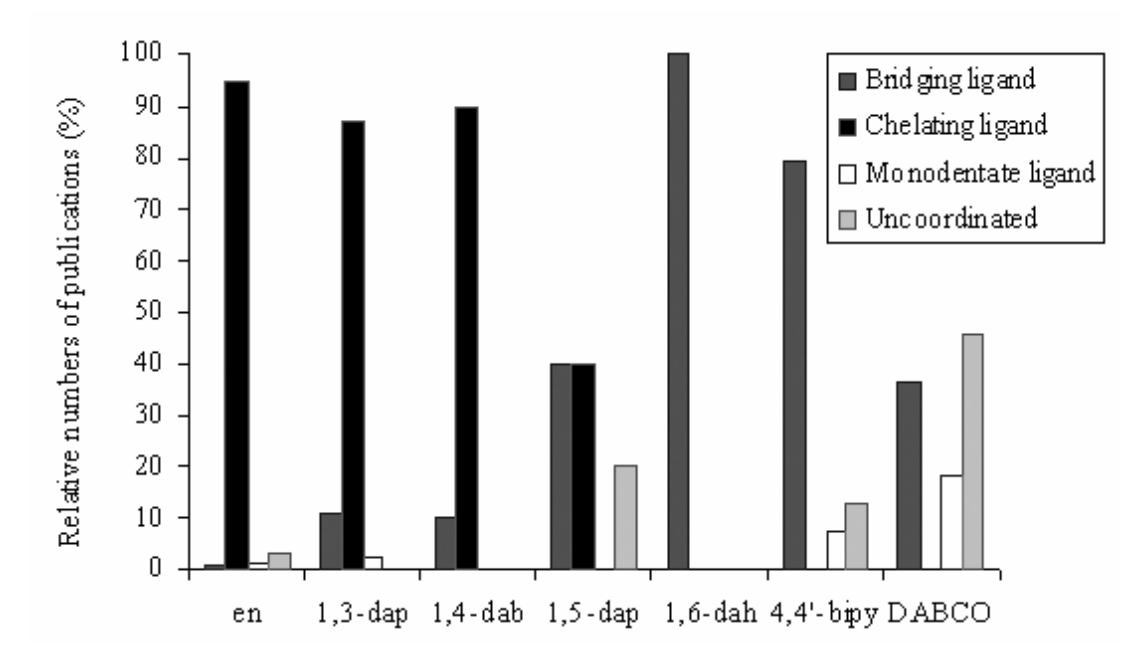


Figure 2.22 Percentages of metal-diamine IOH structures categorized by different roles of the diamines (metal = Co, Ni and Fe).

■ Cobalt-Organodiamine IOHs

Among the top three magnetic ions generally employed in the formation of the IOH materials - Co, Ni and Fe -, the most popular magnetic ion employed in the preparation of the IOH materials is Co (Figure 2.23), among which the en is also the most widely studied organic molecule (Figure 2.24). Figure 2.25 shows statistically the observed functionalities of the diamines in the Co-diamine IOH compounds.

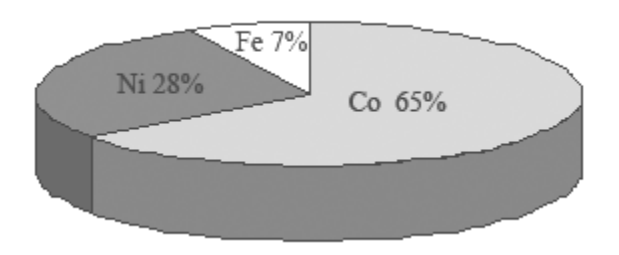


Figure 2.23 Relative numbers of publications on metal-diamines IOH compounds, classified by type of the magnetic ion.

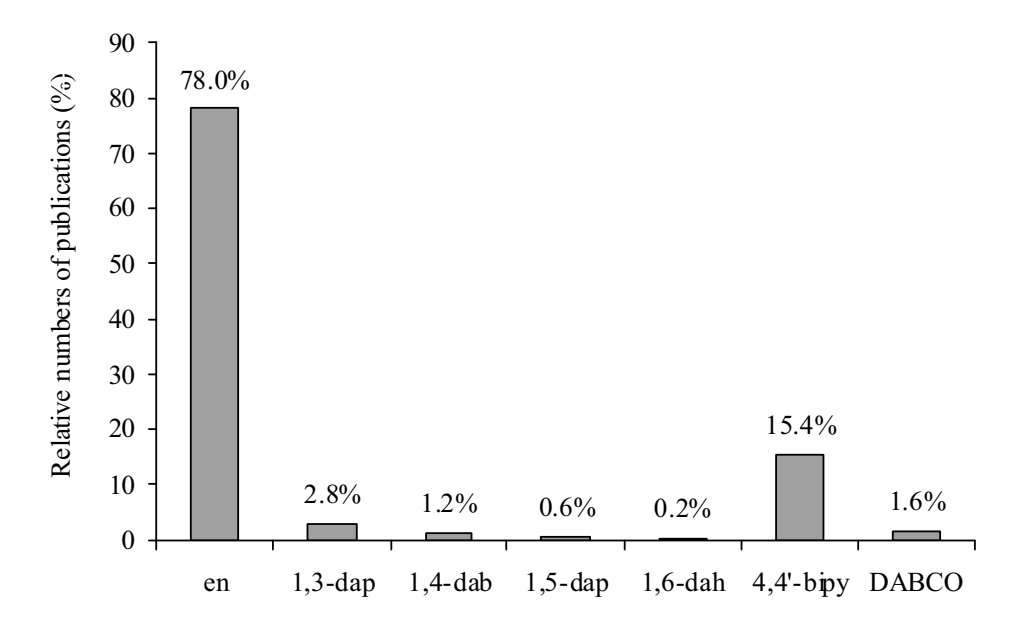


Figure 2.24 Relative numbers of publications on the Co-diamine IOH compounds grouped by different type of diamines.

Regarding the Co-diamine IOH compounds, it is rather intriguing to note that the Co^{III} compounds are over three times more abundant than the Co^{II} compounds (Figure 2.26). It is also apparent as shown in Figure 2.27 that most of the Co^{III} compounds are found with the diaminoalkanes, particularly with en acting as an organic component, e.g. $Co^{III}(en)_2(N_3)_2$]· $C_0H_{11}SO_3$ ·o.5 H_2O [18] and $[Co^{III}(C_3H_{10}N_2)_3]$ Cl₃·H₂O [19]. The Co^{II} compounds, on the other hand, are mostly found with more rigid diamine, *e.g.* $[Co^{II}(C_8H_4NO_2)_2(C_{10}H_8N_2)(H_2O)_2]$ [20], $[Co^{II}(C_5H_3N_2O_4)_2(H_2O)_2]$ · $C_{10}H_8N_2$ [21] and $[Co^{II}(C_8H_4O_4)(C_6H_{12}N_2)(H_2O)_2]$ · C_3H_7NO [22]. Reviews on these materials are already well documented [23,24].

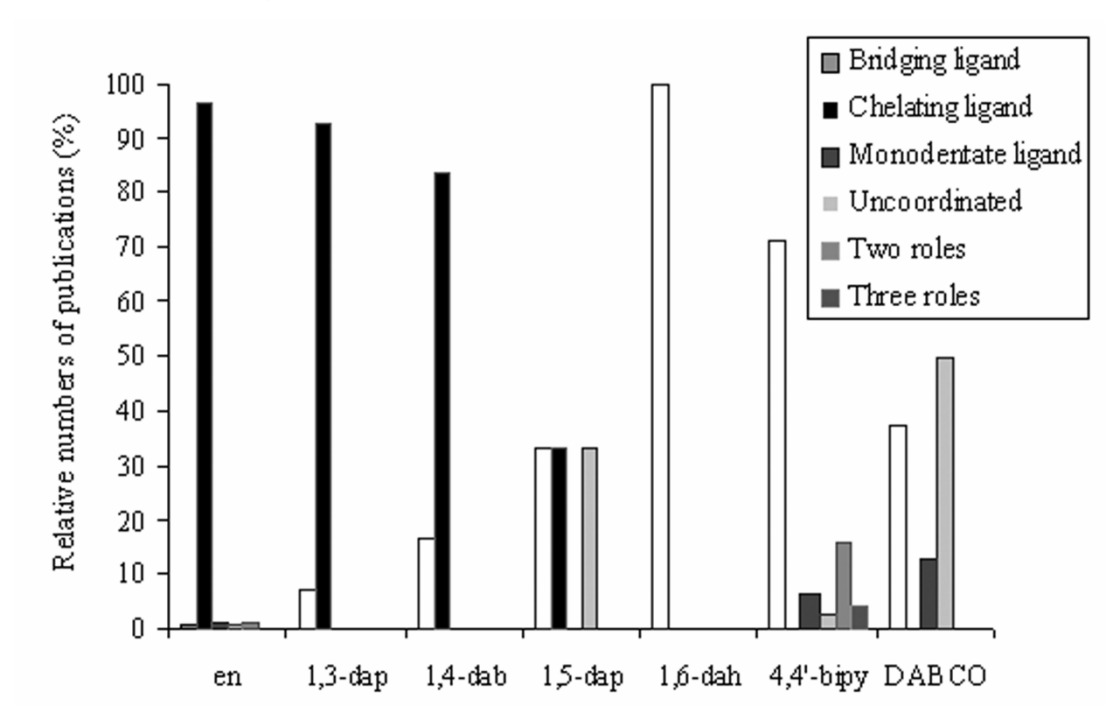


Figure 2.25 Relative numbers of the Co-diamine IOH compounds classified by different roles of the diamines.

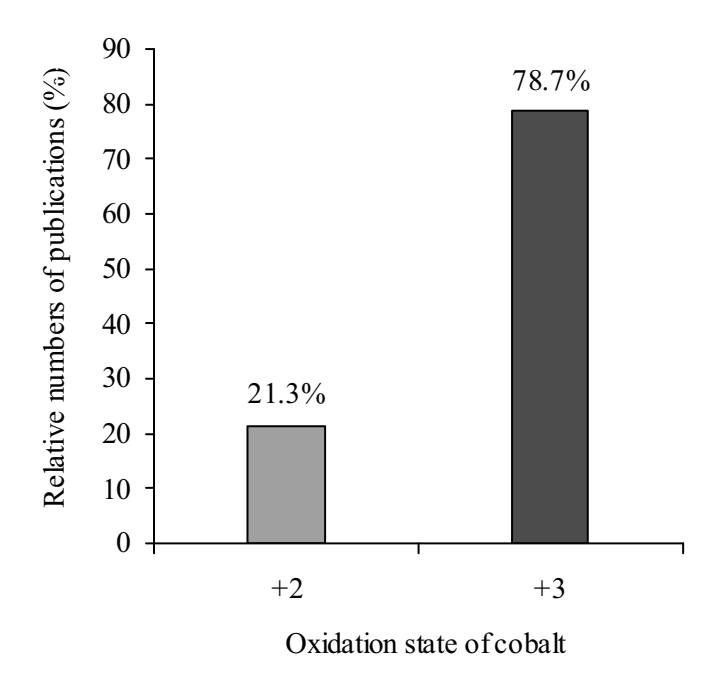


Figure 2.26 Comparison of the oxidation states of the Co present in the Co-diamine IOH compounds.

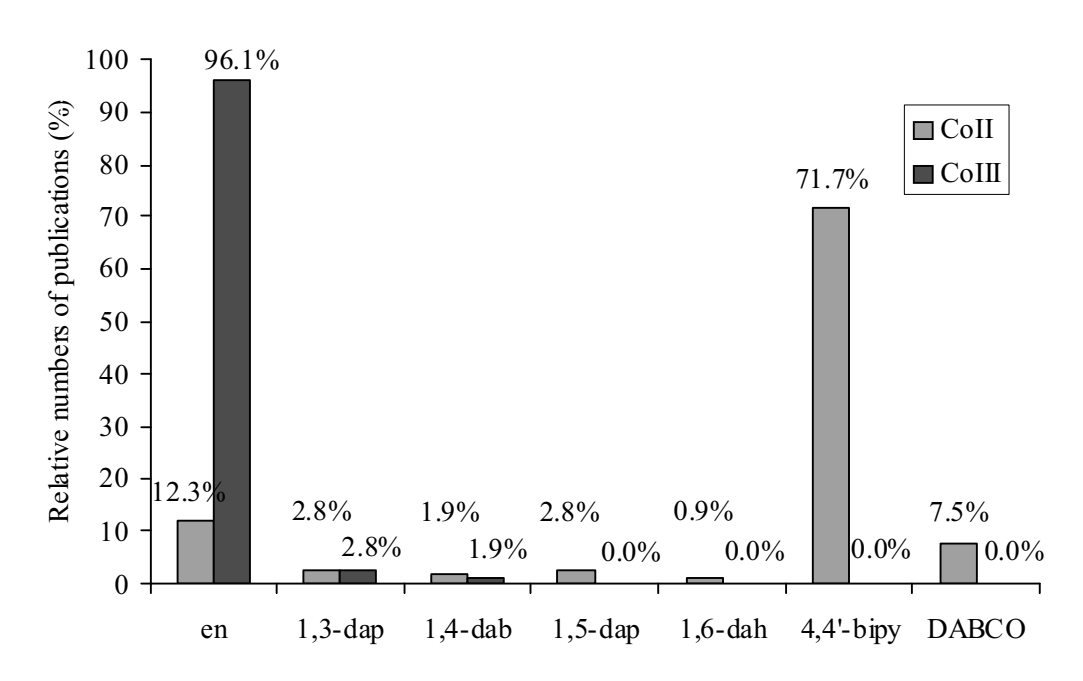


Figure 2.27 Number of publications showing relation between the oxidation states of Co and different roles of the diamines.

Beside the en, the symmetric 4,4'-bipy has also been widely used in the preparation of the IOH frameworks with Co metal ion. Table 2.8 lists typical examples of the Co-4,4'-bipy IOH compounds . The 4,4'-bipy commonly acts as either a bridging ligand, e.g. $[Co(4,4'-bipy)(SO_4)(H_2O)_3]\cdot 2H_2O$ [25], or concurrently as a bridging ligand and an uncoordinated guests in the same structure, e.g. [Co(4,4'bipy) $(H_2O)_4$] $(C_{10}H_8O_6)$ · o.5(4,4'-bipy)·2 H_2O [26]. The triple roles of being a bridging ligand, an uncoordinated guest and a monodentate ligand as found in, for examples, $(ClO_4)_2 \cdot 1.4(4,4'-bipy) \cdot 3(H_2O)$ $[Co(4,4'-bipy)_3(H_2O)_2],$ [27] and $[Co_2(4,4)^2]$ bipy) $_3(C_{10}H_8O_6)_2(H_2O)_6]\cdot(4,4'-bipy)\cdot7H_2O$ [28], are on the other hand rarely observed.

Table 2.8 Typical examples of Co-4,4'-bipy IOH materials.

	Roles of 4,4'-bipy						
Co-diamine derivative compounds	Bridging	Monodentate	Guests	Organizing forces	Network dimen- sionality	Metal coor- dination	Ref.
[Co ₂ (4,4'-bipy) ₃ (NO ₃) ₄]	•			Coordination H-bond	1D 3D	Oct	29
[Co(4,4'-bipy)(CH ₃ COO) ₂]	•			Coordination H-bond	1D 3D	Oct	30
[Co(4,4'-bipy)(DMSO) ₂ Cl ₂]	•			Coordination 3D	1D 3D	Oct	30
$[Co(4,4'-bipy)(C_4O_4)$ $(H_2O)_2]\cdot (H_2O)_3$	•			Coordination H-bond	2D 3D	Oct	31
$[Co(4,4'-bipy)(SO_4)$ $(H_2O)_3] \cdot 2H_2O$	•			Coordination H-bond	1D 3D	Oct	30
[Co(4,4'-bipy) (C ₈ H ₆ ClO ₃ S) ₂ (H ₂ O) ₂]	•			Coordination H-bond	1D 3D	Oct	32
[$Co(4,4'-bipy)$ ($C_9H_9O_2S)_2(H_2O)_2$]	•			Coordination H-bond	1D 3D	Oct	33
$[Co(4,4'-bipy)(H_2O)_4]$ $(C_4H_4O_4)\cdot 4H_2O$	•			Coordination H-bond	1D 3D	Oct	34
$[Co(4,4'-bipy)(H_2O)_4]$ $(C_9H_6O_5)\cdot H_2O$	•			Coordination H-bond	1D 3D	Oct	35
[Co(4,4'-bipy)(SO ₄) (H ₂ O) ₃]·C ₂ H ₆ O ₂	•			Coordination H-bond	1D 3D	Oct	36
$[Co(4,4'-bipy)(H_2O)_4]$ $(C_8H_4O_4)\cdot 2H_2O$	•			Coordination H-bond	1D 3D	Oct	37
$[Co(4,4'-bipy)_2(NO_3)_2]$ ·2 PNA	•			Coordination H-bond	2D 3D	Oct	38
$[Co_2(4,4'-bipy)_2(C_8H_4NO_2)_4]$ ·2H ₂ O·4C ₃ H ₇ NO	•			Coordination H-bond	1D 3D	Oct	39
[Co(4,4'-bipy) ($C_{10}H_8O_6$)($H_2O)_2$]	•			Coordination H-bond	2D 3D	Oct	40
[Co(4,4'-bipy) ($C_8H_4NO_2$) ₂ (H_2O) ₂]	•			Coordination H-bond	2D 3D	Oct	20
[Co(4,4'-bipy) ($C_9H_7O_5$) ₂ (H_2O) ₂]·2 H_2O	•			Coordination H-bond	2D 3D	Oct	41
[Co ₂ (4,4'-bipy) (C ₇ H ₃ NO ₄) ₂ (H ₂ O) ₆]·2H ₂ O	•			Coordination H-bond	2D 3D	Oct	42
[Co(4,4'-bipy) ₂ (C ₉ H ₇ O ₅) ₂ (H ₂ O) ₂]·4H ₂ O	•			Coordination H-bond	2D 3D	Oct	43
$[Co_2(4,4'-bipy)_2$ $(C_{16}H_8O_8)_2(H_2O)_2]\cdot 4H_2O$	•			Coordination H-bond	2D 3D	Oct	44

Table 2.8 Typical examples of Co-4,4'-bipy IOH materials. (*continued*)

		oles o 4'-bip	_				
Co-diamine derivative compounds	Bridging	Monodentate	Guests	Organizing forces	Network dimen- sionality	Metal coor- dination	Ref
$[Co(4,4'-bipy)_2 (C_{16}H_8O_8)]$		•		Coordination H-bond	1D 3D	Oct	45
$[Co(4,4'-bipy)_2(H_2O)_4]$ $(C_{10}H_8NO_3S)_2\cdot 6H_2O$		•		Coordination H-bond and π - π stacking	1D 3D	Oct	46
$[Co(C_5H_3N_2O_4)_2(H_2O)_2]$ ·4,4'-bipy			•	Coordination H-bond and π - π stacking	1D 3D	Oct	21
$(C_{10}H_{10}N_2)[Co(H_2O)_6]$ $(SO_4)_2$			•	Coordination H-bond	oD 3D	Oct	47
$\begin{aligned} & [Co(4,4'\text{-bipy})(H_2O)_4] \\ & (C_{10}H_8O_6)\cdot o.5(4,4'\text{-bipy})\cdot 2H_2O \end{aligned}$	•		•	Coordination H-bond and π - π stacking	1D 3D	Oct	48
$ \begin{array}{l} [\text{Co}(4,4'\text{-bipy}) \\ (\text{H}_2\text{O})_2(\text{C}_6\text{H}_3\text{OH}(\text{COO})_2)] \cdot (4,4'\text{-bipy}) \cdot (\text{CH}_3)_2\text{SO} \end{array} $	•		•	Coordination H-bond and π - π stacking	1D 3D	Oct	49
$[Co(4,4'-bipy)_3(H_2O)_2]$ $(ClO_4)_2\cdot 1.4 (4,4'-bipy)\cdot 3H_2O$	•	•	•	Coordination H-bond and π - π stacking	1D 3D	Oct	50
$[Co_2(4,4'-bipy)_3(C_{10}H_8O_6)_2$ $(H_2O)_6]\cdot(4,4'-bipy)\cdot7H_2O$	•	•	•	Coordination H-bond and π-π stacking	1D 3D	Oct	51
$[Co_3(4,4'-bipy)_4 (C_9H_3 O_6)_2(H_2O)_{10}]\cdot (4,4'-bipy)\cdot 8H_2O$	•	•	•	Coordination H-bond and π - π stacking	1D 3D	Oct	52

The influences of the organic molecules on the framework dimensionality crucially depend on the function of the organic component. It is apparent that the introduction of small changes to the organic molecular structure can lead to profound effect on the final framework topology obtained under similar reaction conditions. This is due to the fact that the structural information exerting from the organic molecule can be read by the inorganic parts via various organizing forces, e.g. coordinate covalent bond, hydrogen bonds and π - π interactions. The organic molecule therefore acts as the so-called "template" or "structure directing agent",

although the role of being a template is not completely understood. The influences of the diamine chain length and functionalities on the final IOH topology are exemplified in Table 2.9. Two trends can be observed. First, the structures of the frameworks are evolved as the diamine chain lengths are increased. Second, the formation of high dimensional structure, particularly the three dimensional, is distinctively pronounced when the organic molecule plays a bridging role. In addition to these commonly used diamines, cyclic diamine *e.g.* DABCO is also the favored cyclic organic template. The typical Co-DABCO IOH compounds are listed in Table 2.10, in which the bridging function of DABCO becomes more pronounced with increasing framework dimensionality.

According to the examples listed in Table 2.9 and Table 2.10, the coordination environment of Co ion shows no relation to type of the diamine compounds, and a variety of network topologies can be accessed by exploiting a variety of coordination geometries adopted by Co ion. A wide variety of structural architectures including adamantoid, cubic, ladder, honeycomb, helical staircase and brick-wall structures, as examples, have been reported. Although the overall structural topology is predominantly controlled by the organic building unit and the coordination preference of the transition metal ion, more subtle effects, *e.g.* ligand functionalities and counter ions, can have a profound effect upon network topology. For instance, increasing ability of the ligands to form π - π interactions does encourage the construction of longer-range arrays on the solid-state packing of chains from a simple linear chains of $[Co(4,4'-bipy)(SO_4)(H_2O)_3]\cdot 2H_2O$ [25], to a two dimensional sheets of $[Co(4,4'-bipy)_2(C_9H_7O_5)_2(H_2O)_2]\cdot 4H_2O$ [43], and to a pseudo-three dimensional $[Co(4,4'-bipy)_3(H_2O)_2](ClO_4)_2\cdot 1.4(4,4'-bipy)\cdot 3H_2O$ [50]. The higher dimensional networks are evolved by the increasing of the connecting units or forces.

A development of the IOH architectures can alternatively be made by modification of synthetic techniques and/or conditions, *e.g.* pH, solvent, and temperature, instead of the application of new organic feature. Three one-dimensional coordination polymers, namely $Co(SO_4)(H_2O)_3(4,4'-bipy)\cdot 2H_2O$, $CoCl_2(DMSO)_2(4,4'-bipy)$ and $Co(CH_3COO)_2(4,4'-bipy)$ (Figure 2.28), were obtained from the reactions using only different Co precursors, *i.e.* $CoSO_4$, $CoCl_2$ and $Co(CH_3COO)_2$ in different solvent system, *i.e.* water/ethanol, water/DMSO and water/acetonitrile, respectively [30].

Table 2.9 Examples of Co-diaminoalkanes IOH materials.

		Ro	les of noalkar	nes		Network	Metal	
Co-diamine compounds	bridging	Chelating	Monodentate	Guests	Organizing forces	dimen- sionality	coor- dination	Ref.
[cis-Co(en) ₂ (N ₃) ₂]C ₉ H ₁₁ SO ₃ ·o.5H ₂ O		•			coordination	oD	Oct	18
$[Co(C_3H_{10N_2})_3]Cl_3\!\cdot\!H_2O$		•			coordination	oD	Oct	19
[CoCl(en) ₂ (enH)]Cl(ZnCl ₄)		•	•		coordination	oD	Oct	53
cis-[Co(en) ₂ (enH)(imH)]Br ₄		•	•		coordination	oD	Oct	54
[Co(NH ₃) ₅ (enH)]Cl ₄			•		coordination	oD	Oct	54
$[Co(C_4H_7N_2O_2)_2(enH)_2][Co(C_4H_6N_2O_2)Cl_2(C_4H_8N_2O_2)]Cl_2\cdot o.75H_2O$			•		coordination	oD	Oct	55
[Co(benzeneseleninato) ₂ (en) ₃]			•		coordination	oD	Tbp	56
[Co(NH ₃) ₅ (en)]Br ₃			•		coordination	oD	Oct	57
cis-[Co(en) ₂ (enH)Cl]Cl ₃ . H ₂ O			•		coordination	oD	Oct	58
enH ₂ [Co(H ₂ O) ₆](HPO ₄) ₂				•	coordination	oD	Oct	59
$(enH_{2})_{0.5(1-x)}\cdot Al_{x}Co_{1-x}PO_{4}(x\approx 0.15)$				•	coordination	2 D	Tet	60
rac-μ-en[cis-CoCl(en) ₂] ₂	•	•			coordination	ıD	Oct	53
$(ZnCl_4)_2$ $[H_2N(CH_2)_2NH_2]_{0.5}$ ·CoSeO ₃	•				coordination	3D	Tet	61
Co ₄ (SO ₄)(OH) ₆ (en) _{0.5} ·3H ₂ O	•				coordination	3D	Oct & Tet	62
CoCd(NCSe) ₄ ·4en	•				coordination	3D	Sq. pl	63
CoZn(NCSe) ₄ .4en	•				coordination	3D	Sq. pl	63
$[\operatorname{Co}(\operatorname{C_3N_2H_8})(\operatorname{SO_4})]$	•				coordination	3D	Oct	64
$[Co(C_4N_2H_{10})(SO_4)]$	•				coordination	3D	Oct	64
$[Co(C_5N_2H_{12})(SO_4)]$	•				coordination	3D	Oct	64
$[\operatorname{Co}(\operatorname{C}_6\operatorname{N}_2\operatorname{H}_{14})(\operatorname{SO}_4)]$	•				coordination	3D	Oct	64

Table 2.10 Examples for Co-DABCO IOH materials.

	Roles of dia	mine					
Metal-amine derivative compounds	Bridging Monodentate	Guests	Organizing forces	Network dimen- sionality	Metal coor- dination	Ref.	
$[Co(C_8H_4O_4)(DABCO)$ $(H_2O)_2] \cdot C_3H_7NO$	•		Coordination H-bond	1D 3D	Oct	22	
[Co(1,4-benzene dicarboxylate)(DABCO) _{0.5}]	•		Coordination H-bond	3D	Oct	65	
$Co_4(SO_4)(OH)_6(DABCO)_{0.5}$ $\cdot H_2O$	•		Coordination H-bond	3D	Oct , Tet	66	
[CoCl ₃ (HDABCO) (DABCO)]	•		Coordination H-bond	oD 1D,3D	Tbp	67	
$(H_2DABCO)[Co(H_2O)_6]$ $(SO_4)_2$		•	Coordination H-bond	oD 1D,3D	Oct	68	
(H₂DABCO)[CoCl₄]		•	Coordination H-bond	oD 1D,3D	Tet	69	
$(H_2DABCO)[Co_2(HPO_4)_3]$		•	Coordination H-bond	oD 3D	Tet	70	
(a) (b) C8 SC7 C1 C1 C1 C1 C1 C1 C2							
(c) C14 O3C C13 O1C C0 O2C C11 O2C							

Figure 2.28 (a) View of the infinite linear chain of $Co(H_2O)_3(4,4'-bipy)SO_4\cdot 2H_2O$ (1) and (b) $Co(DMSO)_2(4,4'-bipy)Cl_2$ (2), compared to (c) the infinite double chain of $Co(4,4'-bipy)(CH_3COO)_2$ (3) [30].

REFERENCES

- [1] H.R. Godwin, B. Hoffan, K. Bowman-James, The Frontiers of Inorganic Chemistry, National Science Foundation, Colorado (2001).
- [2] P. Gomes-Romero, C. Sanchez, Functional Hybrid Materials, Wiley-VCH Verlag GmbH & Co. KGaA (2004).
- [3] P. Yang, The Chemistry of Nanostructured Materials: Crystalline Microporous and Open Framework Materials, Berkeley, California (2003).
- [4] A.Y. Robin, K.M. Fromm, Coord. Chem. Rev. 250 (2006) 2127.
- [5] K. Eller, E. Henkes, R. Rossbacher, H. Höke, "Amines, Aliphatic" in Ullmann's Encyclopedia of Industrial Chemitry, Wiley-VCH Verlag, Weinheim (2005).
- [6] Sigma-Aldrich Co., Material Safety Data Sheet, Sigma-Aldrich, Germany (2007).
- [7] M. Bohnet, C.J. Brinker, B. Cornils, Ullmann's Encyclopedia of Industrial Chemistry, 7th ed., Wiley and Sons, Inc., New York (2006).
- [8] International Labour Organization, International Occupational Safety and Health Information Centre (CIS) (1998).
- [9] T.L. Ho, Synthesis (1972) 702.
- [10] N.N. Greenwood, A. Earnshaw, Chemistry of the Elements, 2nd edn., Elsevier Butterworth-Heinemann, Oxford (2003).
- [11] P.J. Hargman, R.C. Finn, J. Zubieta, Solid State Sci. 3 (2001) 745.
- [12] M. Schindler, F.C. Hawthorne, W.H. Baur, Chem. Mater. 12 (2000) 1248.
- [13] D. Shriver, P. Atkins, Inorganic Chemistry, 3rd edn., W.H. Freeman and Company, New York (1999).
- [14] Y.-G. Li, Y. Lu, G.-Y. Luan, E.-B. Wang, Y.-B. Wang, Y.-B. Duan, C.-W. Hu, N.-H. Hu, H.-Q. Jia, *Polyhedron* 21 (2002) 2601.
- [15] A.S.J. Wery, J.M. Gutierres-zorrilla, A. Luque, M. Ugalde, P. Roman, *Chem. Mater.* 8 (1996) 408.
- [16] Y. Zhang, R.C. Haushalter, A. Clearfield, Inorg. Chem. 5 (1996) 4950.
- [17] P.Y. Zavalji, M.S. Whittingham, Acta Crystallogr. B55 (1999) 627.
- [18] R.P. Sharma, R. Sharma, R. Bala, K.N. Singh, L. Pretto, V. Ferretti, *J. Mol. Struct.* 784 (2006) 109.
- [19] R. Nagao, F. Marumo, Y. Saito, *Acta Cryst. B*29 (1973) 2438.
- [20] H.-Y. He, A.-Q. Ma, L.-G. Zhu, Acta Cryst. E59 (2003) 333.
- [21] Y.-L. Wang, R. Cao, W.-H. Bi, Acta Cryst. C60 (2004) 609.

- [22] A.-Q. Ma, Acta Cryst. E63 (2007) 1073.
- [23] H.W. Roesky, M. Andruh, Coord. Chem. Rev. 236 (2003) 91.
- [24] A.J. Blake, N.R. Champness, P. Hubberstey, W.-S. Li, M.A. Withersby, M. Schröder, *Coord. Chem. Rev.* 183 (1999) 117.
- [25] J. Lu, C. Yu, T. Niu, T. Paliwala, G. Crisci, F. Somosa, A.J. Jacobson, *Inorg. Chem.* 37 (1998) 4637.
- [26] J.-S. Gao, G.-F. Hou, Y.-H. Yu, Y.-J. Hou, P.-F. Yan, Acta Cryst. E62 (2006) 2913.
- [27] J.D. Woodward, R. Backov, K.A. Abboud, H. Ohnuki, M.W. Meisel and D.R. Talham, *Polyhedron* 22 (2003) 2821.
- [28] S. Gao, J.-W. Liu, L.-H. Huo, H. Zhao, S.W. Ng, Acta Cryst. E60 (2004) 1590.
- [29] P. Losier, M.J. Zaworotko, Angew. Chem. Int. Ed. 108 (1996) 2957.
- [30] J. Lu, C. Yu, T. Niu, T. Paliwala, G. Crisci, F. Somosa, A.J. Jacobson, *Inorg. Chem.* 37 (1998) 4637.
- [31] J. Greve, I. Jeß, C. Näther, J. Solid State Chem. 175 (2003) 328.
- [32] Y.-J. Hou, Y.-H. Yu, Z.-Z. Sun, B.-Y. Li, G.-F. Hou, Acta Cryst. E63 (2007) 1560.
- [33] X.-Y. Zheng, H. Su, Y.-L. Feng, *Acta Cryst. E62* (2006) 1393.
- [34] S.-M. Ying, J.-G. Mao, Y.-Q. Sun, H.-Y. Zeng, Z.-C. Dong, *Polyhedron* 22 (2003) 3097.
- [35] J.-G. Zhao, C.-S. Gu, S. Gao, L.-H. Huo, J.-W. Liu, Acta Cryst. E61 (2005) 33.
- [36] W.-J. Lu, Y.-M. Zhu, K.-L. Zhong, Acta Cryst. C62 (2006) 448.
- [37] C.-Z. Xie, B.-F. Zhang, X.-Q. Wang, G.-Q. Shen, D.-Z. Shen, *Acta Cryst. E60* (2004) 1703.
- [38] B. Moulton, E.B. Rather, M.J. Zaworotko, *Cryst. Eng.* 4 (2001) 309.
- [39] H.-Y. He, L.-G. Zhu, S. W. Ng, Acta Cryst. E61 (2005) 311.
- [40] Y.-M. Dai, E. Tang, Z.-J. Li, Y.-G. Yao, Acta Cryst. C61 (2005) 61.
- [41] J.-S. Gao, G.-F. Hou, Y.-H. Yu, Y.-J. Hou, G.-M. Li, Acta Cryst. E62 (2006) 2685.
- [42] X.-M. Zhang, Acta Cryst. E61 (2005) 1332.
- [43] Z.-P. Deng, S. Gao, L.-H. Huo, J.-G. Zhao, *Acta Cryst. E*61 (2005) 2550.
- [44] J.-Y. Xu, D. S. Contreras, F. R. Fronczek, B. Chen, Acta Cryst. E62 (2006) 1906.
- [45] C. Qin, X.-L. Wang, E.-B. Wang, Acta Cryst. E63 (2007) 3073.
- [46] M.-J. Wu, P.-X. Dai, X.-G. Wang, E.-C. Yang, X.-J. Zhao, *Acta Cryst. E*63 (2007) 2413.
- [47] X.-H. Li, Q. Miao, H.-P. Xiao, M.-L. Hu, Acta Cryst. E60 (2004) 1784.
- [48] J.-S. Gao, G.-F. Hou, Y.-H. Yu, Y.-J. Hou, P.-F. Yan, Acta Cryst. E62 (2006) 2913.

- [49] H.-Y. He, Y.-L. Zhou, L.-G. Zhu, Zeitschrift fuer Kristallographie New Crystal Structures 220 (2005) 445.
- [50] J.D. Woodward, R. Backov, K.A. Abboud, H. Ohnuki, M.W. Meisel, D.R. Talham, Polyhedron 22 (2003) 2821.
- S. Gao, J.-W. Liu, L.-H. Huo, H. Zhao, S. W. Ng, Acta Cryst. E60 (2004) 1590.
- [52] X. H. Zhen, L.Z. Feng, Z.Y. Qing, *Acta Cryst.* C63 (2007) 30.
- [53] D.A. House, P.J. Steel, *Inorg. Chim. Acta* 288 (1999) 53.
- [54] R.L. Fanshawe, A. Mobinikhaledi, C.R. Clark, A.G. Blackman, Inorg. Chim. Acta 307 (2000) 26.
- [55] X.-J. Shen, L.-P. Xiao, R.-R. Xu, *Acta Cryst. E6*1 (2005) 1185.
- [56] C. Preti, G. Tosi, P. Zannini, *Transition Metal Chemistry* 6 (1977) 232.
- [57] H. Ogino, N.Tanaka, Chem. Lett. 7 (1975) 687.
- [58] M.D. Alexander, C.A. Spillert, *Inorg. Chem.* 9 (1970) 2344.
- [59] Y. Shan, S. D. Huang, *Acta Cryst. C*55 (1999) 921.
- [60] X. Bu, P. Feng, T.E. Gier, G.D. Stucky, J. Solid State Chem. 136 (1998) 210.
- [61] D. Xiao, H. An, E. Wang, C. Sun, L. Xu, J. Coord. Chem. 59 (2006) 395.
- [62] A. Rujiwatra, C.J. Kepert, M.J. Rosseinsky, Chem. Commun. (1999) 2307.
- [63] P.P. Singh, A.K. Srivastava, S.B. Sharma, Indian J. Chem. A14 (1976) 714.
- [64] J.N. Behera, C.N.R. Rao, Can. J. Chem. 83 (2005) 668.
- [65] T. Takei, T. Ii, J. Kawashima, T. Ohmura, M. Ichikawa, M. Hosoe, Y. Shinya, I. Kanoya, W. Mori. Chem. Lett. 36 (2007) 1136.
- [66] A. Rujiwatra, C.J. Kepert, J.B. Claridge, M.J. Rosseinsky, H. Kumagai, M. Kurmoo, J. Am. Chem. Soc. 123 (2001) 10584.
- [67] R.G. Pritchard, M. Ali, A. Munim, A. Uddin, *Acta Cryst.* C62 (2006) 507.
- [68] Y.-J. Zhao, X.-H. Li, S. Wang, Acta Cryst. E61 (2005) 671.
- [69] C.A. Bremner, W.T.A. Harrison, *Acta Cryst. E*59 (2003) 425.
- [70] S. Natarajan, S. Neeraj, C.N.R. Rao, Solid State Sciences 2 (2000) 87.

CHAPTER III

CRYSTAL STRUCTURE, THERMAL AND MAGNETIC BEHAVIOR OF INORGANIC-ORGANIC HYBRID $[V^{IV}_{4}O_{10}V^{V}_{2}O_{4}](C_{6}H_{14}N_{2}).H_{2}O\ POLYMERIC\ FRAMEWORK$

T. Settheeworrarit, C. Pakawatchai, S. Maensiri, J. Limtrakul, A. Rujiwatra*, J. Inorg. Organomet. Polym. Mater. 16(3) (2006) 231-239.

Crystal Structure, Thermal and Magnetic Behavior of Inorganic-Organic Hybrid [VIV4O10 VV2O4] (C6H14N2)·H2O Polymeric Framework

Thapanon Settheeworrarit, ¹ Chaveng Pakawatchai, ² Santi Maensiri, ³ Jumras Limtrakul, ⁴ and Apinpus Rujiwatra ^{1,5}

Submitted May 30, 2006; Accepted August 8, 2006

Submitted May 30, 2006; Accepted August 8, 2006

The inorganic-organic hybrid [V^W, Q₁₀V^C, Q₄] (C.3k₁₆N₂)H₂Q polymeric framework was prepared under mild bydrothermal conditions from a mixture of DABCO and V₂Q₃ and the described water with a 1:1450 mole ratio, at neutral pH. The reaction was carried out at 180 °C for 3 days under autogenous pressure yielding phase pure crystal product. The crystal structure was studied using both powder and single crystal X-ray crystallography, reunling the structure was the first the structure to be of the (UuSh)[T*y²] type in the SP+T class and Z-T subclass. The researcher of the organic cation was confirmed by FT-IR, spectrum and chemical composition analysis. The structure was thermally stable up to over 400 °C, and showed ferromagnetic distribution of the confirmed with the maximum molar susceptibility of 8.26 × 10⁻⁷ cm³ at zero applied field.

EVY WOREN. Vanadium oxide: inoregatic-organic hybrid polymer; hydrothermal synthesis crystal

XEY WORDS: Vanadissin oxide; inorganic-organic hybrid polymer, hydrothermal synthesis; crystal structure; thermal behavior; magnetic characterization.

L INTRODUCTION

Transition metal oxide based solids are cur-rently attracting the most attention of the numerous morganic materials. They have been developed for a wide range of applications, e.g. high temperature

compositional range and notable structural diver compositional range and notable structural diversity together with the profusion in their chemistry. This has resulted in efforts to design and engineer the transition metal oxides, particularly those with inorganic-organic hybrid (IOH) polymeric structures [6]. One of the most appealing IOH materials is the

INTRODUCTION

Transition metal oxide based solids are currently attracting the most attention of the numerous inorganic materials. They have been developed for a wide range of applications, *e.g.* high temperature resistant materials, artificial bones, catalysts, molecular electronics, energy storage devices, magnetic and optical devices [1-5]. The foundation for promoting such applications is the immense chemical compositional range and notable structural diversity together with the profusion in their chemistry. This has resulted in efforts to design and engineer the transition metal oxides, particularly those with inorganic-organic hybrid (IOH) polymeric structures [6]. One of the most appealing IOH materials is the vanadium based polymeric framework [3-7]. Thorough reviews on crystal structures and coordination chemistry of vanadium oxide with open frameworks were recently reported by Zavalji *et al.* and Schindler *et al.* [8-9].

The vanadium oxide layer framework $(C_6H_{14}N_2)V_6o_{14}.H_2o$ with the most structural uniqueness and potential applications was first reported by Nazar *et al*, in 1996 [5]. The article focused on the investigation of its electrochemical behavior, while the preparation and structural characterization were only briefly reported. The purpose of this present study is, therefore, to further investigate the structure of the compound as an extension of the preliminary study reported earlier. The preparation of the material for this study was performed differently and, in addition, the thermal and magnetic properties were examined.

EXPERIMENTAL

Hydrothermal Preparation

The title compound, revealed later by single crystal X-ray diffraction to be $[V^{IV}_4O_{10}V^V_2O_4](C_6H_{14}N_2).H_2O$ or NVDAB henceforth, was prepared under mild hydrothermal conditions. A mixture of vanadium(V) oxide (V_2O_5) , Fluka Chemika 99%) and 1,4-diazabicyclo[2.2.2]octane, or so-called DABCO, $(C_6H_{12}N_2)$, Fluka Chemika 95%) was prepared in deionized water with the molar ratio V_2O_5 :DABCO:450 H_2O . The reaction mixture was stirred vigorously for 30 minutes, and transferred to the hydrothermal reaction vessel with a filling factor of ca. 50%. The pH of the mixture was measured and read 6.52. No pH adjustment was performed before the reaction. The reaction was conducted under autogeneous

pressure at 180°C for 3 days before being cooled down to room temperature at a cooling rate of 0.1 °Cmin⁻¹. The solid product was lustrously dark crystals, which were recovered by filtration, washed with deionized water and ethanol before being left to dry in air. The use of sodium metavanadate (Na₃VO₄, Fisher Laboratory Chemical 99%), as an alternative for V₂O₅, was also attempted, but led to nearly amorphous brown powder, according to powder X-ray diffraction. No crystals were obtained from the reactions with Na₃VO₄.

Structural Characterization

The purity and crystallinity of the obtained crystals were characterized by powder X-ray diffraction (Bruker D8 Advance, CuK_{α} , Ni Filter, λ =1.540558 Å, 48 kV, 30 mA). The morphology and elemental composition of the bulk crystals were analyzed by field emission scanning electron microscope equipped with an energy dispersive X-ray spectroscopic microanalyzer (FESEM-EDS, JEOL JSM-6335F) and a CHNS/O analyzer (Perkin Elmer Series II 2400), respectively. The presence of the organic motif in the structure was ensured by Fourier transform infrared spectroscopy (FT-IR, Bruker Tensor 27, 4000-400 cm⁻¹, resolution 0.5 cm⁻¹) using a KBr disc prepared from ground crystals.

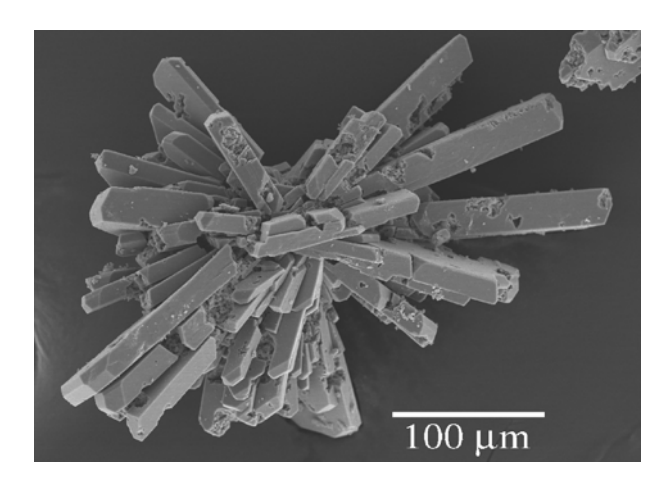


Figure 3.1 Scanning electron micrograph showing the agglomeration of the NVDAB crystal prisms.

Reflection data of the chosen prismatic single crystal of 0.22 x 0.14 x 0.04 mm³ in size were collected on a Bruker SMART APEX CCD diffractometer at 298(2) K using graphite monochromated MoK_{α} radiation (λ =0.71073 Å). The crystals were

present mostly as an agglomeration (Figure 3.1) and dark in color, corresponding to the presence of mixed valent vanadium (IV, V) [10]. The collected data were reduced **Table 3.1** Crystallographic data for structural solution and refinement of the NVDAB compared with the earlier reported $(C_6H_{14}N_2)V_6O_{14}.H_2O$.

Crystallographic data	NVDAB	Nazar et al. [5]
Formula	$[V_6O_{14}](C_6N_2H_{14}).H_2O$	$[V_6O_{14}](C_6N_2H_{14}).H_2O$
Formula weight	661.85	661.85
Crystal description	dark violet prism	dark prism
Crystal size/mm³	0.22 × 0.14 × 0.04	Not reported
Crystal system	Monoclinic	Monoclinic
Space group	I121	C ₂
a/ Å	7.5945(7)	19.202(9)
b/ Å	6.6779(6)	6.625(3)
c/ Å	18.0246(16)	7.547(4)
β/°	91.787(6)	111.28(2)
Unit cell volume/ ų	913.68(14)	894.6(7)
Z	2	2
$\rho_{calc}/g.cm^{-3}$	2.402	2.457
T/K	298(2)	293(2)
Radiation (λ /Å)	Mo K _α (0.71073)	Mo K _α (0.71073)
μ/mm^{-1}	3.022	3.087
θ_{min} , θ_{max}	2.3, 27.5	2.28, 24.98
Total data collected	3943	1723
Unique data	2043	1571
Parameters refined	127	132
Restraints no.	1	1
Goodness of fit	1.098	1.028
R , R_w (all data)	0.0227, 0.0565	0.0476, 0.0975
$R, R_w(I>2\sigma(I))$	0.0222, 0.0563	0.0394, 0.0925

by using the program SAINT [11] and empirical absorption correction was done by using the SADABS [12] program. The structure was solved and refined by direct method and successive different Fourier maps using SHELXS-97 [13] and SHELXL-97 [14] via the WinGX [15] program interface. All non-hydrogen atoms were located from

direct and different Fourier maps and refined anisotropically, whereas the hydrogen atoms were located geometrically and refined using a riding model provided by the SHELXL-97 program. The crystallographic data for structural solution and refinement are summarized in Table 3.1, in comparison with the data of the earlier reported (C₆H₁₄N₂)V₆O₁₄.H₂O [5]. Notably, the final residue values of the NVDAB structure reported here; R=0.0227 and $wR(F^2)=0.0565$ for the total 2043 unique reflections, are better than the reported $(C_6H_{14}N_2)V_6O_{14}$. H_2O case; R=0.0476 and $wR(F^2)$ =0.0975 for the total 1571 unique reflections.

Thermogravimetric and Magnetic Investigation

The thermal behavior of the NVDAB compound was studied on thermogravimetric analyzer (Perkin Elmer TGA7) using ground crystals. The measurement was conducted in the temperature range between 50-600°C with a heating rate of 20 °Cmin⁻¹ under flow of nitrogen gas. The magnetic behavior of the ground crystals was examined at room temperature (298 K) in a magnetic field range of ±10kOe, using a vibrating sample magnetometer (VSM 7403, Lake Shore, USA).

RESULTS AND DISCUSSION

Hydrothermal Preparation

The nature of the vanadium precursor apparently was a crucial factor for the successful preparation of the NVDAB compound. The attempt to employ Na₃V^VO₄ under the described hydrothermal condition at approximately neutral pH led to a nearly amorphous powder with no presence of the NVDAB compound. The vanadium(V) oxide, $V_{2}^{V}O_{5}$, precursor with vanadium in the same pentavalent oxidation state, by contrast, yielded a phase containing pure NVDAB crystals under the same condition. This can be accounted for by the amphoteric character of $V_2^VO_5$ giving an acidic aqueous solution, and the mild oxidizing power of the precursor, which can be readily reduced to the crucial component in the structure of NVDAB, i.e. vanadium(IV), in aqueous solution at neutral pH [16]. According to the earlier report on the preparation of $(C_6H_{14}N_2)V_6O_{14}H_2O$ [5] using NaV^VO₃ precursor, a pH adjustment down to 2 was apparently necessary for the reduction of vanadium(V) to occur. It should also be mentioned that the amount of DABCO in the reaction mixture was twice as much compared to the synthetic route reported here.

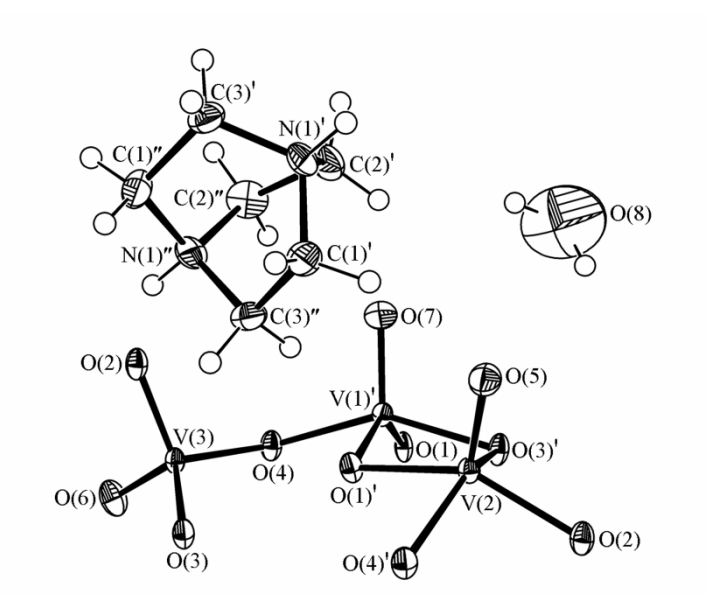


Figure 3.2 ORTEP drawing of the extended asymmetric unit of NVDAB with atomic numbering scheme for non-hydrogen atoms. Thermal ellipsoids are shown at 50%probability.

Table 3.2 Atomic coordinates (x10⁴) and equivalent isotropic displacement parameters (Å $^2\,x\,10^3)$ for all non-hydrogen atoms. U_{eq} is defined as one third of the trace of the orthogonalized $U_{ij}\ tensor. \label{eq:constraint}$

	X	У	Z	U_{eq}
V(1)	12688(1)	126(1)	2144(1)	12(1)
V(2)	5107(1)	2373(1)	3212(1)	12(1)
V(3)	8759(1)	2446(1)	2206(1)	12(1)
O(1)	12303(2)	-2675(3)	2168(1)	16(1)
O(2)	7634(2)	2300(3)	3016(1)	17(1)
O(3)	10061(2)	220(3)	2074(1)	16(1)
O(4)	10090(3)	4657(3)	2233(1)	17(1)
O(5)	5093(3)	2167(4)	4095(1)	24(1)
O(6)	7340(3)	2671(4)	1532(1)	25(1)
O(7)	13333(3)	789(4)	1343(1)	27(1)
O(8)	5000	6280(12)	5000	140(3)
N(1)	6002(3)	6098(4)	556(2)	24(1)
C(1)	6800(4)	4853(6)	-35(2)	28(1)
C(2)	5781(5)	8179(5)	282(2)	31(1)

C(3) 4267(4) 5243(6) 754(2) 26(1)

Structural Characterization

The structure of the NVDAB compound, $[V^{IV}_4O_{10}V^V_2O_4](C_6H_{14}N_2).H_2O$, was successfully solved and refined in monoclinic I_{121} , which is a non-standard setting of monoclinic C_2 , with the final refined cell parameters a=7.5945(7) Å, b=6.6779(6) Å, c=18.0246(16) Å, $\beta=91.787(6)^\circ$, V=913.68(14) Å³. The ORTEP plot of the extended asymmetric unit showing the coordination environment of the NVDAB structure and atomic numbering scheme is shown in Figure 3.2. Table 3.2 summarizes the refined atomic coordinates and isotropic displacement parameters.

There are three distinct sites of vanadium, two of which are in tetravalent state (V(1), V(2)) whereas the other one is in pentavalent state (V(3)), indicated by the bond valence calculations based on a single point energy model [17], and refined bond distances (Table 3.3). The tetravalent V(1) and V(2) are characterized by square pyramidal geometry, and can both be described as 4+1: four long equatorial bonds (1.894(2)-2.022(2) Å) and one short V(1)=O(7) vanadyl bond (1.602(2) Å) in V(1)^{IV}O₅, and four longer equatorial bonds (1.934(2)-1.987(2) Å) and one V(2)=O(5) short vanadyl bond (1.597(2) Å) in V(2)^{IV}O₅. The pentavalent V(3) shows a tetrahedral coordination to four oxygen atoms. The bond lengths found in the constructed V^VO₄ motif can be assigned to short terminal V(3)-O(2) and V(3)-O(6) bonds (1.718(2) and 1.605(2) Å) and long bridging V(3)-O(3) and V(3)-O(4) bonds (1.805(2) and 1.789(2) Å). These values do well agree with those reported by Nazar *et al.* [5] and Schindler *et al.* [9]. The structural motifs of V^{IV}O₅ square pyramids and V^VO₄ tetrahedra are thus linked *via* V-O-V oxo-bridges to form a naked vanadium oxide two-dimensional layer structure (Figure 3.3(a)).

The layered structure can be described as being constructed from one-dimensional polymeric chains of $V^{IV}O_5$ square pyramids. The chains are built up from the binuclear units of $V^{IV}O_5$, which share their edges in a *trans* conformation, as shown in Figure 3.3(a). The binuclear units are then fused to each other through *cis* edge sharing, directing in opposite directions, to produce a zig-zag profile. Each chain is linked to the adjacent chains *via* a V^VO_4 tetrahedra to form a mixed valence infinite two-dimensional vanadium oxide layer. Each constructive layer is anionic in character with the chemical formula of $[V^{IV}_4O_{10}V^V_2O_4]^{2^c}$, suggested by EDS semi-quantitative results; found. V:O, 6:13.3; calc. V:O, 6:14. This layer can be symbolized

as $(\{UuDd\}:T^*)\alpha'$ in SP+T class and Z-T subclass according to the abbreviations and classification suggested by Zavalij *et. al.* [8]. The projection along the *b*-axis of the **Table 3.3** Selected bond lengths (Å) and angles (°).

Bond lengths			
V(1)-O(7)	1.602(2)	V(3)-O(6)	1.605(2) 1.7177(19)
V(1)-O(1)	1.894(2)	V(3)-O(2)	1.789(2) 1.805(2)
V(1)-O(1)#3	1.922(2)	V(3)-O(4)	1.495(4)
V(1)-O(3)	1.9962(18)	V(3)-O(3)	
V(1)-O(4)#4	2.022(2)	N(1)-C(1)	
V(2)-O(5)	1.597(2)	N(1)-C(2)	1.482(4) 1.489(4)
V(2)-O(1)#1	1.9343(18)	N(1)-C(3)	1.529(4) 1.538(7)
V(2)-O(2)	1.9628(19)	C(1)-C(3)#5	
V(2)-O(3)#1	1.973(2)	C(2)-C(2)#5	
V(2)-O(4)#2	1.987(2)		
Bond angle			
O(7)-V(1)-O(1)	110.19(10)	O(6)-V(3)-O(2)	107.99(11)
O(7)-V(1)-O(1)#3	112.06(11)	O(6)-V(3)-O(4)	108.02(11)
O(1)-V(1)-O(1)#3	137.51(5)	O(2)-V(3)-O(4)	108.57(10)
O(7)-V(1)-O(3)	105.52(11)	O(6)-V(3)-O(3)	109.60(11)
O(1)-V(1)-O(3)	82.98(8)	O(2)-V(3)-O(3)	110.72(10)
O(1)#3-V(1)-O(3)	90.02(8)	O(4)-V(3)-O(3)	111.83(8)
O(7)-V(1)-O(4)#4	105.65(10)	V(3)-O(2)-V(2)	131.80(11)
O(1)-V(1)-O(4)#4	87.78(8)	V(3)-O(3)-V(2)#2	142.82(10)
O(1)#3-V(1)-O(4)#4	76.93(8)	V(3)-O(3)-V(1)	124.61(11)
O(3)-V(1)-O(4)#4	148.79(9)	V(2)#2-O(3)-V(1)	92.43(8)
V(1)-O(1)-V(1)#4	140.51(11)	V(3)-O(4)-V(2)#1	134.94(11)
V(1)-O(1)-V(2)#2	96.93(9)	V(3)-O(4)-V(1)#3	127.20(11)
V(1)#4-O(1)-V(2)#2	103.03(9)	V(2)#1-O(4)-V(1)#3	97.70(8)
O(5)-V(2)-O(1)#1	108.38(10)	C(2)-N(1)-C(3)	110.3(3)
O(5)-V(2)-O(2)	102.37(10)	C(2)-N(1)-C(1)	109.1(3)
O(1)#1-V(2)-O(2)	148.83(8)	C(3)-N(1)-C(1)	109.8(3)
O(5)-V(2)-O(3)#1	109.93(11)	N(1)-C(3)-C(1)#5	108.2(2)
O(1)#1-V(2)-O(3)#1	82.57(8)	N(1)-C(1)-C(3)#5	107.1(2)
O(2)-V(2)-O(3)#1	91.84(9)	N(1)-C(2)-C(2)#5	107.31(18)
O(5)-V(2)-O(4)#2	108.73(11)		
O(1)#1-V(2)-O(4)#2	77.49(8)		
O(2)-V(2)-O(4)#2	88.09(9)		
O(3)#1-V(2)-O(4)#2	140.39(8)		
Symmetry transformation	s used to gener	ate equivalent atoms:	
#1 -x+3/2,y+1/2,-z+1/2		#4 -x+5/2,y-1/2,-z+1/2	1
#2 -x+3/2,y-1/2,-z+1/2		#5 -x+1,y,-z	
#3 -x+5/2,y+1/2,-z+1/2			

unit cell, as shown in Figure 3.3(b), reveals that the layers are not planar but sinusoidal wave-like. The anionic layers subsequently stack along the c-axis with a repeating distance of ca. 1.80 nm into a three-dimensional framework. The largest interlayer distance of ca. 1.48 nm is observed at the location of the occluded organic motif, indicating the influence of the organic species on the construction of the inorganic polymeric sub-structure.

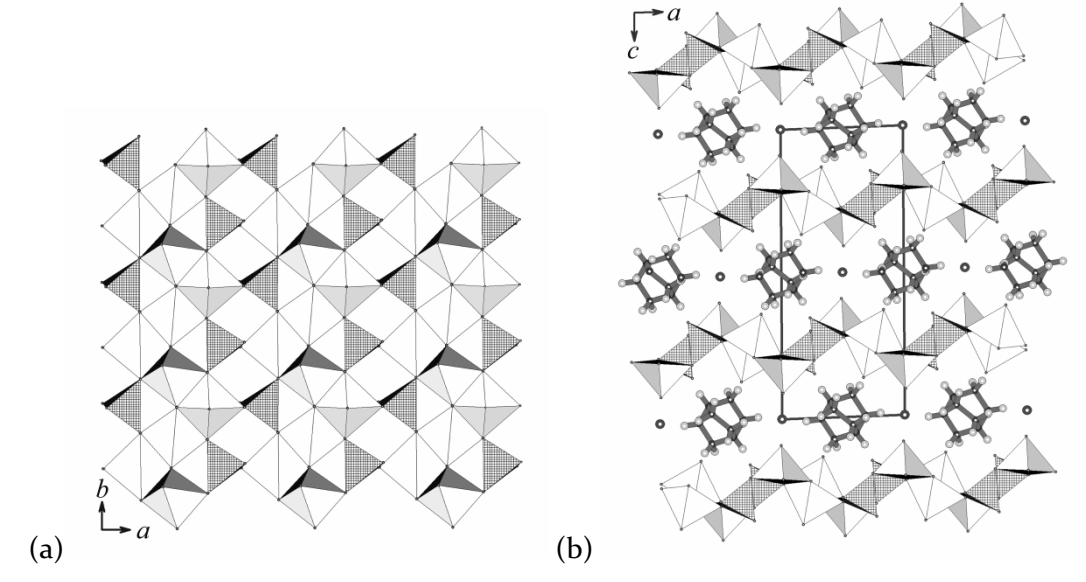


Figure 3.3 (a) A polyhedral view projected along c axis of the vanadium oxide layer constructed from edge-shared $[V^{IV}_{2}O_{8}]_{n}$ one-dimensional chain and the linkage $[V^{V}O_{4}]$ tetrahedral (hatched), and (b) the three-dimensional framework structure of NVDAB formed by the stacking of the vanadium oxide layers along the *[ooi]* direction.

The interlamellar galleries are evenly occupied by water of crystallization and diprotonated 1,4-diazabicyclo[2.2.2]octane, H₂DABCO. The dipositive charges of H₂DABCO ensure the electrical neutrality of the structure. The existence of the H₂DABCO cation was confirmed by the FT-IR spectrum (Figure 3.4), revealing characteristic vibrations of C-H stretching at 2925 cm⁻¹, C-H bending at 1470 cm⁻¹ and C-N stretching at 1047 cm⁻¹. The N-H stretching and N-H bending absorption peaks at 3560 and 1605 cm⁻¹ indicate the protonation of the nitrogen atoms of DABCO. The H₂O-derived O-H stretching mode ranges from 3250 to 3600 cm⁻¹, overlapping with the amine N-H stretching. The CHN analytical result also provided consistent results; found. C, 10.94%; H, 2.22%; N, 4.32%; calc. C, 10.88%; H, 2.42%; N, 4.23%. The

stretching vibration of the vanadyl bond was also observed and gave rise to the intense peak at about 683 cm⁻¹.

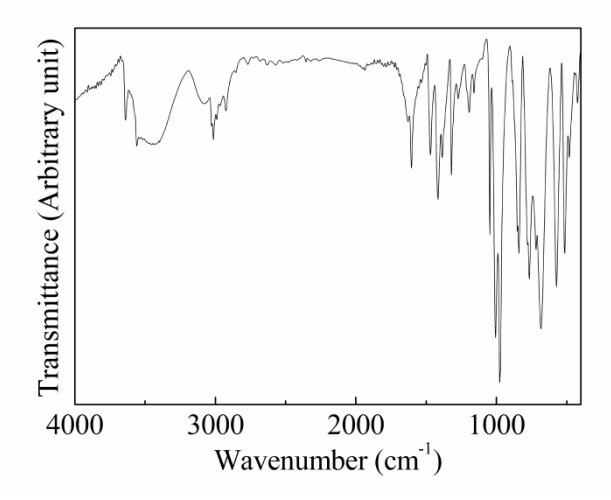


Figure 3.4 The FT-IR spectrum collected on the ground NVDAB crystals, confirming the presence of the organic cation and vanadyl bond.

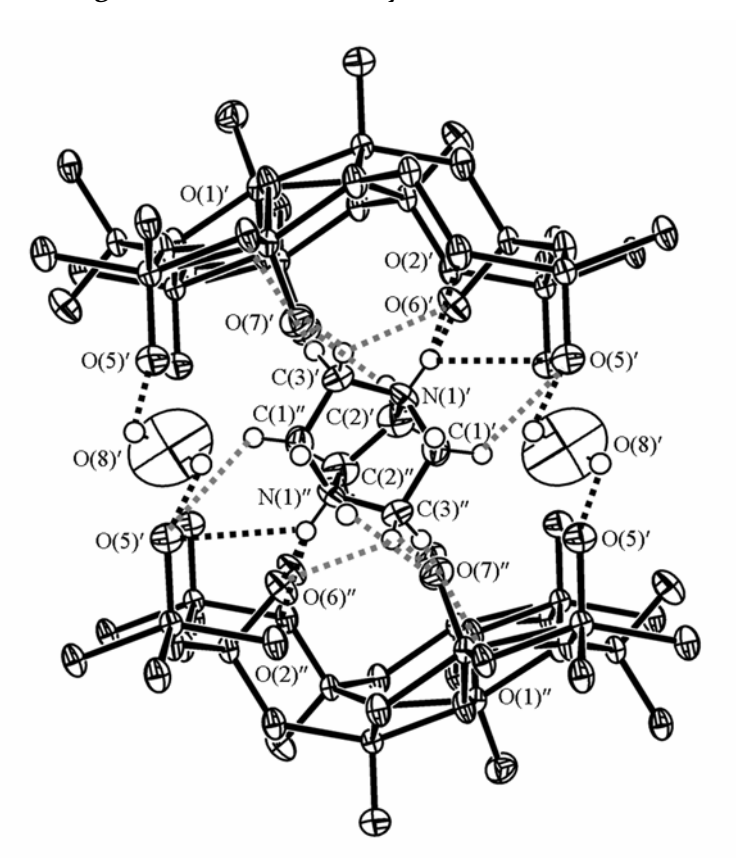


Figure 3.5 Diagram showing the presence of strong (black) and weak (grey) hydrogen bonds in the NVDAB structure.

Table 3.4 List of hydrogen bonds occurred in the NVDAB structure.

D-H····A (Å)	d(H····A) (Å)	d(D····A) (Å)	D-H····A angle (°)			
Strong hydrogen bonds:						
O(8)-H(8)O(5)#6	2.52	3.197(7)	126.9			
N(1)-H(1)O(6)	2.54	3.041(4)	115.0			
N(1)-H(1)O(2)#1	2.05	2.859(3)	148.1			
N(1)-H(1)O(5)#1	2.52	3.096(3)	121.8			
Weak hydrogen bonds:						
C(1)-H(12)···O(5)#5	2.54	3.368(4)	144			
C(2)-H(21)···O(7)	2.38	3.220(4)	145			
$C(3)-H(31)\cdots O(1)$	2.39	3.300(4)	156			
C(3)-H(32)···O(6)#7	2.52	3.187(4)	126			
C(3)-H(32)···O(7)#8	2.38	3.244(5)	148			
Symmetry transformations used to generate equivalent atoms:						
11 1 1		11				

^{#1 -}x+3/2,y+1/2,-z+1/2

#7 X+1,Y-1,Z

#8 x,y-1,z

#6 -x+1,y,-z+1

The overall structure of NVDAB is stabilized by hydrogen bonds which transfix water and H₂DABCO to the vanadium oxide framework, and *vice versa*. The hydrogen bonds were analyzed, revealing both strong and weak interactions [18, 19] as depicted and described in Figure 3.5 and Table 3.4, respectively. Strong hydrogen bonds are those between polar hydrogen atoms bound to nitrogen donor atoms of H₂DABCO and oxygen atoms of the vanadium oxide framework. Weak hydrogen interactions occur between hydrogen atoms attached to the carbon atoms of H₂DABCO and oxygen atoms of the vanadium oxide framework and water of crystallization. The presence of hydrogen bonds in the structure also confirmed by the broadening effect observed in the FT-IR spectrum. The occurring hydrogen bonds, as described, help in regulating the spatial orientation of the H₂DABCO with respect to the sinusoidal arrangement of the vanadium oxide layer, and hence the three-dimensional long-range order.

The powder X-ray diffraction pattern taken from ground crystals of NVDAB is shown in Figure 3.6, confirming the layered character of the structure by the presence of the preferred orientation effect. Every peak present in the powder pattern could be indexed based on the crystallographic data, indicating the chosen single crystal to be representative for the bulk sample. The d-spacing of 1.79 nm calculated from the oot peak at 2θ =9.88° agreed well with the repeating distance of 1.80 nm obtained from the single crystal structure.

^{#5 -}x+1,y,-z

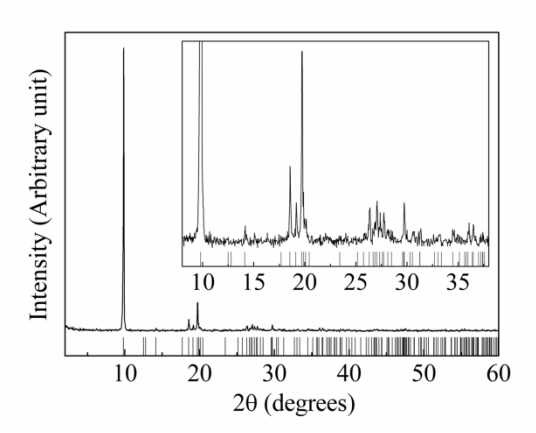


Figure 3.6 The powder X-ray diffraction pattern taken from the ground crystals of NVDAB compared with the pattern generated from the crystallographic structure.

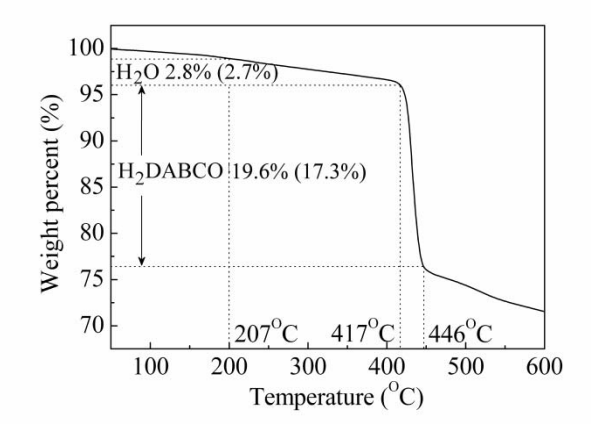


Figure 3.7 The TGA curve shows three major weight losses on heating the NVDAB, which correspond to the exile of surface water, water of crystallization and organic combustion respectively. The experimented figures are compared with the calculated figures present in the brackets.

Thermogravimetric Analysis

Three steps of weight losses were observed upon heating the ground crystals sample from 50 to 600°C with a constant heating rate of 20°Cmin⁻¹ under flow of nitrogen gas. The TGA curve is shown in Figure 3.7 with the measured weight losses shown in comparison with the theoretical figures calculated from the crystallographic chemical formula. Below 200°C, a small weight loss of ca. 1.2% was observed, which could be due to the loss of surface water. This was followed by another gradual loss of water of crystallization which was completed by 417°C, contributing to ca. 2.8% of the total sample weight. The last step was an abrupt loss of ca. 19.6% of the total sample weight, and was completed by 450°C, which corresponded to the combustion of the

 H_2DABCO , resulting in dark powder of poorly crystallinity. The thermal stability of the compound was apparently better under the nitrogen atmosphere than that in air, as reported earlier [5]. The organic combustion temperature was slightly higher (ca. $10^{\circ}C$) and there was no weight gain after the organic combustion, which was reportedly due to the oxidation of the framework V^{IV} to V^{V} [5-20].

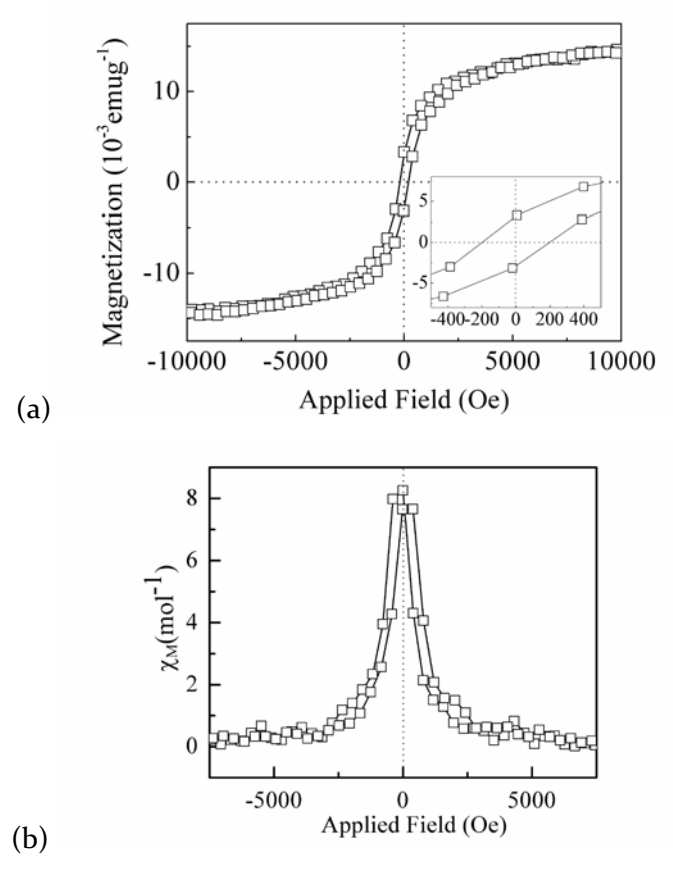


Figure 3.8 (a) Field dependent specific magnetization of the ground NVDAB crystals at room temperature, and (b) the corresponding molar susceptibility curve.

Magnetic Property

The field dependent specific magnetization, M(H), curve obtained from the isothermal VSM measurement at room temperature is shown in Figure 3.8(a). It indicates clear hysteresis ferromagnetism in the field range of *ca.* ±4 kOe and the increasing of the specific magnetization (M_s) with the increased field outside this range. No clear magnetization saturation was observed within the investigated field of ±10 kOe. The values of the remanent magnetization (M_r) and the coercive forces (H_c) on the decreasing and increasing field of the hysteresis were 3.08 x 10⁻³ emug⁻¹, -201.38 Oe and 197.50 Oe, respectively. Differentiation of the M(H) curve with respect to the applied field, followed by the multiplication with the formula weight yielded

the molar susceptibility, χ_M , curve (Figure 3.8(b)). The maximum χ_M of 8.26 x 10⁻³ emumol⁻¹ was observed at zero applied field, leading to the effective magnetic moment of 4.46 μ_B per formula unit. The χ_M was decreased under the applied field, and close to a constant value of zero outside the hysteresis. The observed magnetism should result only from the presence of V^{IV} ($S=\frac{1}{2}$) in the polymeric chain substructure, since V^{V} ions do not possess an effective magnetic moment. As there are four $\boldsymbol{V}^{\text{IV}}$ magnetic centers in the formula, the measured effective magnetic moment is slightly lower than the expected effective magnetic moment for four $S=\frac{1}{2}$ magnetic ions. This can be assigned to the effective superexchange coupling [21] between the V^{IV} ions via non-magnetic oxo-bridges. The intervening $O^{\text{2-}}$ anions involved in the $V^{\text{IV}}\text{-O-V}^{\text{IV}}$ linkages of the edge-shared binuclear substructures form angles ranging from 92.43(8)° to 103.03(9)° (Table 3). These are slightly deviated from orthogonality, and therefore result in ferromagnetic coupling of ferromagnetic binuclear units. The edge-share linkage between the two adjacent binuclear subunits (Figure 3.3(a)) in the cis transformation however prompts the triangular arrangement of the V^{IV} magnetic centers, and thus the anticipated spin frustration. The partial antiferromagnetic interaction is expected under the circumstance and accounts for the lowering of the bulk effective magnetic moment. It should be noted that an antiferromagnetic interaction below room temperature was observed for the analogous structures [22].

CONCLUSIONS

The inorganic-organic hybrid $[V^{IV}_4O_{10}V^V_2O_4](C_6H_{14}N_2).H_2O$ polymeric framework was prepared under mild hydrothermal conditions from a mixture of DABCO and V_2O_5 in deionized water at neutral pH. The structure of the title compound was studied by single crystal X-ray crystallography, revealing the structure to be of the ({UuDd}:T*) α' type in the SP+T class and Z-T subclass. The presence of the organic cation was confirmed by the FT-IR spectrum and the chemical composition analysis. The structure was thermally stable up to over 400° C, and showed ferromagnetic character at room temperature with the maximum effective magnetic moment of $4.46~\mu_B$ per formula unit at zero applied field.

REFERENCES

- [1] S. Cheng, H. D. Hwang, G. E. Maciel, J. Mol. Struct. 470 (1998) 135.
- [2] S. Cheng, *Catal. Today* 49 (1999) 303.

- [3] P. J. Hagrman, R. C. Finn, J. Zubirta, Solid State Sci. 3 (2001) 745.
- C. H. Lu, W. C. Lee, S. J. Liou, G. T. K. Fey, J. Power Sources 81 (1999) 696. [4]
- [5] L. F. Nazar, B. E. Koene, J. F. Britten, Chem. Mater. 8 (1996) 327.
- [6] P. G. Romero, C. Sanchez, Functional Hybrid Materials, WILEY-VCH, Weinheim (2004).
- [7] F. N. Shi, F. A. Almeida Paz, J. Rocha, J. Klinowski, T. Trindade, Inorg. Chem. Acta 358 (2005) 927.
- [8] P. Y. Zavalij, M. S. Whittingham, Acta Cryst. B55 (1999) 627.
- [9] M. Schindler, F. C. Hawthrone, W. H. Baur, Chem. Mater. 12 (2000) 1248.
- P. J. Ollivier, J. R. D. DeBoard, P. J. Zapf, J. Zubieta, L. M. Meyer, C. -C. Wang, T. [10] E. Mallouk, R. C. Haushalter, J. Mol. Struct. 470 (1998) 49.
- [11] Siemens, SAINT v4: Software Reference Manual, Siemens Analytical X-Ray Systems, Madison, WI, USA (1996).
- G.M. Sheldrick, SADAB: Program for Empirical Absorption correction of Area [12] Detector Data, University of Goettingen, Germany (1996).
- [13] G. M. Sheldrick, SHELXS-97: A Program for Solving Crystal Structure, University of Goettingen, Germany, Release 97-2 (1997).
- [14] G. M. Sheldrick, SHELXL-97: A Program for Crystal Structure Refinement, University of Goettingen, Germany, Release 97-2 (1997).
- [15] L. J. Farrugia, J. Appl. Cryst. 32 (1999) 837.
- [16] N. N. Greenwood, A. Earnshaw, Chemistry of the Elements, 2nd ed. Elsevier-Butterworth-Heinemann, Oxford (2003).
- [17] V. S. Urusov, I. P. Orlov, Cryst. Rep. 44 (1999) 686.
- [18] A. L. Spek, *A preliminary Introduction to the PLATON Program*, Utrecht, Netherlands (1997).
- [19] G. A. Jeffrey, An Introduction to Hydrogen Bonding, Oxford University Press, New York (1997).
- [20] T. Whitfield, X. Wang, L.-M. Zheng and A. J. Jacobson, J. Solid State Chem. 175 (2003) 13.
- [21] J. B. Goodenough, Magnetism and the Chemical Bond, Interscience Publisher, New York (1963).
- [22] Y. Zhang, J. R. D. DeBord, C. J. O'Connor, R. C. Haushalter, A. Clearfield, J. Zubieta, Angew. Chem. Int. Ed. Engl. 35 (1996) 989.

CHAPTER IV

CRYSTAL STRUCTURES, THERMOGRAVIMETRIC AND MAGNETIC PROPERTIES OF FOUR ORGANODIAMINE **TEMPLATED VANADIUM OXIDE FRAMEWORKS: INFLUENCES OF DIAMINOALKANE TEMPLATES**

T. Settheeworrarit, T.J. Prior, S. Meansiri, J. Limtrakul, A.Rujiwatra. *J. Inorg. Organomet. Polym. Mater.* 18(2) (2008) 253-263.

J Inorg Organismet Polym DOI 10.1007/s10904-007-9171-y

Crystal Structures, Thermogravimetric and Magnetic Properties of Four Organodiamine Templated Vanadium Oxide Frameworks: Influences of Diaminoalkane Templates

Thapanon Settheeworrarit · Timothy J. Prior · Santi Meansiri · Jumras Limtrakul · Apinpus Rujiwatra

Received: 29 August 2007 / Accepted: 3 October © Springer Science+Business Media, LLC 2007

 $H_{10}N_2\lambda$, $[V_2^VO_8V_2^VO_2](C_3H_{12}N_2)$, $[V_4^VO_{10}V_2^VO_4(C_4H_{14}N_2)]$ and $[V_4^VO_8V_2^VO_4)(C_3H_{16}N_2)$, have been successfully prepared under hydrothermal conditions. The crystal structures are fully characterized revealing byered structures composed of common inorganic building units, namely $|V^VO_3\rangle$ square pyramids and $|V^VO_4\rangle$ tetrahedra. The layer registries are different depending on the molecular terms of the distribute the period of the distribute the distribute the distributed the dist the tayer registation are unrevious departuring on the second ular structure of the diaminoalkanes, and can be accounted for by the organic-inorganic interface interactions. The analysis of hydrogen bonds indicates their important role in directing two- and three-dimensional structural architecsurecting two- and three-dimensional structural architec-tures. The influences of different diaminoals area are also apparent in both thermogravimetric and complex magnetic

1 Introduction

Besides being important for technological applications, inorganic oxides have long been attracting scientists and technologists worldwide because of their structural and technologists worldwide occasion of their structural and functional diversities. Although the most abundant inor-ganic oxides are those of the main group elements, such as clay minerals and aluminosilicates, current interest have been focused on materials with transition and/or posttransition elements [1-3]. The complex and flexible structural and physical chemistry make variadium oxides one of the most studied groups of compounds [1, 4, 5]. The concept of structural design has also been applied to extend further the range of structures and, therefore, the properties of these compounds. One important strategy employed is to

INTRODUCTON

Besides being important for technological applications, inorganic oxides have long been attracting scientists and technologists worldwide because of their structural and functional diversities. Although the most abundant inorganic oxides are those of the main group elements, such as clay minerals and aluminosilicates, current interest have been focused on materials with transition and/or posttransition elements [1-3]. The complex and flexible structural and physical chemistry make vanadium oxides one of the most studied groups of compounds [1,4,5]. The concept of structural design has also been applied to extend further the range of structures and, therefore, the properties of these compounds. One important strategy employed is to use organic templates to direct the structures, although complete control over the final frameworks has not yet be achieved. The structural directing function of organic templates, however, has been assumed to be due to organicinorganic interface interactions including, for example, hydrogen bonding and electrostatic interactions [1]. The design of the structures may, therefore, require the assembly of specific arrays of interactions to direct the product geometry. At present current expertise is well short of ab initio structure prediction for materials of this type. Therefore, further examples of frameworks templated by specific interactions are actively being sought.

Inspired by our success in the preparation of the layered structure of $[V^{IV}_4O_{10}V^V_2O_4](C_6H_{14}N_2)\cdot H_2O$ [6] and the attempt to synthesize nickel-vanadium oxide frameworks, we sought to explore further the influences of various diaminoalkanes on the structures of the layered vanadium oxides. Of particular interest was to establish the influence upon the vanadium oxide frameworks of the chain length of terminal diaminoalkanes. To this end, a series of four crystals, *i.e.* $[V^{IV}_2O_8V^V_2O_2](C_2H_{10}N_2)$, $[V^{IV}_2O_8V^V_2O_2](C_3H_{12}N_2)$, $[V^{IV}_4O_{10}V^V_2O_4](C_4H_{14}N_2)$ and $[V^{IV}_4O_{10}V^V_2O_4](C_5H_{16}N_2)$ have been isolated and structurally characterized. It should be noted that the structure of $[V^{IV}_2O_8V^V_2O_2](C_3H_{12}N_2)$ is analogous to a formerly reported structure, deduced from crystals prepared *via* different route [7]. Although all of these structures are assembled from common structural building units and exhibit similar gross structure, they differ substantially in their layer topologies, three-dimensional architectures, thermal properties and magnetic behavior. The differences discussed in the present work reflect the influences of synergistic

Table 4.1 Single crystal growth conditions and crystallographic data for structural solutions and refinements of 1, 2, 3 and 4.

	1	2 ⁽¹⁾	3	4
	Cryst	tal growth conditions		
Starting materials	NiSO ₄ ·6H ₂ O: V ₂ O ₅ :	NiSO ₄ ·6H ₂ O: V ₂ O ₅ :	NiSO ₄ ·6H ₂ O: V ₂ O ₅ :	(CH ₃ COO) ₂ Ni·4H ₂ O:
and mole ratios	3C ₂ H ₈ N ₂ : 450H ₂ O	${}_{2}C_{3}H_{10}N_{2}$: ${}_{4}50H_{2}O$	2C ₄ H ₁₂ N ₂ : 450H ₂ O	V_2O_5 : $2C_5H_{14}N_2$:
and more ratios				450H₂O
Stirring times	0	30	30	30
pH of reaction mixtures	8	8.33	8.97	8.41
Reaction temperatures (°C)	180	180	180	160
Reaction times (hr)	72	72	72	72
Cooling rates (ºC/min)	1.0	3.0	3.0	1.0
	Cr	ystallographic data		
Empirical formula	$[V_4O_{10}](C_2N_2H_{10})$	$[V_4O_{10}](C_3N_2H_{12})$	$[V_6O_{14}](C_4N_2H_{14})$	$[V_6O_{14}](C_5N_2H_{16})$
Formula weight	425.90	439.90	619.81	633.84
Crystal description	Dark green plate	Black plate	Black prism	Black prism
Crystal size/mm ³	$0.2 \times 0.035 \times 0.035$	$0.10 \times 0.20 \times 0.06$	$0.12 \times 0.02 \times 0.02$	$0.04 \times 0.02 \times 0.01$
Crystal system	Triclinic	Monoclinic	Monoclinic	Monoclinic
Space group	$P\overline{1}$	P_{2_1}/n	P_{2_1}/n	P_{2_1}/n
a/ Å	5.995(1)	7.971(2)	9.688(3)	10.105(3)
b/ Å	6.609(1)	9.977(2)	6.789(2)	6.757(2)
c/ Å	7.627(1)	15.651(3)	12.642(4)	12.659(4)
α/ º	82.390(2)	90.00(0)	90.00(0)	90.00(0)
β/ º	70.413(1)	100.47(2)	96.279(2)	95.202(3)
γ/ º	75.286(2)	90.00(0)	90.00(0)	90.00(o)
	1	2 ⁽¹⁾	3	4
	Cryst	tal growth conditions		
Ctanting materials	NiSO ₄ ·6H ₂ O: V ₂ O ₅ :	NiSO ₄ ·6H ₂ O: V ₂ O ₅ :	NiSO ₄ ·6H ₂ O: V ₂ O ₅ :	(CH ₃ COO) ₂ Ni·4H ₂ O:
Starting materials	3C ₂ H ₈ N ₂ : 450H ₂ O	2C ₃ H ₁₀ N ₂ : 450H ₂ O	2C ₄ H ₁₂ N ₂ : 450H ₂ O	V_2O_5 : $2C_5H_{14}N_2$:
and mole ratios				450H₂O
Stirring times	0	30	30	30
pH of reaction mixtures	8	8.33	8.97	8.41
Reaction temperatures (°C)	180	180	180	160
Reaction times (hr)				
- 1. ()	72	72	72	72
Cooling rates (°C/min)	72 1.0	72 3.0		
Cooling rates (ºC/min)	1.0	-	72	72
	1.0	3.0	72	72
Cooling rates (ºC/min) Empirical formula Formula weight	1.0 <i>Cr</i>	3.0 ystallographic data	72 3.0	72 1.0
Empirical formula	1.0 Cr [V ₄ O ₁₀](C ₂ N ₂ H ₁₀)	ystallographic data [V ₄ O ₁₀](C ₃ N ₂ H ₁₂)	72 3.0 [V ₆ O ₁₄](C ₄ N ₂ H ₁₄)	72 1.0 [V ₆ O ₁₄](C ₅ N ₂ H ₁₆)
Empirical formula Formula weight	1.0 Cr $[V_4O_{10}](C_2N_2H_{10})$ 425.90	3.0 ystallographic data [V ₄ O ₁₀](C ₃ N ₂ H ₁₂) 439.90	72 3.0 [V ₆ O ₁₄](C ₄ N ₂ H ₁₄) 619.81	72 1.0 [V ₆ O ₁₄](C ₅ N ₂ H ₁₆) 633.84
Empirical formula Formula weight Crystal description	1.0 Cr $[V_4O_{10}](C_2N_2H_{10})$ 425.90 Dark green plate	3.0 ystallographic data [V ₄ O ₁₀](C ₃ N ₂ H ₁₂) 439.90 Black plate	72 3.0 [V ₆ O ₁₄](C ₄ N ₂ H ₁₄) 619.81 Black prism	72 1.0 [V ₆ O ₁₄](C ₅ N ₂ H ₁₆) 633.84 Black prism
Empirical formula Formula weight Crystal description Crystal size/mm ³	1.0 Cr $[V_4O_{10}](C_2N_2H_{10})$ 425.90 Dark green plate 0.2 × 0.035 × 0.035 Triclinic	3.0 ystallographic data [V ₄ O ₁₀](C ₃ N ₂ H ₁₂) 439.90 Black plate 0.10 × 0.20 × 0.06	72 3.0 [V ₆ O ₁₄](C ₄ N ₂ H ₁₄) 619.81 Black prism 0.12 × 0.02 × 0.02	72 1.0 [V ₆ O ₁₄](C ₅ N ₂ H ₁₆) 633.84 Black prism 0.04 × 0.02 × 0.01
Empirical formula Formula weight Crystal description Crystal size/mm³ Crystal system Space group	1.0 Cr $[V_4O_{10}](C_2N_2H_{10})$ 425.90 Dark green plate 0.2 × 0.035 × 0.035 Triclinic $P\bar{1}$	ystallographic data $[V_4O_{10}](C_3N_2H_{12})$ 439.90 Black plate $0.10 \times 0.20 \times 0.06$ Monoclinic $P2_1/n$	72 3.0 $[V_6O_{14}](C_4N_2H_{14})$ 619.81 Black prism 0.12 × 0.02 × 0.02 Monoclinic P_{2_1}/n	72 1.0 [V ₆ O ₁₄](C ₅ N ₂ H ₁₆) 633.84 Black prism 0.04 × 0.02 × 0.01 Monoclinic P2 ₁ /n
Empirical formula Formula weight Crystal description Crystal size/mm³ Crystal system Space group a/ Å	1.0 Cr $[V_4O_{10}](C_2N_2H_{10})$ 425.90 Dark green plate 0.2 × 0.035 × 0.035 Triclinic $P\bar{1}$ 5.995(1)	3.0 ystallographic data $[V_4O_{10}](C_3N_2H_{12})$ 439.90 Black plate $0.10 \times 0.20 \times 0.06$ Monoclinic P_{2_1}/n 7.971(2)	72 3.0 $[V_6O_{14}](C_4N_2H_{14})$ 619.81 Black prism 0.12 × 0.02 × 0.02 Monoclinic P_{2_1}/n 9.688(3)	72 1.0 $[V_6O_{14}](C_5N_2H_{16})$ 633.84 Black prism 0.04 × 0.02 × 0.01 Monoclinic P2 ₁ /n 10.105(3)
Empirical formula Formula weight Crystal description Crystal size/mm³ Crystal system Space group a/ Å b/ Å	1.0 Cr $[V_4O_{10}](C_2N_2H_{10})$ 425.90 Dark green plate 0.2 × 0.035 × 0.035 Triclinic $P\bar{1}$ 5.995(1) 6.609(1)	3.0 ystallographic data [V ₄ O ₁₀](C ₃ N ₂ H ₁₂) 439.90 Black plate 0.10 × 0.20 × 0.06 Monoclinic P2 ₁ /n 7.971(2) 9.977(2)	72 3.0 [V ₆ O ₁₄](C ₄ N ₂ H ₁₄) 619.81 Black prism 0.12 × 0.02 × 0.02 Monoclinic P ₂₁ /n 9.688(3) 6.789(2)	72 1.0 [V ₆ O ₁₄](C ₅ N ₂ H ₁₆) 633.84 Black prism 0.04 × 0.02 × 0.01 Monoclinic P2 ₁ /n 10.105(3) 6.757(2)
Empirical formula Formula weight Crystal description Crystal size/mm³ Crystal system Space group a/ Å b/ Å c/ Å	1.0 Cr $[V_4O_{10}](C_2N_2H_{10})$ 425.90 Dark green plate 0.2 × 0.035 × 0.035 Triclinic $P\bar{1}$ 5.995(1) 6.609(1) 7.627(1)	3.0 ystallographic data [V ₄ O ₁₀](C ₃ N ₂ H ₁₂) 439.90 Black plate 0.10 × 0.20 × 0.06 Monoclinic P2 ₁ /n 7.971(2) 9.977(2) 15.651(3)	72 3.0 [V ₆ O ₁₄](C ₄ N ₂ H ₁₄) 619.81 Black prism 0.12 × 0.02 × 0.02 Monoclinic P2 ₁ /n 9.688(3) 6.789(2) 12.642(4)	72 1.0 [V ₆ O ₁₄](C ₅ N ₂ H ₁₆) 633.84 Black prism 0.04 × 0.02 × 0.01 Monoclinic P2 ₁ /n 10.105(3) 6.757(2) 12.659(4)
Empirical formula Formula weight Crystal description Crystal size/mm³ Crystal system Space group a/ Å b/ Å	1.0 Cr $[V_4O_{10}](C_2N_2H_{10})$ 425.90 Dark green plate 0.2 × 0.035 × 0.035 Triclinic $P\bar{1}$ 5.995(1) 6.609(1)	3.0 ystallographic data [V ₄ O ₁₀](C ₃ N ₂ H ₁₂) 439.90 Black plate 0.10 × 0.20 × 0.06 Monoclinic P2 ₁ /n 7.971(2) 9.977(2)	72 3.0 [V ₆ O ₁₄](C ₄ N ₂ H ₁₄) 619.81 Black prism 0.12 × 0.02 × 0.02 Monoclinic P ₂₁ /n 9.688(3) 6.789(2)	72 1.0 [V ₆ O ₁₄](C ₅ N ₂ H ₁₆) 633.84 Black prism 0.04 × 0.02 × 0.01 Monoclinic P2 ₁ /n 10.105(3) 6.757(2)

 $^{^{(1)}}$ The crystallographic data of 2 were extracted from the supporting information of reference [7].

interactions between the organic and inorganic components on structural details and, therefore, on their properties.

EXPERIMENTAL

Hydrothermal crystal growth

Single crystals of $[V^{IV}_{2}O_{8}V^{V}_{2}O_{2}](C_{2}H_{10}N_{2})$ (1), $[V^{IV}_{2}O_{8}V^{V}_{2}O_{2}](C_{3}H_{12}N_{2})$ (2), $[V^{IV}_{4}O_{10}V^{V}_{2}O_{4}](C_{4}H_{14}N_{2})$ (3) and $[V^{IV}_{4}O_{10}V^{V}_{2}O_{4}](C_{5}H_{16}N_{2})$ (4) were grown under hydrothermal conditions from suspensions of vanadium(V) oxide $(V_{2}O_{5}, Fluka Chemika, 99\%)$, nickel(II) salts $(NiCl_{2}\cdot6H_{2}O, Univar Analytical Reagent, 99\%; NiSO_{4}\cdot6H_{2}O, Carlo Erba, 99\%; (CH_{3}COO)_{2}Ni, BDH, 98\%)$, and various diaminoalkanes, *i.e.*, ethylenediamine $(C_{2}H_{8}N_{2}, Carlo Erba, 98\%)$, 1,3-diaminopropane $(C_{3}H_{10}N_{2}, Fluka Chemika, 99\%)$, 1,4-diaminobutane $(C_{4}H_{12}N_{2}, Fluka Chemika, 98\%)$, and 1,5-diaminopentane $(C_{5}H_{14}N_{2}, Fluka Chemika, 97\%)$ in deionized water. The crystals were recovered by filtration, washed with deionized water and ethanol before being left to dry in air. The nature, mole ratios of the starting chemicals and optimal reaction conditions, which afforded single crystals suitable for further structural characterization are summarized in Table 4.1. It should be noted that the nickel salts were used in the experiments in an attempt to introduce nickel into the framework. There was no evidence, however, for incorporation of nickel within any of the frameworks.

Structure characterizations

The single crystal X-ray diffraction experiments were conducted on Station 16.2SMX at the Darebury SRS, UK using synchrotron radiation on a D8 3-circle diffractometer equipped with Bruker-Nonius APEXII charge coupled device (CCD) area detector. The collected data were reduced and corrected with an empirical absorption correction by using the SAINT [8] and SADABS [9] programs, respectively. The structures were solved by direct method using SHELXS-97 [10] and further refined by full-matrix least-squares analysis against F^2 using the SHELXL-97 [11] via the WinGX [12] program interface. Non-hydrogen atoms could be assigned directly from the electron density maps, whereas the hydrogen atoms were located and refined using a riding model provided in the SHELXL-97 program. The hydrogen atoms were not introduced to 1,5-diaminopentane due to the presence of disorder at

the carbon atoms. The crystallographic data for 1, 3 and 4 are summarized in Table 4.1. The preliminary crystallographic data suggest that 2 is isostructural with the formerly reported structure, $(H_3N(CH_2)_3NH_3)[V_4O_{10}]$ [7], therefore, the full data set of 2 was , which are not collected. Structural details of 2 described further in this work in order to compare with those of 1, 3 and 4, are extracted from the supporting information accompanying the previous report [7].

The powder X-ray diffraction (PXRD) patterns were obtained on a Bruker D8 Advance diffractometer, operating with a Ni filtered CuKα radiation (λ =1.540558 Å). The infrared spectra were collected on a Bruker Tensor 27 FT-IR (4000–400 cm⁻¹, resolution 0.5 cm⁻¹) spectrometer as KBr (BDH, 98.5%) pellets prepared from ground crystals. The quantities of carbon, hydrogen and nitrogen were analyzed by a Perkin Elmer Series II 2400 CHNS/O analyzer. Thermogravimetric analyses (TGA) were performed with an Elmer TGA7 thermal analysis system in the temperature range 50-600 °C with a heating rate of 20 °C min⁻¹ under a nitrogen atmosphere. The magnetic behavior of the ground crystals of 2, 3 and 4 were examined at 273K in a magnetic field range of ±10kOe, using a VSM 7403 magnetometer.

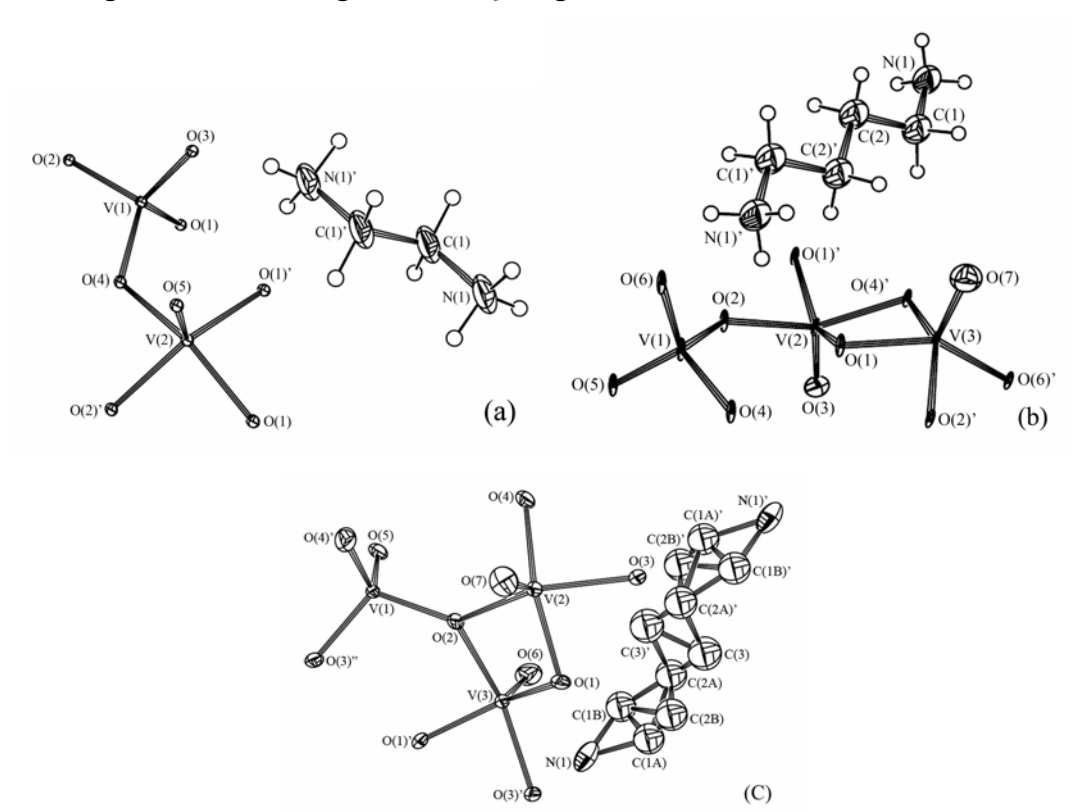


Figure 4.1 ORTEP diagrams showing extended asymmetric units of (a) 1, (b) 3 and (c) 4 with atomic numbering scheme for non-hydrogen atoms, and thermal ellipsoids of 99% for 1 and 3, and 70% for 4.

Table 4.2 Selected bond distances (Å) and angles (deg) of 1, 3 and 4.

1 ⁽¹⁾			3 ⁽²⁾			4 ⁽³⁾		
V(1)-O(1)	1.834	1 (4)	V(1)-O(2)	1.826	(3)	V(1)-O(5)	1.598	3(6)
V(1)-O(2)	1.735	(4)	V(1)-O(4)	1.795	(3)	V(1)-O(4)#3	1.702	(5)
V(1)-O(3)	1.633	3(4)	V(1)-O(5)	1.604	(3)	V(1)-O(2)	1.789	0(4)
V(1)-O(4)	1.695	5(4)	V(1)-O(6)	1.712(3)	V(1)-O(3)#6	1.809	o (5)
V(2)-O(1)	1.996	5(4)	V(2)-O(1)	1.880	(3)	V(2)-O(7)	1.598	3(5)
V(2)-O(1)#2	1.958	3(4)	V(2)-O(1)#2	1.909	(3)	V(2)-O(1)	1.924	(5)
V(2)-O(2)#3	1.929	9(4)	V(2)-O(2)#2	1.985	(3)	V(2)-O(4)	1.933	(5)
V(2)-O(4)#4	1.928	3(4)	V(2)-O(3)#2	1.613(3)	V(2)-O(3)	1.977	(5)
V(2)-O(5)	1.608	3(4)	V(2)-O(4)	2.016	(3)	V(2)-O(2)	2.011	(5)
			V(3)-O(1)#2	1.925((3)	V(3)-O(6)	1.607	
			V(3)-O(2)#5	1.978	(3)	V(3)-O(1)#4	1.882	2(5)
			V(3)-O(4)	2.024	(3)	V(3)-O(1)	1.907	7(5)
			V(3)-O(6)#4	1.929	(3)	V(3)-O(3)#4	1.989	o(5)
			V(3)-O(7)#4	1.613(3)	V(3)-O(2)	2.027	7(5)
O(3)-V(1)-O(4)		109.64(19)	O(5)-V(1)-O(6)		109.11(16)	O(5)-V(1)-O(4)	#3	109.22(29)
O(3)-V(1)-O(2)		109.82(19)	O(5)-V(1)-O(4)		107.65(15)	O(5)-V(1)-O(2)		107.88(25)
O(4)-V(1)-O(2)		108.83(18)	O(6)-V(1)-O(4)		109.10(15)	O(4)#3-V(1)-O	(2)	109.68(23)
O(3)-V(1)-O(1)		110.53(18)	O(5)-V(1)-O(2)		108.80(15)	O(5)-V(1)-O(3)	#6	109.25(25)
O(4)-V(1)-O(1)		109.97(18)	O(6)-V(1)-O(2)		111.10(15)	O(4)#3-V(1)-O	(3)#6	109.66(23)
O(2)-V(1)-O(1)		108.01(17)	O(4)-V(1)-O(2)		111.00(14)	O(2)-V(1)-O(3)	#6	111.11(20)
O(5)-V(2)-O(4)		105.25(18)	O(3)#2-V(2)-O		108.80(16)	O(7)-V(2)-O(1)		112.48(26)
O(5)-V(2)-O(2)	-	107.55(18)	O(3)#2-V(2)-O		114.64(16)	O(7)-V(2)-O(4		105.96(25)
O(4)#4-V(2)-O		87.44(16)	O(1)-V(2)-O(1)		136.46(6)	O(1)-V(2)-O(4)		141.46(24)
O(5)-V(2)-O(1)=	‡ 2	111.12(18)	O(3)#2-V(2)-O(3)	(2)#2	104.58(16)	O(7)-V(2)-O(3)		104.84(25)
O(4)#4-V(2)-O		87.72(16)	O(1)-V(2)-O(2)		83.31(14)	O(1)-V(2)-O(3)		82.02(20)
O(2)#3-V(2)-O((1)#2	140.93(16)	O(1)#2-V(2)-O(88.64(13)	O(4)-V(2)-O(3)		90.97(20)
O(5)-V(2)-O(1)		102.14(17)	O(3)#2-V(2)-O(3)		103.83(15)	O(7)-V(2)-O(2))	105.88(25)
O(4)#4-V(2)-O		152.22(16)	O(1)-V(2)-O(4)		90.02(13)	O(1)-V(2)-O(2)		77.57(19)
O(2)#3-V(2)-O(2)		88.73(16)	O(1)#2-V(2)-O(77.22(13)	O(4)-V(2)-O(2		89.74(19)
O(1)#2-V(2)-O(1)	78.12(17)	O(2)#2-V(2)-O		151.47(13)	O(3)-V(2)-O(2)		147.80(22)
			$O(7)#_4-V(3)-O$		112.60(16)	O(6)-V(3)-O(1)		110.21(26)
			$O(7)#_4-V(3)-O$		107.35(16)	O(6)-V(3)-O(1)		113.21(26)
			O(1)#2-V(3)-O(139.93(14)	O(1)#4-V(3)-O		136.51(9)
			$O(7)#_4-V(3)-O$		105.06(15)	O(6)-V(3)-O(3)		104.46(25)
			O(1)#2-V(3)-O(82.33(13)	O(1)#4-V(3)-O	-	82.73(20)
			O(6)#4-V(3)-O		90.48(13)	O(1)-V(3)-O(3)	-	88.95(20)
			O(7)#4-V(3)-O		104.27(15)	O(6)-V(3)-O(2		104.54(24)
			O(1)#2-V(3)-O(76.68(13)	O(1)#4-V(3)-O		89.48(20)
			O(6)#4-V(3)-O	,	90.90(13)	O(1)-V(3)-O(2)		77.56(20)
(1)#1· V V I			O(2)#5-V(3)-O	(4)	148.76(13)	O(3)#4-V(3)-O	(2)	150.91(21)

⁽¹⁾#1: x, y+1, z; #2: -x+1, -y+1, -z; #3: -x+2, -y+1, -z; #4: x, y-1, z; #5: -x+2, -y, -z+1

^{(2)#1: -}x+1/2, y-1/2, -z+1/2; #2: -x+1/2, y+1/2, -z+1/2; #3: x, y-1, z; #4: -x+1, -y+1, -z+1; #5: x, y+1, z; #6: -x+2, -y, -z+1

^{(3) #1: -}x, -y+2, -z; #2: x, y+1, z; #3: -x+1, -y+1, -z; #4: -x+3/2, y-1/2, -z+1/2; #5: -x+3/2, y+1/2, -z+1/2; #6: x, y-1, z; #7: x-1, y, z; #8: -x+1/2, y-1/2, -z+1/2; #9: -x+1/2, y+1/2, -z+1/2; #10: x-1/2, -y+3/2, z-1/2; #11: x-1/2, -y+1/2, z-1/2; #12: -x+1, -y+2, -z

RESULTS AND DISCUSTION

Crystal structures of 1, 3 and 4

The coordination environments of the fundamental building units of the structures of 1, 3 and 4 are shown as the ORTEP plots in Figure 4.1. It is apparent that these structures are constructed from the common inorganic building units, i.e. square pyramidal {VO₅}_{sp} and tetrahedral {VO₄}_{tet} units. Selected refined bond lengths and angles of these structures, which are in good agreement with those of 2 [7], are summarized in Table 4.2. Bond valences (BV) of the vanadium centers were calculated based on these data and a single point energy model with b=0.37, Ro=1.735, 1.784 and 1.803 for V^{IV} =O, V^{IV} -O and V^{V} -O bond, respectively [13,14]; 1, BV[V(1)]=5.04, BV[V(2)]=3.95; 3, BV[V(1)]=4.96, BV[V(2)]=4.00, BV[V(3)]=3.86; 4, BV[V(1)]=5.03, BV[V(2)]=3.92, BV[V(3)]=3.96. The calculation results indicate a mixed valence nature of the vanadium centers, i.e. tetravalence for $\{V^{IV}O_5\}_{sp}$ and pentavalence for $\{V^VO_4\}_{tet}$. According to the refined bond lengths, the coordination environment of {V^{IV}O₅}_{sp} can be described as 4+1, including four long V-O (1.874(7)-2.032(7) Å) equatorial bonds, and a short vanadyl bond, V=O, (1.603(7)-1.615(7) Å) in the apical site. The two adjacent {VIVO5}sp units are further condensed to form a [VIV2O8]2- dimer via transbasal edge-sharing with the apical O atoms of each {VIVO5}sp unit pointing toward opposite sides of the basal plane. The $\{V^{V}O_{4}\}_{tet}$ unit exhibits 3+1 fashion with three long V-O bonds (1.706(7)-1.834(4) Å), manifesting a oxygen bridge character and a short terminal V-O bonds (1.604(3)-1.633(4) Å).

The $\{V^VO_4\}_{tet}$ units together with the $[V^{IV}_2O_8]^{2-}$ dimers are arranged in two distinct fashions, leading to two different two-dimensional layered vanadium oxide frameworks. The small ethylenediamine template used in the preparation of 1 results in the same vanadium oxide framework topology as that of 2, for which 1,3-propanediamine was used as the template. The layer framework can be assigned as an α' -(UD.2T..) type and categorized in SP-T class and UD-T subclass [15]. The framework can also be described as being constructed from $[V^{IV}_2O_8]^{2-}$ dimers, surrounded by six $\{V^VO_4\}_{tet}$ units via the V^{IV} -O- V^V linkages at the equatorial corners of the $[V^{IV}_2O_8]^{2-}$ dimers, as shown in Figure 4.2(a). Each $\{V^VO_4\}_{tet}$ unit, on the other hand, shares its three basal O atoms with three neighboring $[V^{IV}_2O_8]^{2-}$ dimers. The arrangement leads to a sinusoidal $[V^{IV}_2O_8V^V_2O_2]^{2-}$ layer. It should also be noted that the V-V vectors of the $[V^{IV}_2O_8]_{2-}$ dimers within the layer are oriented uniformly in the

same direction, whereas the tetrahedral apexes of the adjacent $\{V^VO_4\}_{tet}$ units are directed in opposing directions throughout.

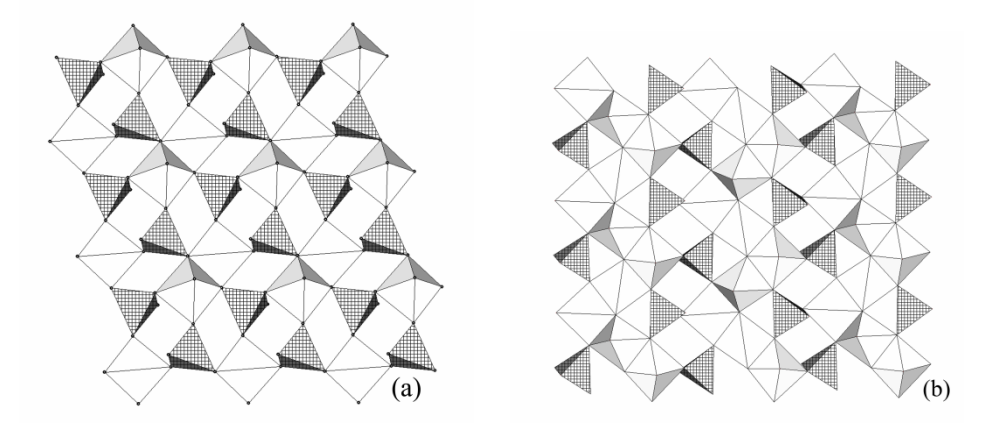


Figure 4.2 Polyhedral representations of vanadium oxide layers of (a) α' -(UD.2T..) for 1 and 2 and (b) β' -({UuDd}:2T..) for 3 and 4.

The employment of the longer diaminoalkanes of 1,4-diaminobutane and 1,5diaminopropane lead to another layer registry in 3 and 4, i.e. α' -({UuDd}:2T.) type, SP-T class and Z-T subclass. The $[V_{2}^{IV}O_{8}]^{2}$ dimers in 3 and 4 are not present as discrete units, but edge-shared in a cis fashion at the basal positions to the adjacent dimers. An extended one-dimensional zigzag chain of $\{[V^{IV}_{2}O_{8}]^{2-}\}_{n}$, as shown in Figure 4.2(b), is then established. The adjacent $\{[V^{IV}_{2}O_{8}]^{2}\}_{n}$ chains are then linked to each other via the {VVO4}tet units, each of which shares two basal corners with one chain and another with the other chain, thereby providing the two dimensional layered framework of $[V^{IV}_4O_{10}V^V_2O_4]^{2-}$. The alternation of the terminal apical O atoms of the $\{V^VO_4\}_{tet}$ units in combination with the tilting nature of the $[V^{IV}_{2}O_8]^{2^-}$ dimers gives rise to the twisting of the layers into a wave-like shape. It may be worth noting that the layer registry of 3 and 4 is similar to α' -({UuDd}:2T.), which is found in the analogous [V^{IV}₄O₁₀V^V₂O₄](C₆H₁₄N₂)·H₂O structure, sharing the common layer composition of $[V^{IV}_{~4}O_{10}V^{V}_{~2}O_{4}]^{2\text{-}}$ [6]. The major difference between and the α and β types is the relative arrangement of the $\{[V^{IV}_{2}O_8]^{2\text{-}}\}_n$ chains. The neighboring $\{[V^{IV}_{2}O_{8}]^{2-}\}_{n}$ chains in the α type are not superimposed as those found in the β type, but translated by one $\{V^{IV}O_{\scriptscriptstyle{5}}\}_{sp}$ unit along the chain direction.

The anionic vanadium oxide layers are subsequently stacked in the third dimension. The interlayer distances (d) of 1, 2, 3 and 4 were calculated from the PXRD patterns (Figure 4.3) and indicate an enlargement of d with length or number of the methylene groups (n) in the organic templates; i.e., 7.18, 7.70, 8.08 and 8.24 Å

for 1, 2, 3 and 4, respectively. The linear correlation between d and n is apparent when n=2-4 (see Figure 4.3 inset). These organic templates are located evenly in the interlayer galleries of the structures and arranged approximately parallel to the layers. The increasing length of the carbon skeleton has, therefore, a modest affect on the interlayer spacing. According to the FT-IR spectra (Table 4.3), these diaminoalkanes are deprotonated, which provide charge-balancing for the anionic framework. The CHN analysis results (Table 4.4), though differing slightly from the theoretical figures, agree well with the presence of the dications.

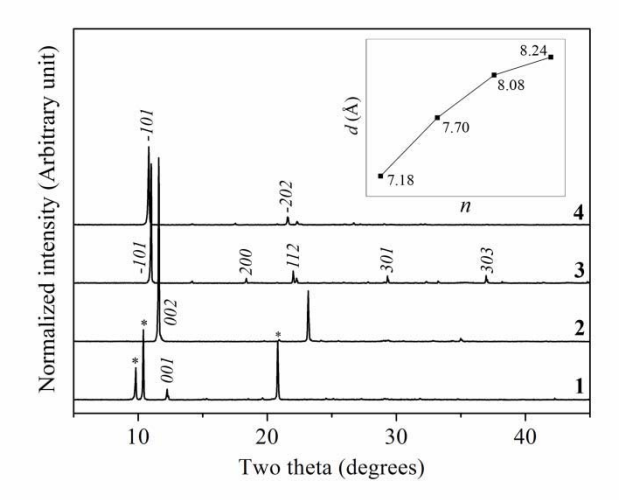


Figure 4.3 The PXRD patterns of 1, 2, 3 and 4 suggesting the correlation between the interlayer distances (d) and the number of methylene groups (n) of the diaminoalkenes (inset). The asterisks indicate impurities.

Table 4.3 FT-IT spectral assignments for 1, 2, 3 and 4.

1					
3328vs	ν(N-H)	1450VS	δ(C-H), CH ₂	779vs	$\nu_{as}(V-O_t)$
2965s	$v_{as}(C-H)$, CH_2	1321VS	$\delta s(N-H), NH_3^+$	514VS	$\nu_s(\text{V-O}_\text{b}\text{-V})$
2882m	$v_s(C-H)$, CH_2	1093VS	v(C-N)	48om	$\nu_{as}(V\text{-}O_b\text{-}V)$
1589vs	$\delta_{as}(N-H)$, NH_3^+	887vs	$v_s(V-O_t)$		
2					
345ovs,br	ν(N-H)	1290S	$\delta_{\rm s}({\rm N-H}),{\rm NH_3}^+$	561vs	$\nu_s(V-O_b-V)$
1603vs	$\delta_{as}(N\text{-H})$	1210S	v(C-N)	461vs	$\nu_{as}(V\text{-}O_b\text{-}V)$
1438m	δ_s (C-H), CH ₂	831vs	$\rho(CH_2 \text{ of } C\text{-}(CH_2)\text{-}C)$		
3					
3445vs,br	ν(N-H)	1459VS	δ_s (C-H, CH ₂)	768m	$\rho(CH_2,C-(CH_2)-C)$
2925W	$v_{as}(C-H, CH_2)$	1280W	$\delta_{\rm s}({ m N-H})$, ${ m NH_3}^+$	450s	$\nu_{as}(V\text{-}O_b\text{-}V)$
1628vs	$\delta_{as}(N-H)$, NH_3^+	1104VS	v(C-N)		
4					
3444s,br	ν(N-H), NH ₃ ⁺	1474VS	$\delta_{\rm s}({\rm C-H}),{\rm CH_2}$	507vs	$\nu_s(V-O_b-O)$
2925S	$v_{as}(C-H)$, CH_2	871vs	$v_s(V-O_t)$	466m	$\nu_{as}(V\text{-}O_b\text{-}V)$
1588vs	$\delta_{as}(N-H), NH_3^+$	762vs	$\rho(CH_2 \text{ of } C\text{-}(CH_2)_3\text{-}C)$		